Hydrological Drivers of Cutoff Regimes in Meandering Rivers

A Study on Overbank Flood Effects on Chute and Neck Cutoffs using Satellite Imagery

L. J. Zwaan

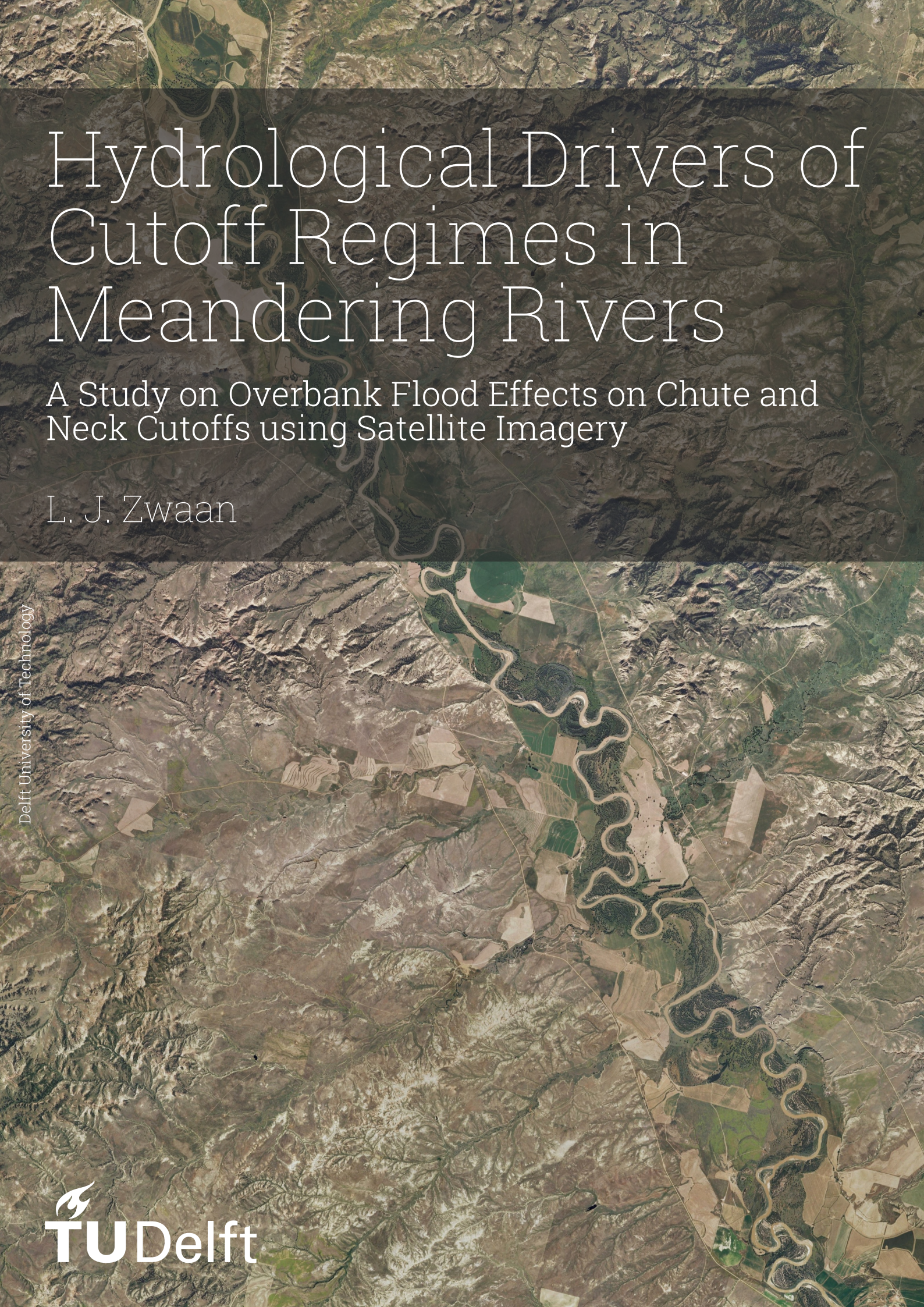

Delft University of Technology

TU Delft

Hydrological Drivers of Cutoff Regimes in Meandering Rivers

A Study on Overbank Flood Effects on Chute and Neck Cutoffs using Satellite Imagery

by

L. J. Zwaan

to obtain the degree of Master of Science
at the Delft University of Technology,
to be defended publicly on Monday July 1st, 2024 at 13:00.

Student number: 4713346
Project duration: January 30, 2024 – July 1, 2024
Thesis committee:

Dr. ir. A. Blom,	TU Delft, chair
Dr. K. B. J. Dunne,	TU Delft, supervisor
Dr. S. C. Toby,	TU Delft, supervisor

Cover: Powder River, Montana, USA. Image source: Google Earth Pro.

TU Delft

Preface

This thesis report shows the research I performed with the goal of receiving the Master's degree in Civil Engineering at the faculty of Civil Engineering and Geosciences of Delft University of Technology. After completing the required courses within the track Hydraulic Engineering with focus on River Engineering, I worked on this thesis from February until June 2024, with a final presentation on the 1st of July.

Time lapse videos of meandering rivers have always intrigued me, so I got in quite a good flow searching for river bend cutoffs on satellite imagery while looking at the beautiful power of nature. Rivers create fascinating shapes in their landscape, which raised a lot of questions for me. If you share this curiosity about rivers and their processes, this can definitely be an interesting read.

It was very enlightening to apply the things that I have learned in all the years that I spent studying Civil Engineering. I encountered a few obstacles and difficulties during this research, but I managed to resolve them or work around those, much like a meandering river. This was possible with the support of my enthusiastic supervisor, Kieran Dunne. I would like to thank him for the valuable brainstorm sessions, discussions, advises, and the opportunities to teach him some Dutch. Also many thanks to my other supervisor, Stephan Toby, for a vision from the other side of the faculty and very insightful feedback. And to the chair of my committee, Astrid Blom, thanks for keeping me grounded and helping me see the bigger picture with a critical view.

I am grateful for all the people who have supported me during my time at TU Delft. Especially my housemates, who endured listening to my stories and struggles for the past few months (and years) and were always there to support and motivate me. And to my family, who have always encouraged me to follow my passion and to work hard to achieve my goals, thank you for the opportunities you have given me and for your unlimited enthusiasm and support.

Linde Zwaan
Delft, June 2024

Abstract

Predicting and modelling meandering river migration is necessary for river engineering, land development, and risk assessment. One chaotic process that makes predicting the migration more difficult is the cutoff of a river bend, which is the subject of this report. This report describes the research process and results of a study on overbank flood effects on chute and neck cutoffs in single-thread meandering alluvial rivers. The following research question is addressed in this report: "*What is the relationship between the duration of overbank flooding and the formation of chute versus neck cutoffs*?". The relationships between the overbank flood shear stress and the frequency of chute versus neck cutoffs, and between the soil type of the floodplain and the frequency of chute versus neck cutoffs are evaluated.

An overbank flood exceeds the bankfull limit of a river, flowing over the floodplain. When a river bend is cut off, two cutoff types are visually distinguished: neck cutoffs and chute cutoffs. Cutoffs of both types were analysed in four rivers in the United States of America: Cheyenne River in North Dakota, Powder River in Wyoming and Montana, Pearl River in Mississippi, and Trinity River in Texas. These rivers have a chute cutoff regime, a mixed cutoff regime, and two neck cutoff regimes, respectively.

For these four rivers satellite imagery on Google Earth Pro was combined with measurements from USGS measurement stations and soil data from SoilWeb. The bankfull river discharge was converted to bankfull river depth to calculate the overbank flood heights and the overbank flood shear stresses acting on the floodplain during floods. Subtraction of the critical shear stresses of the soils resulted in residual shear stresses. These were combined with the corresponding flood durations to calculate the flood impulses of each flood.

The floods associated with chute cutoffs showed larger overbank flood shear stresses than those for neck cutoffs. Rivers with steeper slopes seem to be more prone to a chute cutoff regime than rivers with gentler slopes. The soils in which chute cutoffs were formed contained high sand percentages, while the neck cutoffs occurred in a wider range of soil types. The overbank floods creating chute cutoffs exerted larger residual shear stresses for shorter durations, as opposed to smaller residual shear stresses for longer durations of floods associated with neck cutoffs. The overbank flood impulses associated with chute cutoffs show a larger range and higher values, but are on average not significantly different to those of neck cutoffs.

The processes related to river bend cutoffs are very complex and not entirely understood yet and more research is needed on a local and a greater scale. The formulation of general relationships for chaotic events such as cutoffs will improve the prediction and modelling of meandering rivers. This will be increasingly useful, especially now with more extreme weather events and river floods all over the world.

Contents

1

Introduction

Meandering rivers come in many different shapes and sizes. Naturally meandering rivers never remain in the same shape or position, but carve through surrounding terrain and migrate across the floodplain, eroding, transporting, and depositing sediment (Güneralp & Marston, 2012). People living or working along and with these rivers are directly influenced by their changes. To improve the safety along these rivers, our ability to forecast morphodynamic change and river path migration needs to improve. Farmers, residents, ecosystems, navigation, and infrastructures will benefit from a better understanding and ability to predict the migration of meandering rivers. Predicting the behaviour of meandering rivers can be done by modelling the rivers to reflect reality. To do that, the hydromorphological processes within meandering rivers need to be defined and formulated for implementation into a model. Better prediction and modelling of migration improves river engineering decisions, land development plans, and river-hazard risk assessment (Pannone & De Vincenzo, 2022). Especially now, when more extreme weather events are expected due to climate change, and socio-economic concerns related to rivers are very present.

One of the difficulties that is encountered when a meandering river is modelled, is the occurrence of a river bend cutoff. Compared to the erosion and sedimentation processes on river banks, this process is a chaotic event. The river chooses the shortest path and changes its path, leaving the former bend as an oxbow lake. Figure 1.1 shows two of those cutoff river bends and the remaining oxbow lakes. When a river bend is cut off, the river's course changes suddenly and the river length is shortened abruptly, which can have many consequences for the hydromorphodynamic interaction of the river with the floodplain (Ghosh et al., 2023). These chaotic cutoff events have been difficult to model, especially over a longer time span (Abad et al., 2022; Durkin et al., 2018; Frascati & Lanzoni, 2013).

Figure 1.1: Image of Powder River, Wyoming, including cutoff river bends. The flow direction is from South to North (left to right on the image). Image taken from Google Earth Pro, image date: 5-7-2009, at an eye elevation of 12.26 km.

Cutoff events are placed into two categories: neck cutoffs and chute cutoffs. Neck cutoffs develop over time when two river bends have migrated close enough towards each other to pinch off the river bend, which creates a shorter and steeper path for the river to take (Constantine et al., 2010; Ghosh et al., 2023; J. Li et al., 2020; Martha et al., 2015). This type of cutoff has been modelled in various ways. Simple numerical models, such as 'meanderpy', show some classic examples of meandering rivers (Sylvester et al., 2019), such as the generated image shown in Figure 1.2.

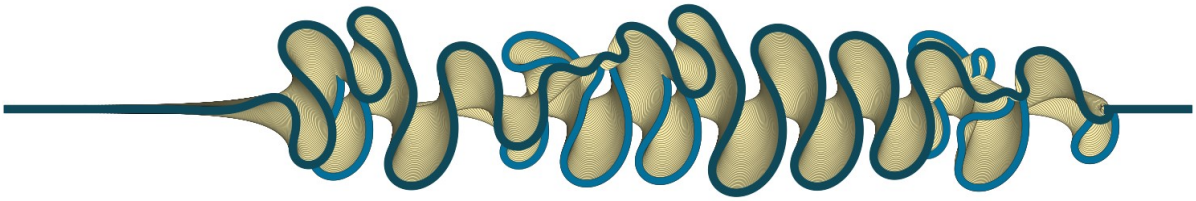

Figure 1.2: Partial image of a result that was generated with the Python module 'meanderpy' (Sylvester et al., 2019), available on Github.

Chute cutoffs cross a larger distance of the floodplain as a result of erosion of the floodplain. Floods incise a channel in the floodplain between river bends when the flood has enough energy to transport sediment from the floodplain (Constantine et al., 2010). Multiple physical processes and conditions have been proposed to initiate and develop the formation of chute cutoffs. One of them is that chute channels can form in swales of scroll bars, which are created by deposition of sediments on the inner bend during lateral migration of the river bend (Fisk, 1947; Grenfell et al., 2012). Another is that, due to local erosion of the river bank and floodplain in the outer river bend, and embayment is created, after which the river shoots across the floodplain and cuts off the original bend (Constantine et al., 2010; Eekhout & Hoitink, 2015). In other situations erosion begins on the downstream side of the floodplain. During a flood, water crosses the floodplain and drops back into the river channel which then results in erosion of the river bank and floodplain, causing a head cut migrating upstream (David et al., 2017; Ghinassi, 2011; Van Dijk et al., 2012; Zinger et al., 2011). This particular process is often assisted by an obstruction in the river in the form of wood or ice (Gay et al., 1998; Keller & Swanson, 1979). A combination of the erosion upstream and downstream of the floodplain is also found in the field and laboratory experiments (Grenfell et al., 2012; Malik et al., 2017; Van Dijk et al., 2012; Zinger et al., 2011). This range of variation and combinations of possible causes of chute cutoffs is something that makes modelling of this event very difficult. Some researchers have been trying to build a model that reflects reality, while focussing on a specific process, which makes that model limited in its applicability (Qiao et al., 2024).

Visually, neck and chute cutoffs are distinguished by the width of the floodplain through which the new cutoff channel is created. When this land width is equal to or smaller than the river width, which is the case for Figure 1.3a, the cutoff is categorised as a 'neck cutoff' (Güneralp & Marston, 2012; G. W. Lewis & Lewin, 2009; Turnipseed, 2017). For all situations where the land width is larger than the channel width, as in Figure 1.3b, the cutoff is called a 'chute cutoff'. After the occurrence of a cutoff, the new channel becomes the main river channel and what remains from the old bend is called an 'oxbow lake', among other names (Constantine & Dunne, 2008; Konsoer et al., 2016; Lauer & Parker, 2008). When a river reach has been subject to both neck and chute cutoffs, it has a 'mixed cutoff regime'. Otherwise, the river has a 'chute cutoff regime' or a 'neck cutoff regime'.

(a) Example of a neck cutoff, number 1 in Pearl River, Mississippi. The flow direction is from North to West. Image taken from Google Earth Pro, image date: 5-11-2011, near coordinates 32.111839, -90.115159.

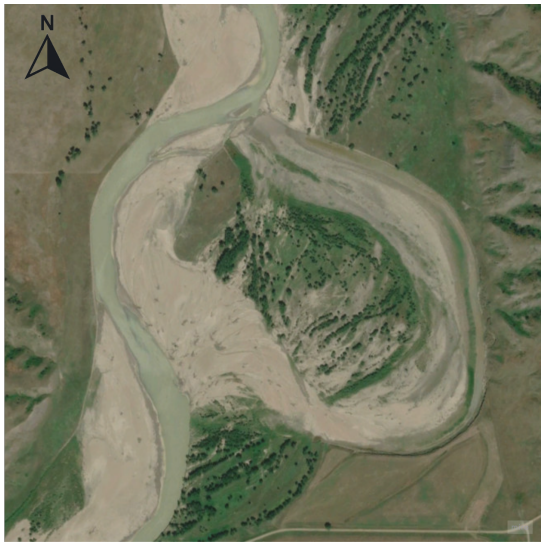

(b) Example of a chute cutoff, number 8 in Cheyenne River, South Dakota. The flow direction is from South to North. Image taken from Google Earth Pro, image date: 16-7-2020, near coordinates 44.291496, -102.032902.

Figure 1.3: Examples of a neck cutoff on the left and a chute cutoff on the right.

The majority of researches in the past centuries have been focused on specific cutoffs in much detail. Field observations, lab experiments (Z. Li et al., 2022; Van Dijk et al., 2012), and modelling have provided insights into the processes connected to meandering and river bend cutoffs, but they lack general relationships on a larger scale over multiple different river bends. This is needed to create a model that can be used for multiple rivers. The hydrological setting and the geological landscape of the rivers need to be incorporated into the models. A better understanding of the general migration of meandering rivers can be gained by finding the extent of influence of specific controlling factors, such as the duration of overbank flooding and the geology of the floodplain, which is what this research aims to do.

For this research, the following research question was drawn up: “What is the relationship between the duration of overbank flooding and the formation of chute versus neck cutoffs?”. An overbank flood exceeds the bankfull limit of a river, flowing over the floodplain. To answer this question, two sub-questions have been formulated: “What is the relationship between the overbank flood shear stress and the frequency of chute versus neck cutoffs?”, and “What is the relationship between the soil type and the frequency of chute versus neck cutoffs?”. This research is limited to single-thread meandering alluvial rivers with naturally created cutoffs.

Key for this research is the use of open source data in the form of Google Earth Pro, showing satellite images starting in 1985 until at least 2022. As oxbow lakes pose difficulties and uncertainties in the assignment of cutoff type, these are not taken into account. This means that the cutoffs analysed in this research happened between 1985 and 2022. Besides the Netherlands, there are few other countries with detailed measurements and documentations on their rivers and soils that are publicly accessible. One of those countries, with meandering rivers and cutoffs within the satellite time frame, is the United States of America (USA). Data was collected for four rivers in the USA: Cheyenne River in South Dakota, Powder River in Wyoming and Montana, Pearl river in Mississippi, and Trinity River in Texas. Google Earth Pro provided satellite imagery, while USGS National Water Information System contributed with hydrological data, and SoilWeb was used to gather geological data. During this data driven research, the different datasets were collected, analysed, reviewed, and filtered before equations and graphs were produced. During the processing of the hydrological data, conversion equations were applied, which are commonly used in hydrology research. The findings were combined to formulate answers to the research questions.

Following this introduction, Chapter 2 will go into depth on the methodology that was followed to collect and process the various data sets. Results of this analysis will be shown and explained in Chapter 3. The implication of these results and the used methods are discussed in Chapter 4, where the research process is reviewed as well. After this, the research questions will be answered, followed by recommendations for further research in Chapter 5. With all this, this report seeks to add to the knowledge of river bend cutoffs in relation to overbank flooding, assisting in the improvement of predicting and modelling meandering river migration.

2

Methodology

This chapter describes the methodology used to eventually answer the research questions: “What is the relationship between the duration of overbank flooding and the formation of chute versus neck cutoffs?”, “What is the relationship between the overbank flood shear stress and the frequency of chute versus neck cutoffs?”, and “What is the relationship between the soil type and the frequency of chute versus neck cutoffs?”. The different methods used for data collection, processing, and analysis are explained in this chapter.

To study the relationship between a river’s flow regime and its cutoff regime, multiple research methods could be used. Field observations, lab experiments, mathematical modelling, visual data analysis, and other methods could be applied to find new information on this topic. Researching these phenomena on a broader scale, looking for general relationships, requires a larger scope. The aim of creating a collection of multiple river bend cutoffs for more than one river reduces the methods to be used, resulting in the use of visual databases, such as Google Earth Pro, to be preferred. Publicly available data has many advantages over closed data. Among ease of use, free access, and provided explanation of terms, definitions, and sources, the major advantage is reproduction and reuse by other researchers. This means that future researchers can not only access this report, but also have the used datasets at their disposal.

In the past, similar methods have proven to be useful to collect data for multiple cutoffs. G. W. Lewis and Lewin (2009), for example, used historic maps and air photographs with which they counted 145 cutoffs in almost 1000 kilometres of river valley in Wales. This was originally published in 1983, when satellite imagery in high quality was not as widely available. Later, Constantine and Dunne (2008) used Google Earth images to measure channel and oxbow lake characteristics with the goal of identifying controls on the production of oxbow lakes in various rivers. On the other side of the world, satellite remote sensing was used to identify fluvial landforms and to map landform changes over time for Sindh River in India (Martha et al., 2015). More recently, researchers in Sri Lanka and Iraq used satellite imagery to learn more about the migration rates and changes of rivers in those countries (Basnayaka et al., 2022; Forti et al., 2022).

By combining the satellite imagery with openly available river gauge data, images gain numerical value. The addition of soil data contributes to the bigger picture of the process of overbank flooding causing erosion and creating cutoffs. The data is divided into three categories: satellite data, river gauge data, and soil data. For each of these categories, the data collection process is described and the steps of the processing and analysis of the data are elaborated. Information and links to the sources used in this research are shown in Appendix A.

First, to narrow the scope of this research, the rivers to be studied were selected by a set of criteria. To be used in this research, a meandering river in a fluvial system has to

- have visibly occurring cutoffs with no direct proof of human interference at a local scale, such as an obstruction of the main channel.
- have one or multiple river gauge stations with sufficiently consistent data collection for daily discharge and field measurements.
- have publicly accessible soil data.
- have a (partial) reach that is not significantly affected by the effects of recently constructed upstream dams or downstream tidal influences.

The satellite imagery time frame at the moment of data collection generally spans from 1985 to 2022. A large amount of meandering rivers with one or more measurement stations can be found in the United States of America (USA), for which open source soil data is also widely available. Many of these rivers are subject to human engineering and contain forced cutoffs in the shape of barricade placements or dredging, but some others show naturally occurring cutoffs without direct human interference. The effects of recently constructed dams would be visible in the discharge data, displayed as great differences in the mean discharge since the construction of that dam. Tidal influences are visible in discharge data when there are negative or significantly reduced discharge values at a tidal interval. After a thorough search through literature on meandering rivers in the USA and corresponding Google Earth Engine and Google Earth Pro images, four rivers were selected for data collection in this research. These rivers are Cheyenne River in South Dakota with only chute cutoffs, Powder River in Wyoming and Montana with chute and neck cutoffs, Pearl River in Mississippi, and Trinity River in Texas, both with only neck cutoffs. These rivers, cutoff regimes, and their locations in the USA are visible on the overview in Figure 2.1. Detailed information on these rivers can be found in Appendix B.

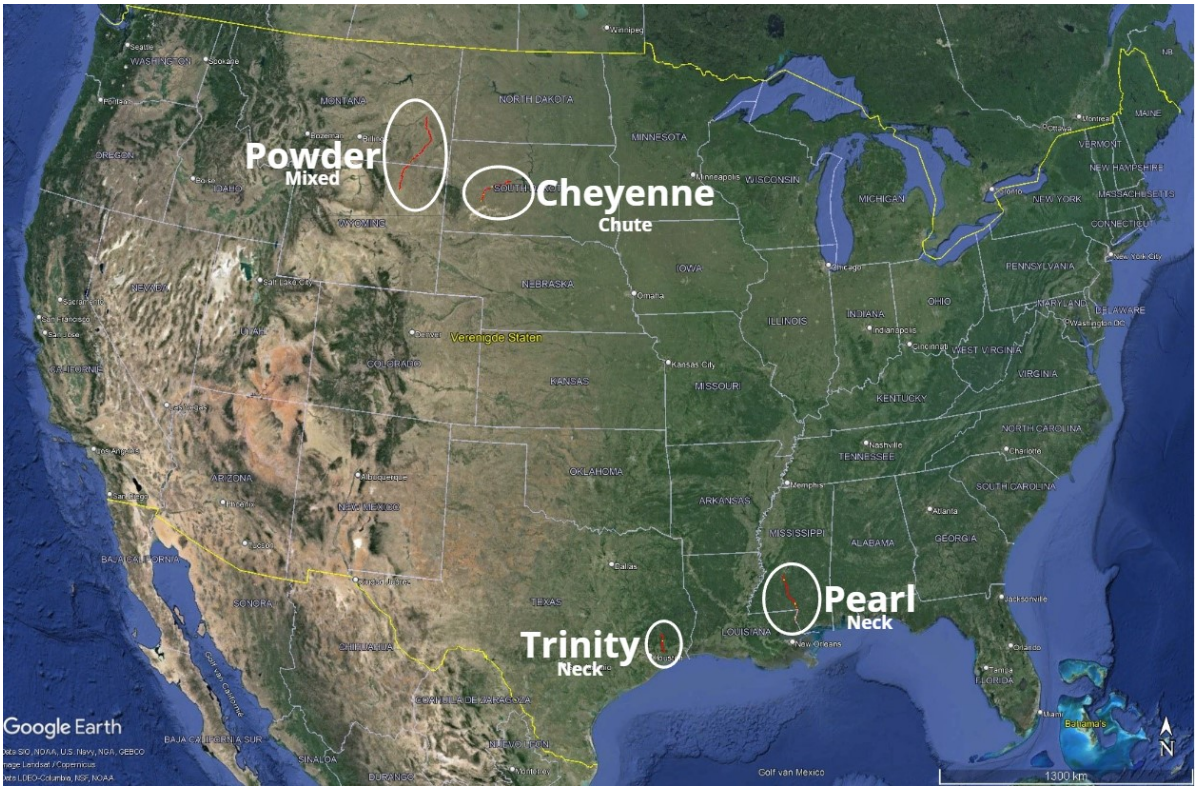

Figure 2.1: Overview of the locations of the four rivers on Google Earth Pro, indicated as red lines within the white circles. From top left to bottom right: Powder River in Wyoming and Montana with a mixed cutoff regime, Cheyenne River in South Dakota with a chute cutoff regime, Trinity River in Texas with a neck cutoff regime, and Pearl River in Mississippi with a neck cutoff regime.

2.1. Satellite Data

Satellite data contributed to the formulation of an answer of the main research question, but it was also used to describe the characteristics of various river bend cutoffs. Google Earth Pro was used to gather detailed information for each cutoff that was found in these four rivers within the time frame from 1985 to 2022. Using the measurement tools provided by Google Earth Pro to draw lines, paths, and circles, each cutoff was measured. Table 2.1 lists which variables were measured and Figure 2.2 shows a visualisation of these measurements on Google Earth Pro. For the measurements of the oxbow channel length and the cutoff channel length of each cutoff, common start and end points were chosen to compare the length ratios and losses. The satellite image dates on which the measurements are based are different per cutoff, which needs to be taken into account when comparing the properties of the oxbow and cutoff channels.

Table 2.1: Overview of the variables measured, with the meaning, unit, and measurement method on Google Earth Pro, corresponding to the figure below.

Symbol	Meaning	Unit	Method
Rad_{ox}	Radius of the oxbow bend	m	Circle
W_{ox}	Width of the oxbow channel	m	Line
W_{cc}	Width of the cutoff channel	m	Line
L_{ox}	Length of the oxbow channel	m	Path
L_{cc}	Length of the cutoff channel	m	Path
W_{land}	Width of land that is crossed by the cutoff event	m	Line

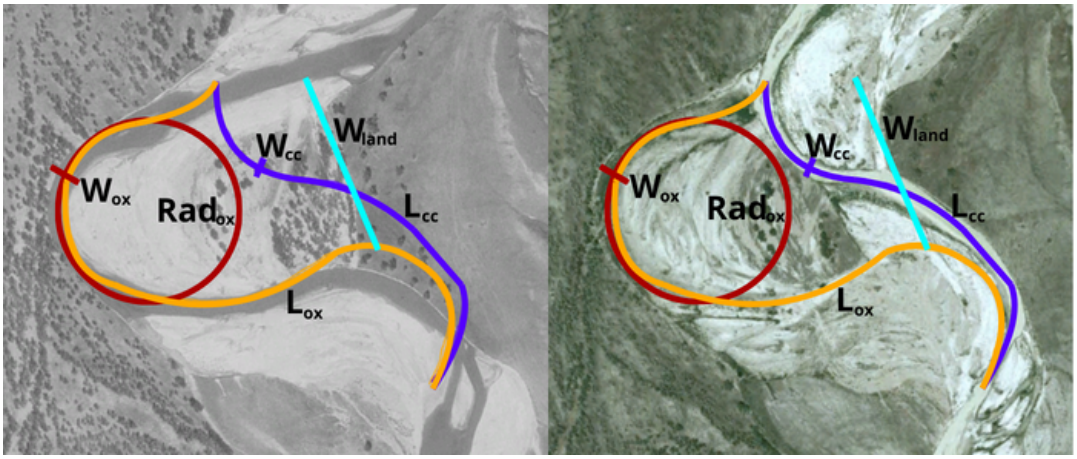

Figure 2.2: Illustration of measurements done on Google Earth Pro before and after the cutoff event. This is cutoff number 5 of Cheyenne River. The measurements can be found in Appendix C.

At relatively straight channel segments near each cutoff, the general bank-to-bank width ($W_{straight}$) of the river was measured to provide the opportunity for the comparison of dimensionless variables. When there was no straight channel segment near the cutoff, the general width was measured at an inflection point. These locations were chosen in such a way that the influence of curvature and river bend erosion on the observed channel width is minimal. All cutoff locations and the recorded measurements are shown in Appendix C. Those tables also show the year(s) assigned to each cutoff. Based on satellite imagery from different eye altitudes the year or years just before the occurrence of the cutoff were reported by selecting the last available image with no visible cutoff channel and the first image with a cutoff channel. The time between these images is the cutoff year(s) that is assigned to that particular cutoff. It is expected that floods occurred within this time frame and one or more of those floods caused the cutoff. The difference in eye altitude of Google Earth Pro gives access to images from a combination of different satellites, using data from sources such as NASA, Airbus, and Landsat. More on these satellites can be found in Appendix A.

The cutoffs were first analysed to see if they were measurable and within the scope of this research. Cutoffs that were incomplete or had significant gaps in satellite imagery were excluded. Rare cases with combined parallel channels or double cutoffs were also excluded, because these were not comparable. The measured variables for the included cutoffs were processed and analysed to see if and what relationships between the various bends of these rivers exist. To do this, Python in Jupyter Notebook was used.

2.2. River Gauge Data

River gauge data was used to estimate the height of overbank flooding, which was used to calculate the overbank flood shear stresses. All to answer the first sub-question: ”What is the relationship between the overbank flood shear stress and the frequency of chute versus neck cutoffs?”. ’Overbank’ is when the bankfull limit is exceeded and the water has gone over the banks and onto the floodplain. The ’bankfull limit’ for river depth and discharge is visible as the red dotted line in the conceptual diagram in Figure 2.3. In this cross-section of a river channel during an overbank flood there is a floodplain on both sides. This a flat area next to the river on which a river migrates laterally, spanning from the river bank until the valley wall (Evers & MacPhee, 2023). The symbols that are used in this chapter and the rest of this report are listed in Table 2.2 with their meanings and units.

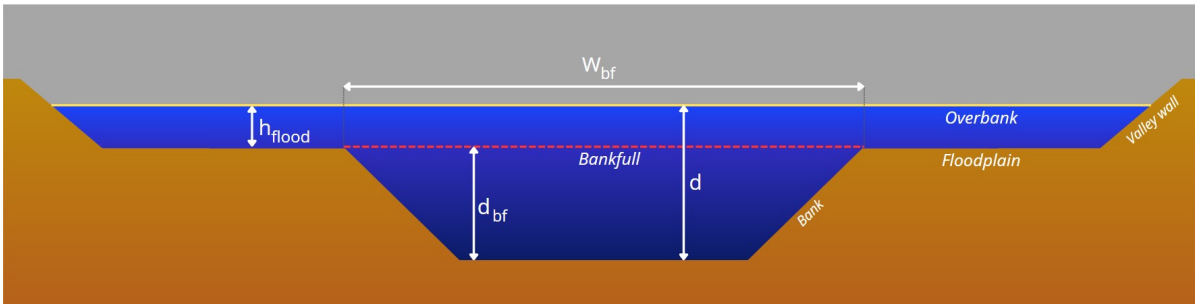

Figure 2.3: Conceptual diagram of a cross-section of a river channel during an overbank flood. The yellow line indicates the water height during the overbank flood and the red dashed line marks the bankfull river depth and the limits for the bankfull river width. Figure is not drawn to scale.

Table 2.2: List of symbols and definitions used to evaluate the river gauge data and to calculate the overbank flood height during overbank flooding.

Symbol	Meaning	Unit
d	River depth	m
d_{bf}	Bankfull river depth	m
W_{bf}	Bankfull river width	m
h_{flood}	Overbank flood height	m

For each of the four rivers, the river gauge stations in the United States Geological Survey (USGS) National Water Information System along the river reach were identified. USGS collects several types of data, of which the field measurements and the daily discharge data are relevant for this research:

- USGS field measurements are performed every six to eight weeks, with local differences. The channel at the measurement site is straight and uniform for a distance long enough to support uniform flow (Jacobson & Kitchen, n.d.). Many of the streamflow measurements are performed with Acoustic Doppler Current Profilers (ADCPs) on a moving boat (Hydroacoustics, n.d.-b). On other occasions, the midsection method is used, during which the channel area and flow velocities at multiple subsections of a cross-section are measured (Hydroacoustics, n.d.-a). Velocities are measured with Acoustic Doppler Velocimeters (ADVs) or ADCPs.

- USGS daily discharge measurements are done by gauge stations working with a stilling well or by measuring pressure. The daily gauge height is measured relative to a certain datum, which is often placed below the river bed. The daily discharge is measured on location or determined by the stage-discharge relationship, which is decided by measurements of discharge at different river stages (Water Science School, 2018).

The datasets for daily discharge data and field measurements were downloaded for the USGS stations along the four rivers. All values were converted from the imperial system to metric values by using the conversion rate of 1 foot = 0.3048 metres. Rows with missing discharge data, or failed measurements due to the presence of ice were removed from the data sets. All files included mean discharge measurements, while some also included maximum and minimum discharge measurements. To compare the values, only the mean discharge measurements were taken for further calculations.

The calculation of the water height on the floodplain during a flood is based on the total discharge at that time. This requires the value for bankfull water level or bankfull discharge. According to the definition of Knighton and Nanson (2002): "The bankfull level is, in effect, the dividing line between the inbank and overbank states", where overbank indicates the flooding of the floodplain. This bankfull discharge (Q_{bf}) can be estimated with the observed bankfull river width (W_{bf}), according to Bjerklie (2007). He compared the results of different possible formulas and other previously calculated and estimated values for bankfull discharge. His research presented a regression equation to estimate the Q_{bf}, for single thread meandering rivers that are unaffected by backwater, in the following form:

$$Q_{bf} = 0.24 \cdot W_{bf}^{1.64} \tag{2.1}$$

With

- Q_{bf} [m^3/s]: Bankfull channel discharge
- W_{bf} [m]: Observed bankfull river width measured on satellite imagery

The value of W_{bf} for each river is the observed bankfull river width of a relatively straight channel part or inflection point near a USGS measurement station. These values are listed in Appendix B in the column called 'River width [m]'. Bjerklie (2007) also gives the corresponding regression statistics for this equation. The lower 95% of the confidence interval is calculated with $Q_{bf} = 0.20 \cdot {W_{bf}}^{1.59}$ and the upper 95% can be found with $Q_{bf} = 0.29 \cdot {W_{bf}}^{1.68}$. This results in the following discharge graph, in Figure 2.4, with the estimated bankfull discharge and corresponding 95% confidence intervals for one of the USGS measurement stations along Trinity River. Discharge graphs with corresponding Q_{bf} values for the other USGS measurement stations can be found in Appendix D.1.

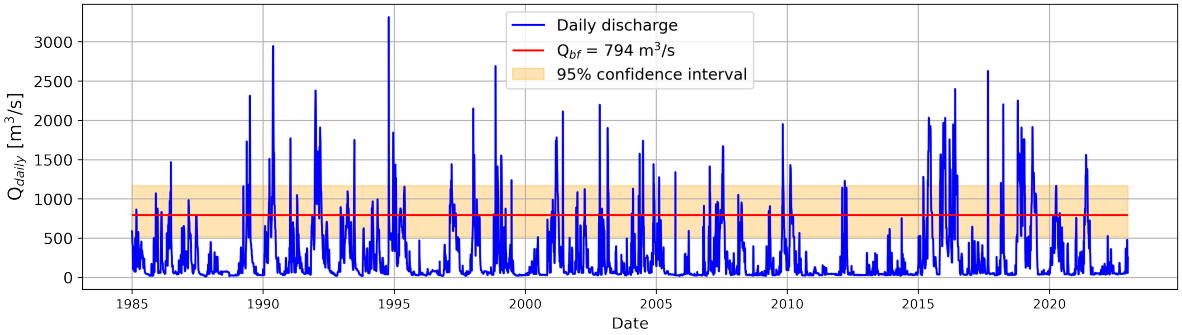

Figure 2.4: Daily discharge (Q_{daily}), plotted in blue over time, taken from USGS station Romayor along Trinity River (ID: 08066500). The red horizontal line represents the bankfull discharge (Q_{bf}), calculated with Bjerklie (2007), with the corresponding 95% confidence interval in light orange with a lower limit of 517 m^3/s and an upper limit of 1169 m^3/s.

For every river, only one measurement station was selected as a reference station for the cutoffs in that river. This was based on the consistency of the data and the location of the stations with regard to the locations of the cutoffs. The consistency of the data collection had to be sufficient, meaning no major gaps in the daily discharge data set. Then, the validity of the daily discharge values compared to the calculated bankfull discharge threshold was checked, taking into account the visual proof of floods on satellite imagery. As a final check, the location of each station with regard to the locations of the cutoffs was analysed. The influence of large bifurcations or conjunctions of tributaries has to be taken into account when selecting the reference station. This was especially the case for Cheyenne River, resulting in the choice for Plainview station, even though it started measuring daily discharge data much later in time than Wasta station which is located further upstream. Plainview station is positioned downstream of the conjunction of Belle Fourche River into Cheyenne River and shows much larger flood discharge values than Wasta station. The majority of the cutoffs is located downstream of this conjunction and the few cutoffs upstream seem to be close enough to the conjunction to be affected by the backwater curve. More information on these stations, including coordinates and data availability can be found in Appendix B.

The selected station for each river is:

- Cheyenne River near Plainview, South Dakota with ID 06438500
- Powder River at Moorhead, Montana with ID 06324500
- Pearl River near Monticello, Mississippi with ID 02488500
- Trinity River at Romayor, Texas with ID 08066500

For these four stations, the daily discharge measurements and field measurements were used to calculate the overbank flood heights. The inbank river depths were calculated with Equation (2.2), based on the field measurements by USGS.

$$d_{calc} = Q_{fm}/(W_{fm} \cdot v_{fm}) \tag{2.2}$$

With

- d_{calc} [m]: The calculated river depth
- Q_{fm} [m^3/s]: Channel discharge measured during field measurements by USGS
- W_{fm} [m]: Channel width measured during field measurements by USGS
- v_{fm} [m/s]: Flow velocity measured during field measurements by USGS

This results in a relationship between discharge and river depth, as long as the bankfull discharge is not exceeded. In the field measurements, critical discharge values near the calculated Q_{bf} were found: one measurement just above the bankfull discharge and one measurement just below it. The corresponding calculated river depths for these critical measurement values and their ratios towards the bankfull value were used to estimate the bankfull river depth.

Limited by the calculated Q_{bf} and the corresponding estimated bankfull river depth, the power law relationship between Q_{fm} and d_{calc} for inbank flow condition was determined, which can be seen in Figure 2.5. The power law is used because of its common use in hydrology (Ashmore & Sauks, 2006; Smith & Pavelsky, 2008). Since these measurements are done in various circumstances and they are only a snapshot of the situation, it is possible that values below bankfull discharge exceed the estimated bankfull river depth and vice versa.

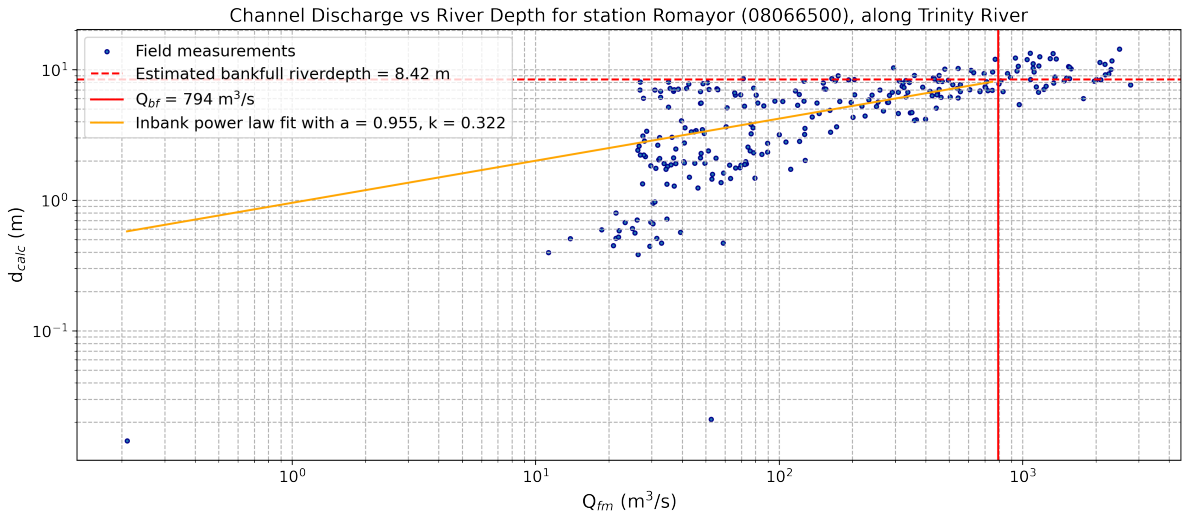

Figure 2.5: Plot with calculated river depths, based on field measurements (d_{calc} [m]) on the y-axis against the measured channel discharge (Q_{fm} [m^3/s]) on the x-axis, both in log scale. The blue scatter dots represent field measurements at different times. The vertical red line is the Q_{bf} limit and the horizontal red dashed line is the corresponding estimation of bankfull river depth. The orange line shows power law scaling with its factor (*a*) and exponent (*k*) shown in the legend, for USGS station Romayor along Trinity River (ID: 08066500).

For each station, the scaling factor and exponent were applied to convert Q_{daily} to daily river depths (d_{scaled}) using Equation (2.3).

$$d_{scaled} = a \cdot Q_{daily}^{k} \tag{2.3}$$

With

- d_{scaled} [m]: Daily river depth resulting from the power law scaling
- *a*: Scaling factor from power law fit on field measurement data
- Q_{daily} [m^3/s]: Daily discharge measured by a USGS station
- *k*: Exponent from power law fit on field measurement data

This relationship was also used to convert Q_{bf} to the bankfull river depth (d_{bf}), which is the horizontal green line in Figure 2.6 below.

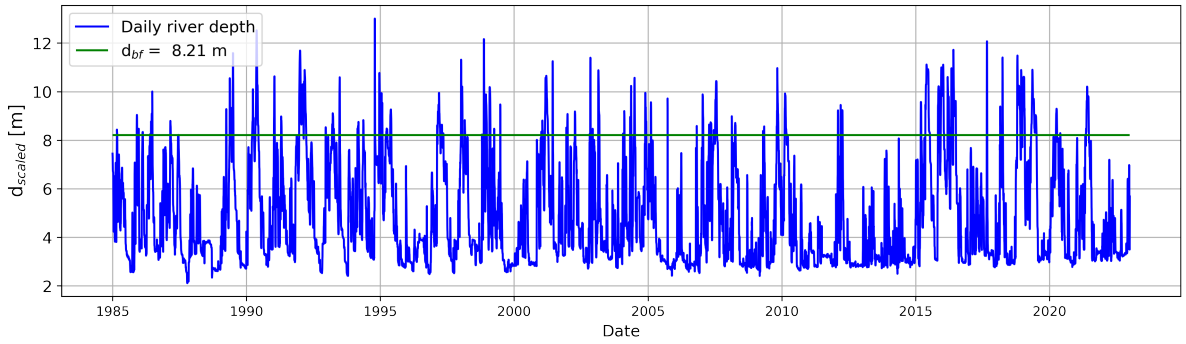

Figure 2.6: Scaled daily river depth (d_{scaled}) in metres shown in blue and the scaled bankfull river depth (d_{bf}) in metres as a green horizontal line with its value displayed in the legend. USGS station Romayor along Trinity River (ID: 08066500).

All peaks above the bankfull river depth threshold are considered to be overbank floods. Those specific floods that happen within the time frames assigned to the cutoffs are collected and appointed to the specific cutoff type. The d_{bf} value is then subtracted from the river depth values to obtain the overbank flood heights.

To calculate the overbank flood shear stress, the local slope at the position of the cutoff is calculated with the overall slope for each river and the length ratio of the cutoff, as is shown in Equation (2.4). This equation takes into account the sudden changes in channel length caused by a cutoff event. The overall slope, shown for each river in Table 2.3, was measured in Google Earth Pro and compared to data of the SWOT River Database (SWORD) (University of North Carolina at Chapel Hill, 2022). An example of the measurements of L_{ox} and L_{cc} for the length ratio of a cutoff is shown in Figure 2.7.

$$S_{local} = S_{river} \cdot L_{ox}/L_{cc} \tag{2.4}$$

With

- S_{local} [m/m]: Local slope of the channel near the cutoff
- S_{river} [m/m]: Overall river slope, found by dividing the change of elevation over the distance of the river path, measured on Google Earth Pro
- L_{ox} [m]: Length of the oxbow lake, as measured on Google Earth Pro
- L_{cc} [m]: Length of the cutoff channel, as measured on Google Earth Pro

Table 2.3: The value for S_{river} for every river, based on elevation and length measurements on Google Earth Pro, checked with SWORD data.

River	S_{river} [m/m]
Cheyenne	$1.028 \cdot 10^{-3}$
Powder	$1.012 \cdot 10^{-3}$
Pearl	$1.318 \cdot 10^{-4}$
Trinity	$3.531 \cdot 10^{-5}$

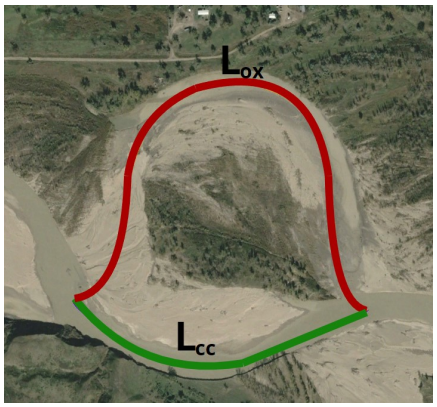

Figure 2.7: L_{ox} in red and L_{cc} in green. This is cutoff 10 in Cheyenne River with flow direction from West to East (left to right on the image). Image taken from Google Earth Pro, image date 05-10-2019.

Since the angle of the river channel to horizontal is very small, and the river width is much larger than the river depth, the average overbank flood shear stress is approximated by Equation (2.5). The average overbank flood shear stress (τ_{flood}) is calculated per flood for the floods that happened within a cutoff time frame.

$$\tau_{flood} = \rho \cdot g \cdot h_{flood} \cdot S_{local} \tag{2.5}$$

With

- τ_{flood} [N/m^2]: Average overbank flood shear stress per flood
- ρ [kg/m^3]: Water density (a value of 1000 is taken)
- g [m/s^2] : Gravity acceleration (taken as 9.81 m/s^2)
- h_{flood} [m]: Average overbank flood height per flood
- S_{local} [m/m]: Local slope of the channel near the cutoff

2.3. Soil Data

In support of answering the second sub-question ”What is the relationship between the soil type and the frequency of chute versus neck cutoffs?”, soil data was collected through SoilWeb. SoilWeb has collected many field measurements that have been performed over the years on a large number of locations during soil surveys performed by USDA-NRCS soil survey (UC Davis, n.d.). Data is collected through digitalised paper manuscripts and surveys directly added to Web Soil Survey.

The SoilWeb map, covering the complete USA, contains the composition of the soil at any location in percentages of soil series, in addition to an enormous amount of data and classifications. Each of these soil series has particular percentages of clay and sand. The top 10 to 20 centimetres are ignored and the values of deeper measurements, often up to 150 or 180 centimetres, are taken, to account for the soil through which the new channel was formed. The clay percentages and sand percentages of the soil classifications were collected and calculated for every cutoff. Sand consists of particles with grain sizes with a diameter between 0.05 mm and 2 mm. This contains the total sand fraction. The clay particles have a diameter smaller than 0.002 mm (U.S. Department of Agriculture, 2022). Any organic matter was ignored and gravel was only taken into account during the calculations of clay and sand percentages when it was explicitly mentioned on SoilWeb. Vegetation on the floodplains was also ignored, because of lack of detailed data. The studied situation represents a simplification of the floodplain, where vegetation is not present or already removed when the erosion of the soil takes place.

The clay percentages were used to calculate the critical shear stresses of the soil ($\tau_{c,soil}$). Based on research and field measurements, done by Dunne et al. (2022), critical shear stress (τ_c) values for clay mixtures can be determined from the graph in Figure 2.8a. These values for τ_c are found for sand-clay mixtures with kaolinite content, which is a well-known clay mineral that is included in the clay percentages found during field measurements (Frost & Kristof, 2004; U.S. Department of Agriculture, 2022). Since clay is the largest contributor to the cohesiveness of the soil, these values were used to calculate the $\tau_{c,soil}$ of the soils of the floodplains of the cutoffs, after interpolation on the experimentally determined values, shown in Figure 2.8b.

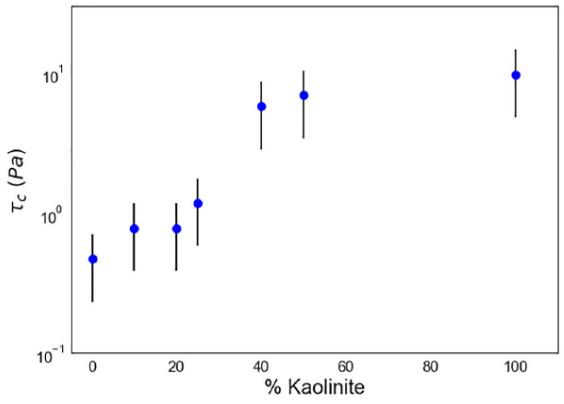

(a) This graph was produced by Dunne et al. (2022), with subscipt: 'Experimentally determined τ_c for sand-clay mixtures with varying kaolinite content. Reported values are for $\tau_c = \tau_{b,n}$. Error bars indicate ± 1 standard deviation.'

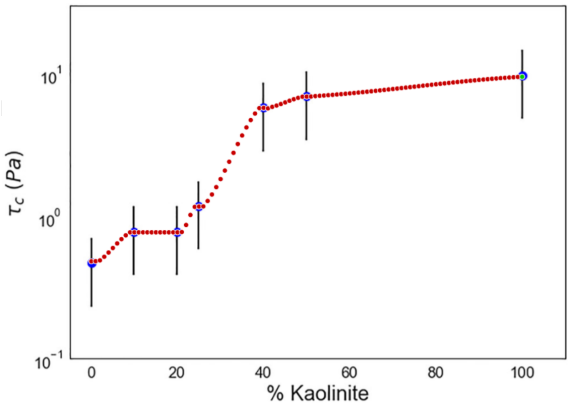

(b) Spline interpolation on the gathered data, done with a step of one unit, with unit being percentage Kaolinite, and no smoothing on the graph. This interpolation was done via WebPlotDigitizer Version 4 using the algorithm 'X Step w/ Interpolation'.

Figure 2.8: Comparison of experimental data and interpolation to calculate critical shear stresses for the soil.

2.4. Data Combination

Visual data from Google Earth Pro satellite images, flood shear stresses based on USGS river gauge data, and critical soil shear stresses calculated with SoilWeb data were combined to answer the main research question: ”What is the relationship between the duration of overbank flooding and the formation of chute versus neck cutoffs?”. The remaining shear stress from a flood on the floodplain is expressed as the average residual shear stress, after the critical shear stress of the soil is subtracted from the overbank flood shear stress. Only the residual shear stresses larger than zero are of importance in the next steps, as those floods eroded the floodplain. These positive residual shear stresses were multiplied with the corresponding durations of those floods within cutoff time frames to quantify an impulse exerted by a singular flood on the floodplain, as can be seen in Equation (2.6). This impulse causes a change in momentum, resulting in the erosion of the floodplain, creating a cutoff. Flood impulse on the floodplain is a concept similar to ’geomorphic work’, which also describes the movement of sediments caused by forces such as the force of flowing water (Wolman & Miller, 1960) and the effect of floods on planform changes (Ielpi et al., 2021). The magnitude of the force is multiplied with the frequency or duration of that force (Leopold et al., 1964).

$$I = \tau_{res} \cdot D \tag{2.6}$$

With

- I [N·s/m^2]: Impulse of a flood on the floodplain, being force applied by a flood over time to cause a change in momentum
- τ_{res} [N/m^2]: Residual shear stress = overbank flood shear stress (τ_{flood}) - critical shear stress of the soil of the floodplain ($\tau_{c,soil}$)
- D [s]: Duration of a singular flood

The duration of every singular flood is based on the converted daily data points that exceed the bankfull river depth. An example of the visualisation of the duration is shown in Figure 2.9. This is a flood that has a duration of 41 days, in Trinity River, where a cutoff was seen at the end of 1990.

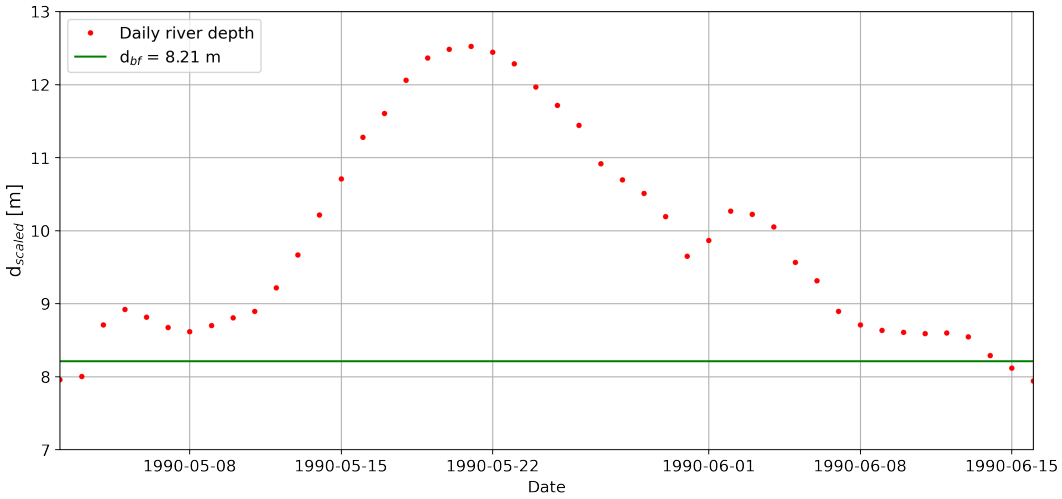

Figure 2.9: Example of a flood in 1990, with a duration of 41 days. The red dots represent daily river depth values. The y-axis shows the scaled daily river depth (d_{scaled}) in metres and the green line is the scaled bankfull river depth (d_{bf}). USGS station Romayor along Trinity River (ID: 08066500).

3

Results

The results following the collection, processing, and analysis of the data are presented in this chapter. The stations that were considered in the calculations for each river are shown in Table 3.1. First, the findings and measurements of the cutoffs from the satellite imagery will be shown. These are followed by the calculated shear stresses of the floods based on measurements taken by the river gauges. The soil types and the corresponding resistance values of the floodplains will then be shown, after which all results combined provide the impulses of the floods on the floodplains. Subsequently, Chapter 4 will go into detail on the interpretations and implications of these results.

Table 3.1: The four selected USGS river gauge stations.

River	USGS station ID	Near	Cutoff regime
Cheyenne	06438500	Plainview	Chute
Powder	06324500	Moorhead	Mixed
Pearl	02488500	Monticello	Neck
Trinity	08066500	Romayor	Neck

3.1. Cutoff Classifications and Measurements

Based on the available Google Earth Pro satellite imagery, the timeframe of interest was set to 1985-2022. All cutoffs found in the four rivers that occurred during that time were analysed and measured. Examples of these measurements are shown in Figure 3.1. The coordinates and measurements of the cutoffs can be found per river in Appendix C.

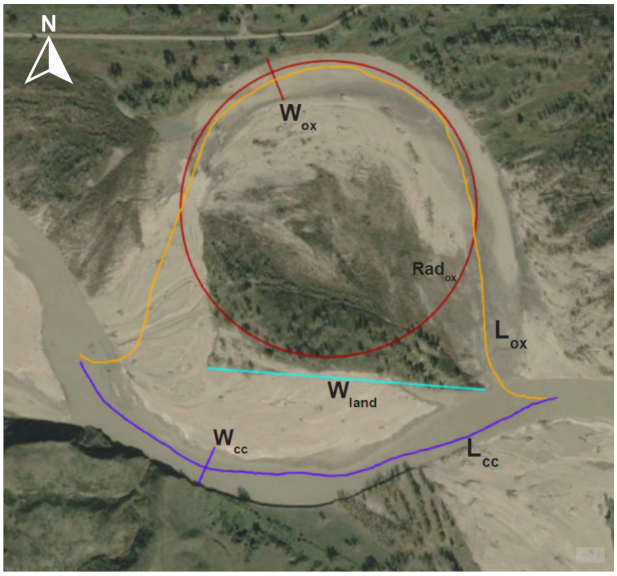

(a) Example of a chute cutoff with measurements drawn on Google Earth Pro. This is cutoff number 10 of Cheyenne River, South Dakota. The flow direction is West to East. Image taken from Google Earth Pro, image date: 5-10-2019.

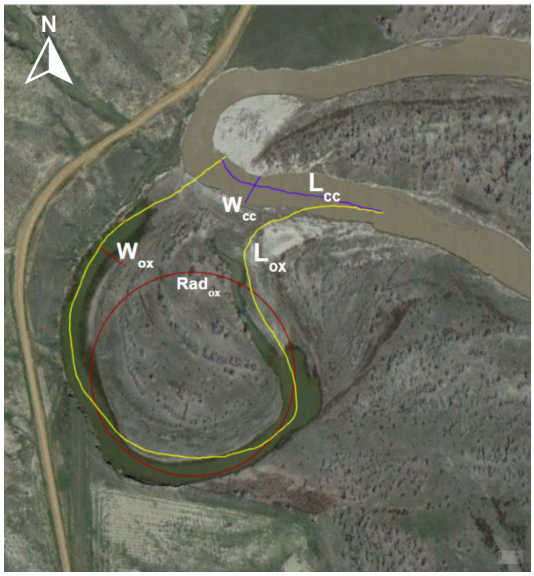

(b) Example of a neck cutoff with measurements drawn on Google Earth Pro. This is cutoff number 7 of Powder River, Wyoming. The flow direction is from South to North. Image taken from Google Earth Pro, image date: 1-5-2014.

Figure 3.1: Measurements done on Google Earth Pro. W_{ox}: oxbow channel width. L_{ox}: oxbow channel length. W_{cc}: cutoff channel width. L_{cc}: cutoff channel length. Rad_{ox}: radius of the oxbow bend. W_{land}: land width between two bends (only measured for chute cutoffs). The values can be found in Appendix C.

After a cutoff event has occurred, the channel length is reduced in all recorded cases, which can be seen in Figure 3.2a. The width loss (W_{ox} - W_{cc}) on the y-axis is plotted against the length loss (L_{ox} - L_{cc}) on the x-axis for the chute cutoffs in orange squares and neck cutoffs in blue circles. These values were made dimensionless by dividing each by their measured width on a straight channel reach near the cutoff ($W_{straight}$). Negative values for width loss indicate an increase of the width of the new cutoff channel compared to the width of the original channel.

On the top right, Figure 3.2b shows the width ratios (W_{ox}/W_{cc}) and length ratios (L_{ox}/L_{cc}) from the old situation over the new situation. The majority of the length ratios (L_{ox}/L_{cc}) for the neck cutoffs are significantly larger than those for the chute cutoffs, which can also be seen in Figure 3.2c. The chute cutoffs have length ratios all below 3, while the length ratios of the neck cutoffs are between 2 and 8. By definition, neck cutoffs have a value of W_{land} that is smaller than or equal to the channel width. This means that the newly created cutoff channel is, in most cases, much shorter than the original channel. For chute cutoffs, this decrease in channel length is often less than for neck cutoffs, as these chute cutoffs have a W_{land} of at least more than the channel width. The width ratios, displayed in Figure 3.2d do not show significant differences between the chutes and necks. In all these boxplots the red line in the box represents the median of the values and the green triangle is the mean of the values in that dataset.

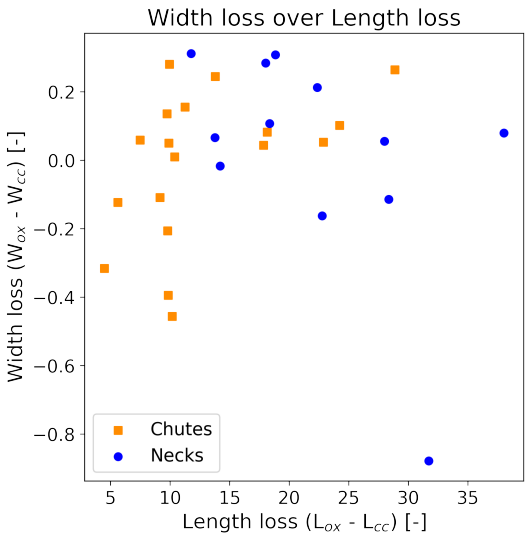

(a) Scatter plot with the dimensionless width loss on the y-axis over the dimensionless length loss on the x-axis.

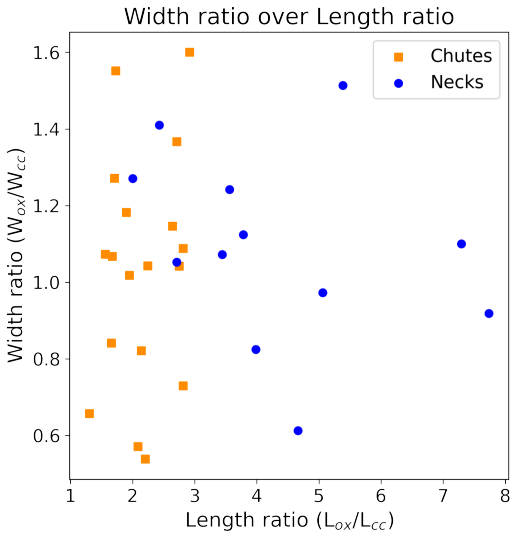

(b) Scatter plot with the width ratio on the y-axis over the length ratio on the x-axis.

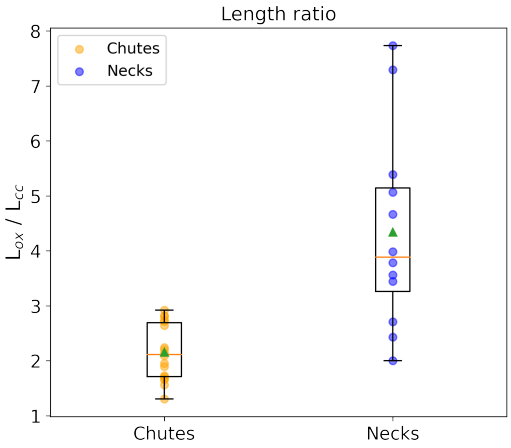

(c) Distributions of the ratios of the oxbow channel length in the old situation over the cutoff channel length in the new situation after the cutoff event.

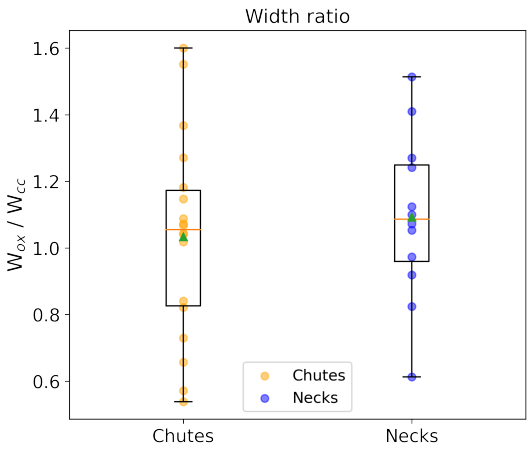

(d) Distributions of the ratios of the oxbow channel width in the old situation over the cutoff channel width in the new situation after the cutoff event.

Figure 3.2: Top row: Scatter plots for the width ratios over length ratios (left) and the width losses over length losses (right). Bottom row: Boxplots showing the distribution of the length ratio (left) and the width ratio (right) of oxbow channels over cutoff channels. Chute cutoffs are shown as orange squares in the scatter plots and as yellow dots on the left in the boxplots. The blue circles represent neck cutoffs in each plot. All values are based on measurements done on Google Earth Pro on images before and after the cutoff event. Those measurement values can be found in Appendix C

3.2. Overbank Flood Shear Stresses

The discharge data and field measurements, collected and performed by USGS stations and employees, were processed, checked, and converted. Equation (2.1) was used to calculate bankfull river discharge and with Equation (2.3) the river depths at the USGS station locations were calculated. Then, overbank flood heights were calculated for floods within the cutoff time frames. This was all done with the aim to answer the sub-question, "What is the relationship between the overbank flood shear stress and the frequency of chute versus neck cutoffs?". The overbank flood shear stress includes the magnitude of overbank floods and takes local properties into account with the local slope.

After calculating the bankfull river depth for each station and checking for floods during the cutoff time frames, it was found that some cutoffs had no record of overbank floods within their assigned time frame. These were thus excluded for further analysis. Of the total number of cutoffs considered, 5 out of 16 cutoffs for Plainview station in Cheyenne River were excluded, in addition to 2 out of 7 cutoffs for Moorhead station in Powder River. For Monticello station in Pearl River and Romayor station in Trinity River, all cutoffs were connected to recorded floods.

In Figure 3.3a below, the calculated overbank flood heights and their distributions are shown for each river. For each flood event, the average overbank flood height during that flood is taken. On the right, Figure 3.3b shows the overbank flood shear stresses, calculated with Equation (2.5).

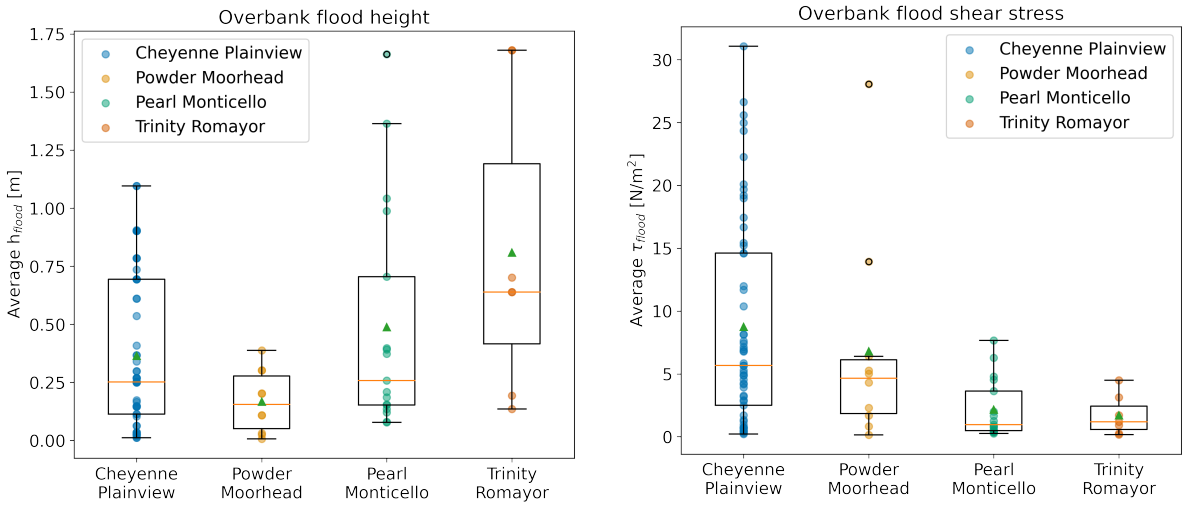

(a) Distributions of the overbank flood heights in metres of the floods within cutoff time frames for every river.

(b) Distributions of the overbank flood shear stresses of each flood for every river in N/m^2.

Figure 3.3: Boxplots for overbank flood heights on the left and overbank flood shear stresses on the right, for each river. From left to right in both plots: Cheyenne River with station Plainview, Powder River with station Moorhead, Pearl River with station Monticello, and Trinity River with station Romayor.

The distribution of the overbank flood heights and overbank flood shear stresses for the two cutoff types are shown in Figure 3.4. In both plots, the yellow dots on the left represent the floods linked to chute cutoffs, and the blue dots on the right depict the floods linked to neck cutoffs.

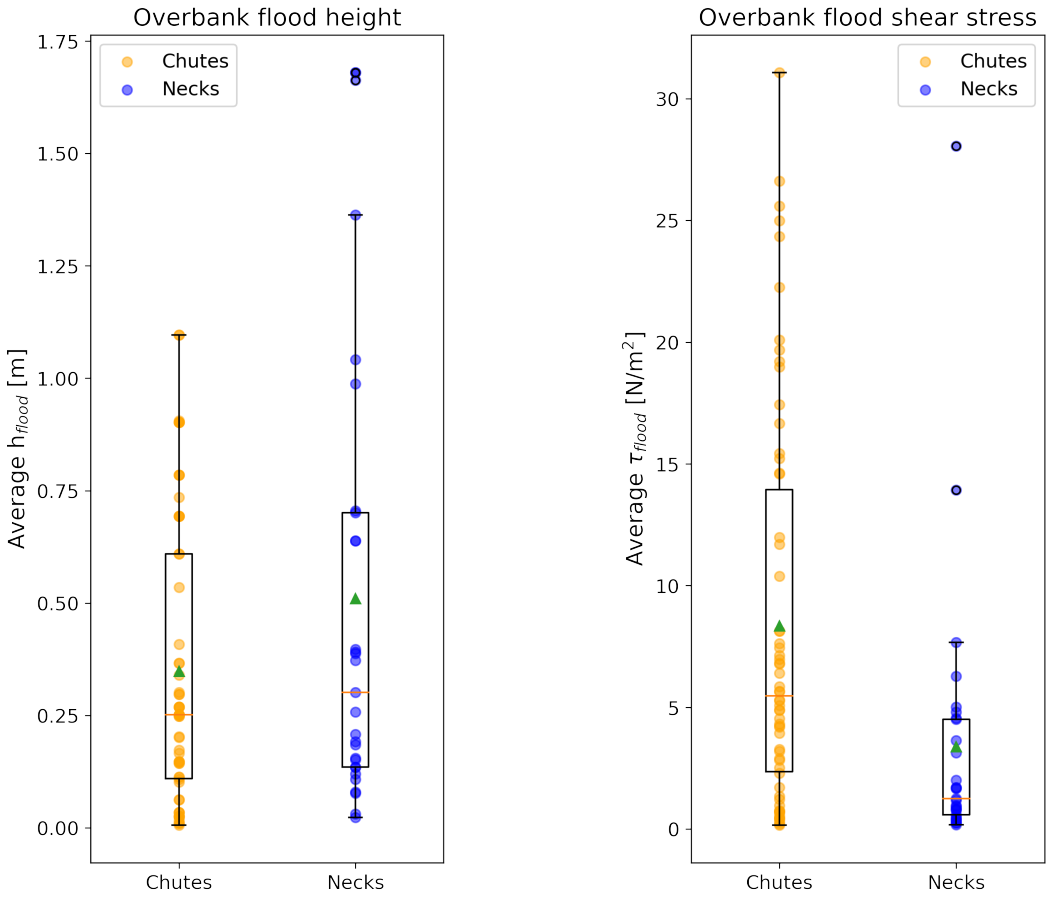

(a) Distributions of the overbank flood heights in metres of all floods within cutoff time frames.

(b) Distributions of the overbank flood shear stresses in N/m^2 of each flood within cutoff time frames, calculated with Equation (2.5).

Figure 3.4: Boxplots for flood data comparing chute and neck cutoffs, with overbank flood height on the left and overbank flood shear stress on the right. The yellow markers show floods linked to chute cutoffs and the blue markers show floods linked to neck cutoffs.

Visible in Figure 3.4a, the overbank flood heights of the chute cutoffs do not seem very different to those of the neck cutoffs. In Figure 3.4b, the differences between the overbank flood shear stresses per cutoff type are much larger. This can be explained by the overbank flood shear stress formula, which includes the local slope of the river based on the overall slope and the length ratio (L_{ox}/L_{cc}). The distributions for S_{local} are shown in Figure 3.5. The outliers in Figure 3.5a in the distribution for the floods associated with the neck cutoffs are cutoff bends in Powder River, which can be seen in Figure 3.5b. While the length ratios of most neck cutoffs showed significantly higher values than those of chute cutoffs, the overall river slopes (S_{river}) of the rivers containing only neck cutoffs were 10 and 100 times smaller than S_{river} of Cheyenne River, which contains the majority of the chute cutoffs.

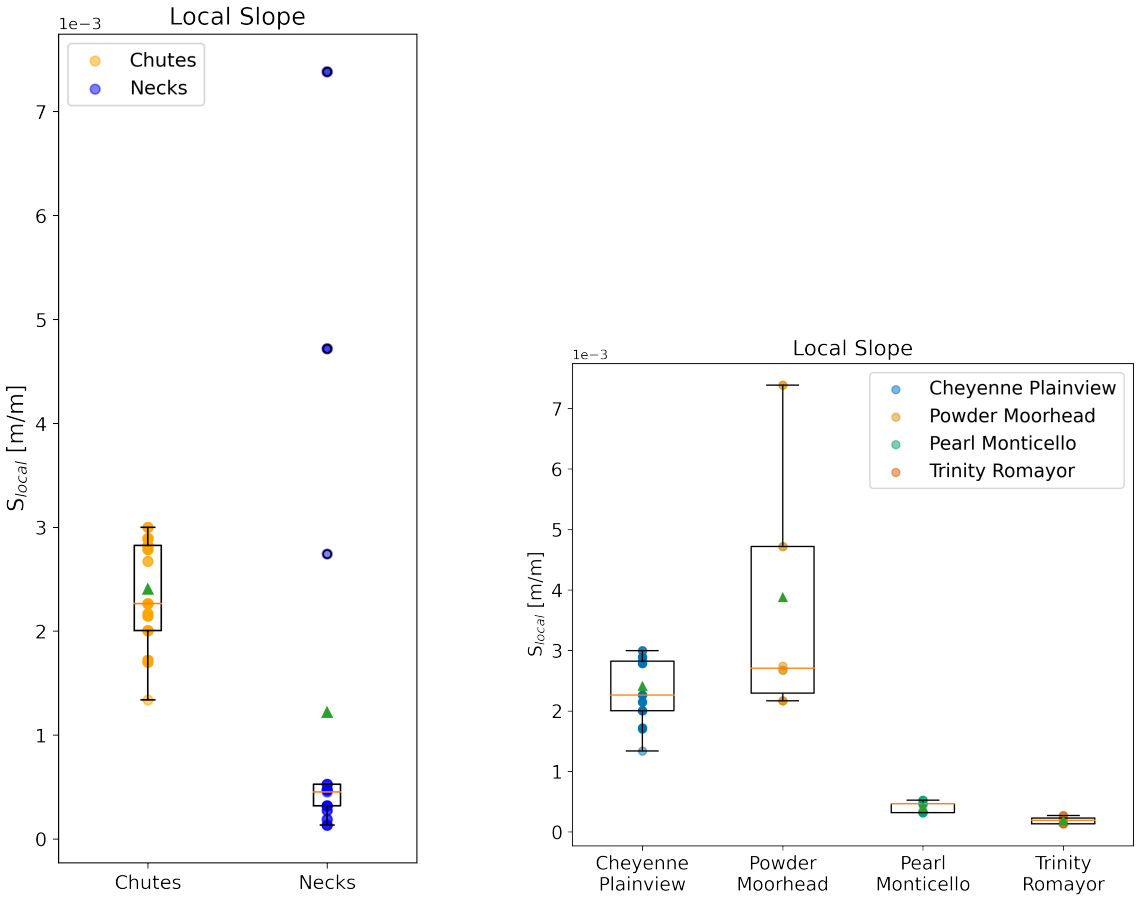

(a) Distributions of the local slopes (S_{local}) for chute cutoffs in yellow on the left and neck cutoffs in blue on the right.

(b) Distributions of the local slopes (S_{local}) for the cutoffs per river.

Figure 3.5: Boxplots for the local slopes (S_{local}) for the neck versus chute cutoffs on the left and for the cutoffs per river on the right, calculated with Equation (2.4). The overall river slope (S_{river}) for Cheyenne River is $1.028 \cdot 10^{-3}$. For Powder River $1.012 \cdot 10^{-3}$. For Pearl River $1.318 \cdot 10^{-4}$ and for Trinity river $3.531 \cdot 10^{-5}$.

3.3. Soil Types and Critical Shear Stresses

With the goal of answering the second sub-question, ”What is the relationship between the soil type and the frequency of chute versus neck cutoffs?”, the collected soil data is displayed in soil texture triangles in Figure 3.6. A soil texture triangle is read in the following way: clay percentage from left to right, silt percentage from the upper right to the lower left, and sand percentage from the bottom towards the upper left. The percentage distribution per cutoff of every river can be found in Appendix E, where the name of the soil, appointed by SoilWeb, is also shown.

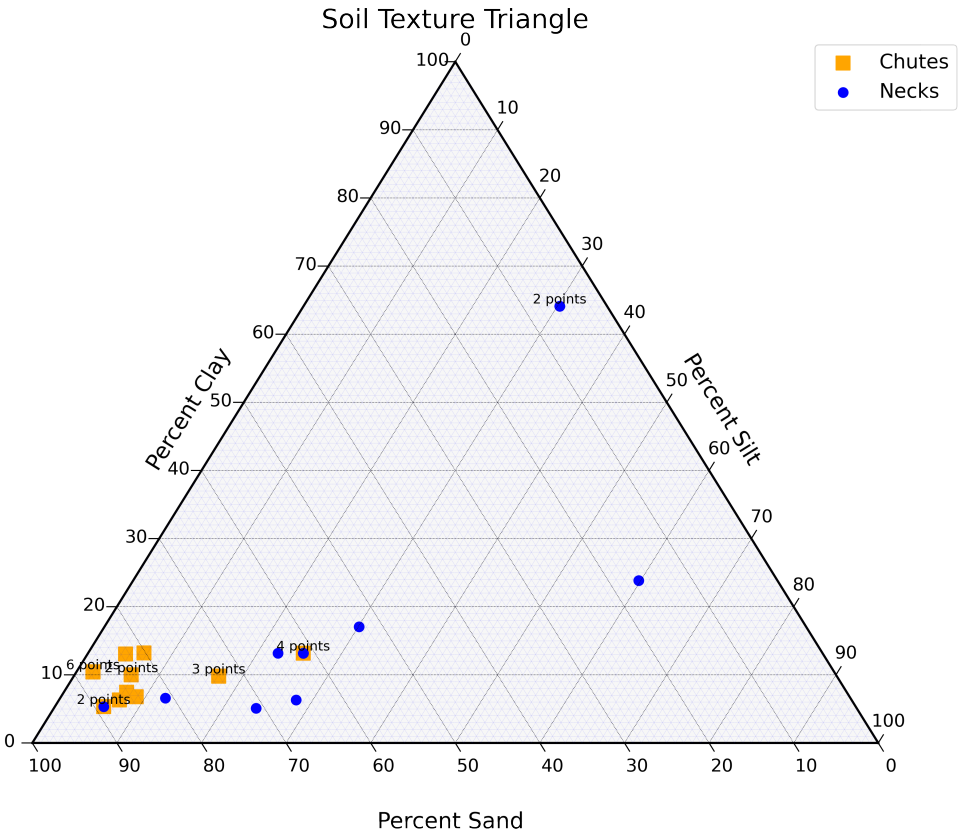

(a) Soil Texture Triangle with soils of the floodplains of chute cutoffs in orange squares and for neck cutoffs in blue circles.

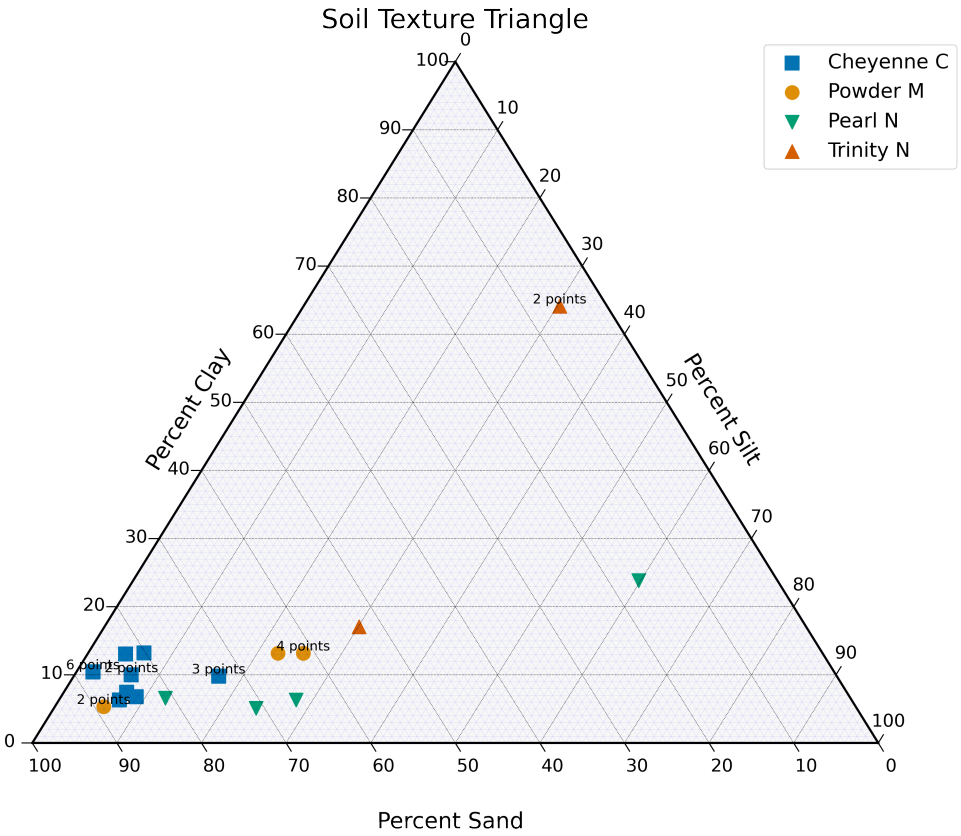

(b) Soil Texture Triangle showing the soils of the floodplains per river. Blue squares for Cheyenne River, with only chute cutoffs. Orange circles for Powder River with a mixed cutoff regime. Green down-pointing triangles for Pearl River, with only neck cutoffs. Red triangles for Trinity River, with only neck cutoffs.

Figure 3.6: Soil texture triangles with annotations to show overlapping points. Above: for chute floodplains versus neck floodplains. Below: for the floodplains of each river.

The soil texture triangle in Figure 3.6a shows that the floodplains of most cutoff bends consist largely of sand, with a very low clay percentage. There are three clear outliers corresponding to floodplains of neck cutoffs. The floodplain of one bend in Pearl River, positioned most right in the triangle, is classified as 'silt loam'. The soil here contains about 60% silt, which is much more than the other floodplains that are located in the range of 0% to 30% silt. The two other outlying cases in the top of the triangle are both in Trinity River and are classified as 'clay'. These floodplain soils have extremely low sand percentages and much higher clay percentages near 65%, which is in large contrast with most other points located below 20% clay. The soil texture of the floodplain of the third cutoff bend of Trinity River is more similar to the soil textures of Cheyenne River, Powder River, and the remaining points of Pearl River, but is below the 60% sand threshold beyond which the other points are clustered.

Based on Figure 3.6a, the chute cutoffs are limited to soil containing a large amount of sand, within the range of 60% to 90%, and small percentages of clay (0-40%), and silt (0-30%). The soil of the floodplains in which the neck cutoffs occurred is more diverse when looking at the soil percentages. The range for sand is 0-90%, while the range for clay is 0-70%, and for silt 0-60%.

The interpolated experimental data from Dunne et al. (2022), visible in Figure 2.8b, was used to relate the clay percentage to the critical shear stress, resulting in the distributions shown in Figure 3.7. The clay percentages for both chute and neck cutoffs are quite low, except for the high extremes for the two neck cutoffs in Trinity River. This results in overall relatively low critical soil shear stresses for the floodplains of these rivers.

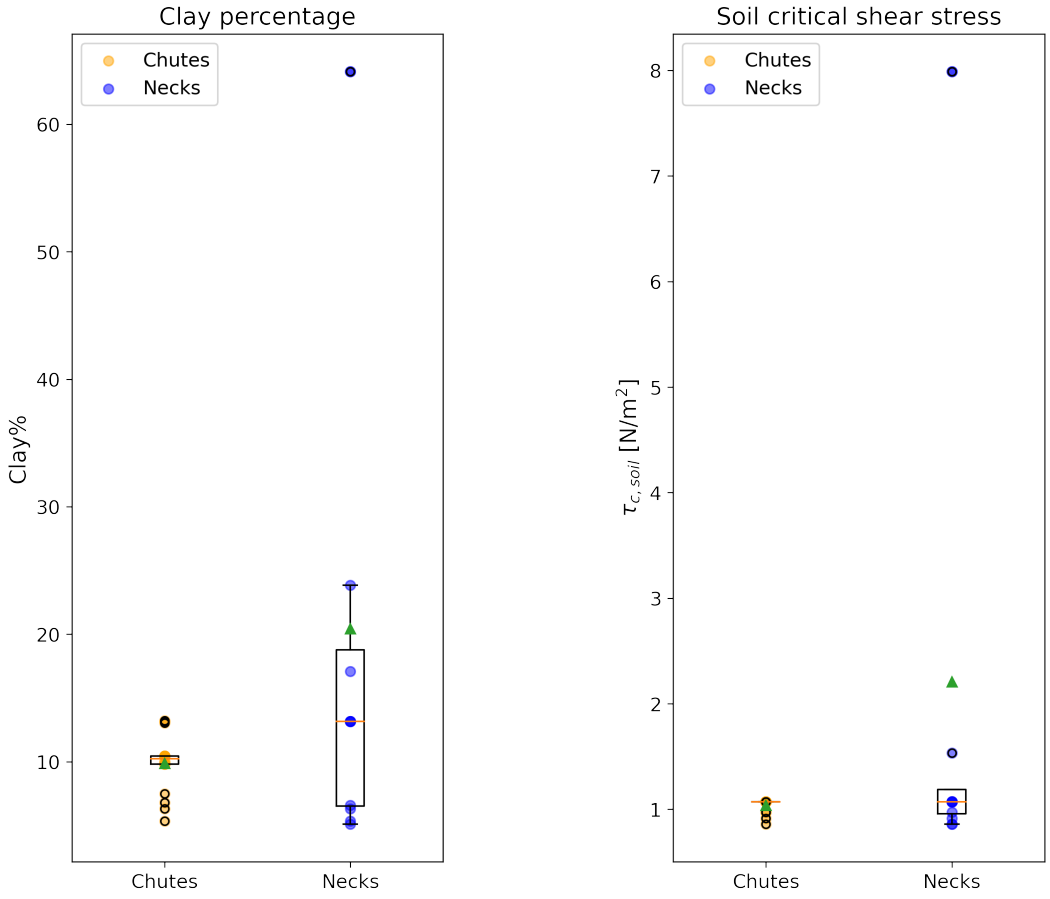

(a) Distributions of the clay percentages of the soil of each cutoff location, as was found through SoilWeb.

(b) Distributions of the critical shear stress of the soil of each cutoff location.

Figure 3.7: Boxplots for soil data with chute cutoffs in yellow on the left and neck cutoffs in blue on the right in both plots.

3.4. Flood Impulse on the Floodplain

To answer the main research question ”What is the relationship between the duration of overbank flooding and the formation of chute versus neck cutoffs?”, the results were combined with the duration of the floods to calculate the flood impulses on the floodplains. The critical shear stress of the soil of the floodplain of each cutoff was subtracted from the overbank flood shear stress acting on that floodplain. This resulted in the residual shear stresses of the floods within the cutoff time frames. There were 62 floods found within chute cutoff time frames and 29 floods within neck cutoff time frames for these four rivers.

Negative values for the residual shear stresses indicate that the threshold for erosion of the floodplain was not exceeded by the average flood shear stress during that particular flood. Those floods are removed from this analysis in which only the effective and eroding floods are of interest. Figure 3.8a contains only those floods with a positive value for the residual shear stress and the corresponding flood durations of each flood are shown in Figure 3.8b. The number of floods within chute cutoff time frames reduced to 50, and the number of floods within neck cutoff time frames reduced to 15.

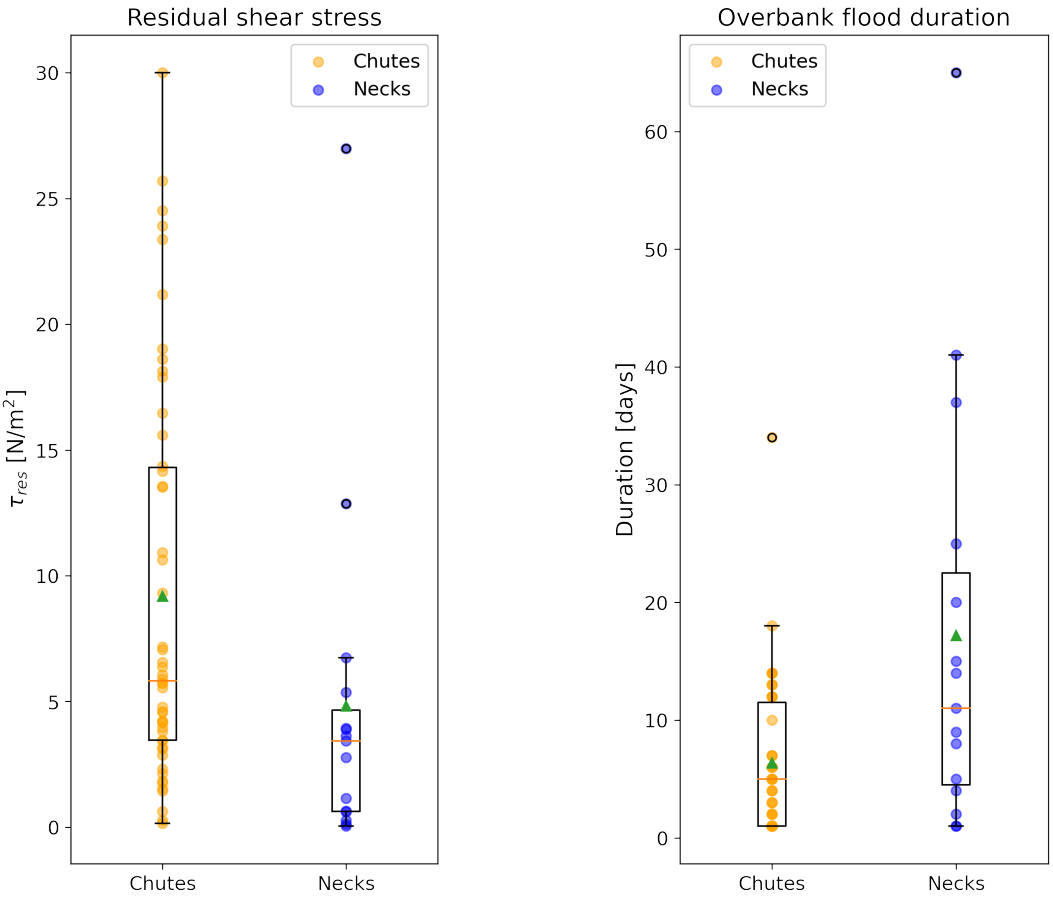

(a) Distributions of the residual shear stresses in N/m^2 when only taking the positive values into account.

(b) Distributions of the durations in days of singular floods, only taking into account those floods for which the residual shear stress is positive.

Figure 3.8: Boxplots for positive residual shear stresses and corresponding flood durations of the floods. Chute cutoffs are in yellow on the left and neck cutoffs are in blue on the right in each plot.

Using Equation (2.6), the flood impulse for each flood with a positive residual shear stress was calculated. The distribution of the values for the flood impulses on an area of 1 m^2 can be seen in Figure 3.9a. On the right, Figure 3.9b shows the distribution of the flood impulses on 1 m^2 for the floods for each river. Mind the y-axes showing flood impulse values times 10^7 N·s.

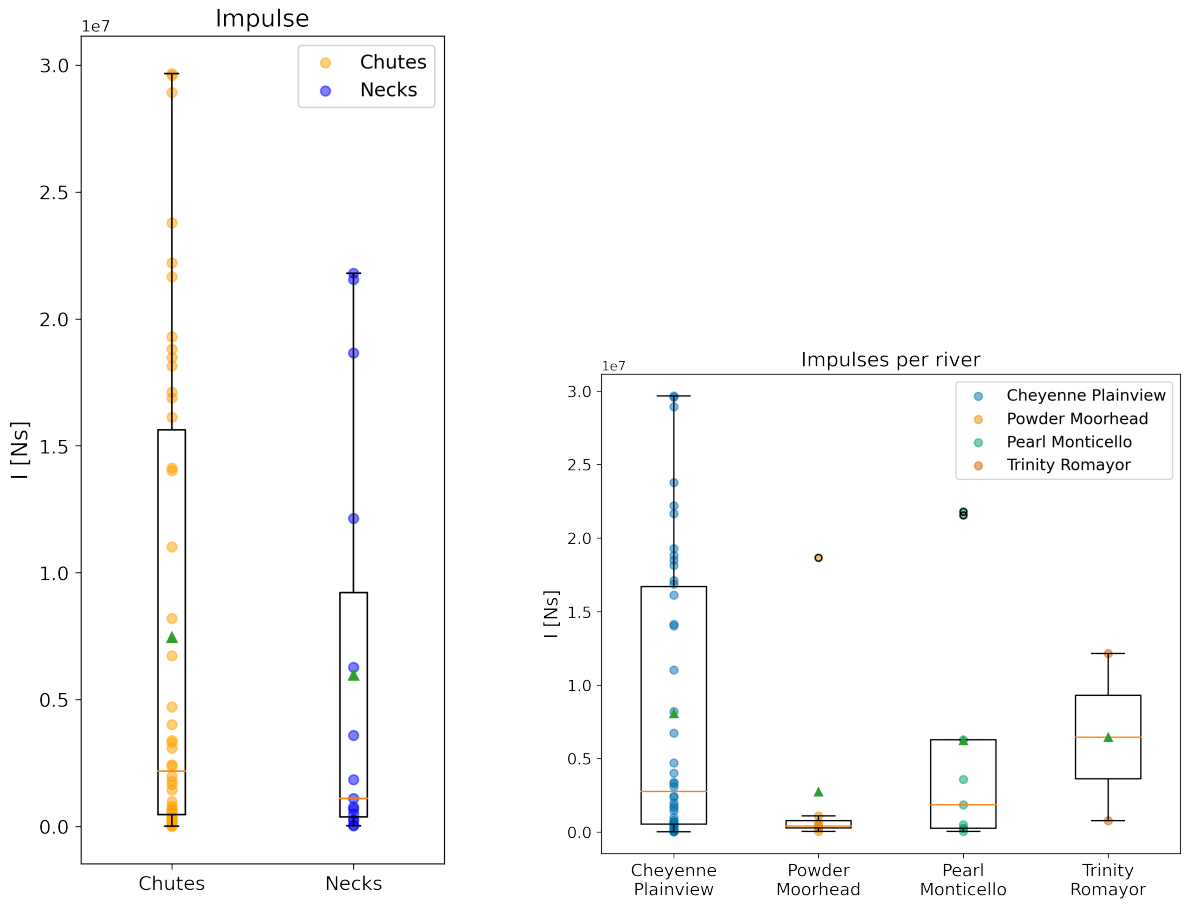

(a) Distributions of the flood impulses in N·s for an area of 1 m^2. On the left, in yellow: flood impulses related to chute cutoffs. On the right, in blue: flood impulses related to neck cutoffs.

(b) Distributions of the flood impulses per river, in N·s for an area of 1 m^2. From left to right: Cheyenne River with station Plainview, Powder River with station Moorhead, Pearl River with station Monticello, and Trinity River with station Romayor.

Figure 3.9: Boxplots for the overbank flood impulses on the floodplain resulting from the multiplication of the positive residual shear stresses with the corresponding flood durations. On the left for chute versus neck cutoffs. On the right per river.

A few of the flood impulses related to chute cutoffs were much higher than those related to neck cutoffs. The mean values are not significantly different, because there is also a large amount of low-impulse floods within the collection for chute cutoffs. These distributions show that the flood impulses connected to chute cutoffs have larger values and are more spread out than those for neck cutoffs. Cheyenne River is the main contributor to those chute cutoff-related high flood impulses, which is clearly visible in Figure 3.9b. Pearl River and Trinity River have less data points to contribute to the spread for the neck cutoffs, but they both have a larger mean flood impulse value than Powder River. The one outlier in Powder River is a flood associated with a neck cutoff.

4

Discussion

After following the steps elaborated in the methodology in Chapter 2, the results shown in Chapter 3 are discussed in this chapter. In addition, this chapter will identify the limitations of the data and discuss the effects of simplifications and assumptions that have been made during this research. The applicability of the methods used during this research on other situations will be examined as well. Structured in the same order in which the results are shown, the classification and measurements of the cutoffs is followed by the overbank flood shear stresses, the soil types and critical shear stresses, and the flood impulses on the floodplain. This chapter will be completed with a section evaluating the overall research process.

4.1. Cutoff Classifications and Measurements

The results following from the assessment of the cutoff properties, displayed in Figure 3.1, show expected ratios and distributions with significant differences for the length ratios. All these cutoff events have decreased the sinuosity of the river, which is the ratio of the channel length to the valley length (Lazarus & Constantine, 2013). This is in agreement with other studies performed on more local scales, such as that of Van Dijk et al. (2014) who studied chute cutoffs in the River Allier in France, and Martha et al. (2015) who focused on neck cutoffs in the Sindh River in India. They found that the development of both chute and neck cutoffs results in a decreasing sinuosity of the river. The width ratio in Figure 3.2d shows no significant differences between chute and neck cutoffs. To really understand the relationship between the widths of the original oxbow channels and the new cutoff channels, local measurements just before, during, and right after the cutoff events should be done. During data collection, the widths were estimated based on satellite imagery of various years, during different weather events. This hindered very detailed measurements and comparisons. For the other cutoff bend properties, such as the radius of the oxbow lake and the land width for chute cutoffs, no clear relationships were found. There was also no clear consistency or relationship detected for the properties of the oxbow lakes and the cutoff bends over the reach of each river individually. The level of detail for the measurements of the channels after the cutoff events was limited by the amount and timing of satellite images. For some bends a satellite image was taken right after the cutoff event, while for other bends detailed images were only available a few years after the event.

When part of the channel is cut off, the local slope change can affect the channel width and/or channel depth for a period of time which could be different per river and river bend. As was found during experiments where a neck cutoff was created on scale in a flume, the cutoff channel width increased due to an increase in the local slope which resulted in a higher flow speed of the water (Z. Li et al., 2019). Neck cutoffs may have multiple (combined) causes leading up to the cutoff event. These specific causes can be very complicated and need detailed analyses and are thus not taken into account in this

research. This means that some of the selected neck cutoffs might not have been caused by overbank flooding, but rather by bank erosion and other river bank failure mechanisms. However, for many of the selected neck cutoffs in this research, the satellite images showed floods around the moment of the cutoff event. The chute cutoffs selected for analysis could also have been caused or assisted by various previous floods, slowly eroding part of the floodplain. For that reason, it is not a problem when a cutoff gets assigned a time frame containing multiple floods.

The use of open source satellite imagery provides opportunities such as remote access and the ability to check multiple years of various rivers. Google Earth Pro also comes with some limits, such as gaps in time, between 1985 and 1996, or 1997 until 2004 for some locations, or unknown image acquisition dates of the image provider (Google, 2024). To cover the gaps in time and to assign smaller time ranges for the occurrences of the cutoffs, Copernicus Landsat on a higher eye elevation was often used, which provided images with acquisition dates on the 31st of December of that particular year. For that reason, the complete previous year was used as the time frame assigned to a cutoff occurrence. The interpretation of these images with less pixels at the cutoff locations took effort and came with some uncertainties, which is why the time frames could not always be limited to one singular year. With a collection of satellite images with smaller time steps, more detailed time frames could be defined for the cutoff events. This would provide the opportunity for more certain assignments of specific floods to specific cutoffs.

4.2. Overbank Flood Shear Stresses

Various steps were taken to calculate the overbank flood heights and overbank flood shear stresses of the floods within cutoff time frames. The daily discharges and field measurements of the USGS river gauge stations were converted and bankfull limits were calculated for the rivers at those locations. For the cutoffs that were included in this analysis, the results in Figure 3.4 imply that the chute cutoffs have been created by larger overbank flood shear stresses than the neck cutoffs. The outliers for neck cutoffs in the distribution of the local slopes, in Figure 3.5a, are neck cutoff bends in Powder River. This river reach with a mixed cutoff regime has a relatively steep slope. The values of the length ratios for the neck cutoffs are higher than for the chute cutoffs. The combination of the steep slope and higher length ratios results in high S_{local} values for these neck cutoffs in Powder River, in comparison to the other river bends. This is clearly visible in Figure 3.5b showing the S_{local} distribution per river.

S_{local} and S_{river} seem to have great influence in the calculation of overbank flood shear stresses. This indicates that local circumstances should be taken into careful consideration when using Equation (2.4) and Equation (2.5) to calculate the overbank flood shear stresses. Overall, S_{local} was larger for chute cutoffs than neck cutoffs. The differences in the values for S_{local} were strongly affected by the overall slope of the river (S_{river}). Cheyenne River, with a chute cutoff regime, has the steepest slope and Powder River, with the mixed cutoff regime, is just a little less steep. The two rivers with a neck cutoff regime have much gentler slopes. Similar trends have been found by Constantine et al. (2010) and Viero et al. (2018), who found that chute cutoffs are more prevailing along rivers with a steeper slope, when other factors such as vegetation are consistent.

Some cutoffs were excluded because no floods were found during their assigned time frames. This was the case for neck cutoffs in Powder River as well as chute cutoffs in Cheyenne River. One of the possible explanations for this is that the bankfull discharges and connected bankfull river depths could have been overestimated, which is connected to the observed river widths at straight channel parts near the locations of the USGS stations. The bankfull channel width is observed and measured at one location, while the cutoffs locations are either upstream or downstream of that measurement location, with possibly another river width and corresponding bankfull discharge in relation to local daily discharges. These differences were not taken into account since there are no detailed discharge or river depth measurements at every cutoff location.

An other explanation for the exclusion of some of the neck cutoffs could be that, in reality, there was no overbank flood event in the year of the cutoff. Instead, the neck cutoff occurred as the

result of continuous bank erosion of the outer banks of the two bends that met each other. Various failure mechanisms could have contributed to these neck cutoffs in addition to floods, as well as the effects of previous cutoffs at other locations. The latter is something that was found by Schwenk and Foufoula-Georgiou (2016) in the Ucayali River in Peru, and researched by Ielpi et al. (2021) for the Humbolt River, Nevada, in the USA. The specific causes of the cutoff events were not analysed during this research due to the scope and chosen level of detail.

Additionally, for Cheyenne River in particular, the choice of the use of the Plainview station as the reference station for the river, already excluded some cutoff time frames which corresponded to the data gap of the station. For these cutoffs, the data from Wasta station could have been used. The magnitude of the discharge recorded at this station displayed such significant differences that it was decided not to include this station and therefore exclude these cutoffs in further steps.

Overall limitations of the USGS gauge data probably also contributed to these gaps and uncertainties. The daily data presented measurement gaps during natural obstructions such as ice, since it is an automatic system at a fixed location. Field measurements are performed by USGS employees on various intervals, some more consistent than others, indicating a possible sampling bias. The data shows some years with measurements every two months, while other years contain multiple measurements per month. This resulted in varying gaps in field data, which could have affected the conversion of discharge to river depth. Despite these limitations, the USGS National Water Information System was a very useful source that provided datasets that span many decades and often include very consistent daily discharge measurements.

During data processing, some simplifications were necessary regarding the area of interest. The overbank flow was assumed to be uniform over time, which was implemented by averaging the overbank water height for each flood period. The high peak or peaks of floods during the flood periods are thus not taken into consideration in this research, while these could have resulted in higher overbank flood shear stresses for shorter durations. The amount of floods that exceeded the critical shear stress threshold would probably increase when taking the peaks of individual floods into account. These threshold-exceeding floods would have relatively short durations, which should also be considered in the analysis. This was too detailed to include in this research, but should be considered when applying this method on other situations.

Although the selected cutoffs were not directly created by humans, human influence can not be completely excluded. The rivers analysed in this research have been affected by humans activities such as farming, construction of infrastructure, river channel modifications, dam placement, and the extraction of water and sediment. This altered the discharge and sediment transport in these rivers compared to circumstances many years ago. The effects of these changes on the rivers during a relatively short time frame of 1985 until 2022 are difficult to quantify and they can not be taken into account in this specific analysis.

The calculation of overbank flood shear stresses included the magnitude of the overbank floods and the local slope of the overbank floods. This method makes comparisons between different rivers and riverbends possible because of the inclusion of local slopes. This not only requires river gauge data, but also additional information such as local elevation level and cutoff properties gathered by field studies or on satellite imagery.

4.3. Soil Types and Critical Shear Stresses

The soil texture triangles in Figure 3.6 show that the chute cutoffs are clustered together within the upper ranges of sand percentages and have low clay percentages. This indicates that these floodplains have low cohesion due to the small amount of clay, which acts as an adhesive within the soil (Ijafiya & Yonnana, 2018). Similar soil textures are found near locations where multiple chute cutoffs have developed, such as in the Obra River in Poland (Slowik, 2016). Additionally, many gravel-bed meandering rivers, such as Ain River in France and River Coquet in the United Kingdom, contain chute cutoffs that have been researched (Fuller et al., 2003; Szewczyk et al., 2022). Chute cutoffs have thus

been reported in sand-dominated rivers as well as rivers with gravel beds and floodplains.

The neck cutoffs in this research have cut through a wider range of soil types and sand and clay percentages, which suggests that neck cutoffs are not as limited by the soil of the floodplain and can occur in more geological environments than the chute cutoffs when solely taking the soil types into account. The critical shear stress distributions seem quite similar for both types of cutoffs, but the neck cutoffs show a wider range in values in this distribution as well. The chute cutoffs are limited to critical shear stresses between 0.8 and 1.1 N/m^2 and that implies that the chute cutoffs might only form in floodplains with a limited soil resistance.

Two outliers are associated with floodplains of neck cutoffs in Trinity River. Trinity River is located in (Deep) East Texas in a humid subtropical climate and the investigated river reach, in the 'Bottomlands' and 'Coastal Prairie', has the gentlest slope of the four rivers (Land et al., 1998). The magnitude and frequency of the water flow in this river are limited by the upstream reservoirs, such as Lake Livingston, which was constructed in 1971 and mirrors river behaviour in its operation (Trinity River Authority of Texas, n.d.). The Livingston Dam also affected sediment transport, which could have affected the composition of the top layer of the floodplain. After placement of the dam, the channel sediment grain size coarsened and the channel slope decreased, in addition to an increase of erosion of the channel (Musselman, 2006). During floodplain soil data collection, the layer beneath the top layer was taken into account, but the effect of this reservoir and upstream dams on the deeper soil layers is unknown, and could be an explanation for these outliers.

The results for the soil texture triangles and $\tau_{c,soil}$ are limited by the number of rivers that have been analysed in this research. When other rivers, located in other areas and climates are added to the data set, one might find a more definite relationship between the soil texture and the cutoff type. This would also require an overview of soil sample collection dates, to ensure that that particular soil was eroded during the cutoff creation, especially for rivers that transport large amounts of sediment. For some cutoffs in this research, the exact soil type of the former floodplain was not entirely clear, particularly in those situations where the soil samples were taken at a time after the cutoff channel was created. In those cases, estimations were done based on the surrounding soil types along the channel. Soil measurements on SoilWeb are often limited to a maximum depth range of 2 metres. Cutoff channels can be deeper than that, depending on the river and the flow regime. In this case, it is assumed that a cutoff channel is visible on satellite imagery when it erodes less than these 2 metres.

The floodplain is assumed to consist of sand, clay, and silt. Many of the floodplains of chute cutoffs have soils with lower clay and silt percentages than those of the neck cutoffs. Since there are only meandering rivers considered in this research, the presence of cohesive material on the floodplain was to be expected (J. Li et al., 2020). Studies, including that of Van Dijk et al. (2013), concluded that fine cohesive sedimentation on the floodplain by overbank floods is necessary for meandering. They also took other variables of the floodplain into account, which have been left out of this research. Organic materials in the floodplains are ignored, since they are very small, and vegetation is excluded, due to lack of data. Grass, trees, and their roots can affect the soil structure and the resistance of the floodplain to overbank flood shear stress (Z. Li et al., 2022; Van Dijk et al., 2014). Before, during, and after a cutoff event, vegetation is subject to various forces and changes. Overall, vegetation would increase the value of the resisting shear stress of the total floodplain (Thornton et al., 2000). The presence of vegetation and its spacing could also contribute to the process of 'healing' of a cutoff by trapping sediment and assisting in the sediment deposition on the eroded area of the floodplain (Constantine et al., 2010).

The results for the critical shear stresses of the floodplains are based on the relationship between clay percentages and τ_c after interpolation of recently experimentally gathered data by Dunne et al. (2022). The effects on the shear stress of internal interaction between the different proportions of sand, clay, and other materials was ignored during this research. To generalise the cutoffs for multiple rivers, simplifications were needed and the knowledge available on this topic is limited (Yin et al., 2021).

The soil properties of each floodplain were compared through visualisation in the soil texture triangles and the boxplots. These comparisons would benefit from an increase in the data amount, which is possible with the datasets available on SoilWeb. For rivers in other countries, this method of soil

data collection and calculations of critical shear stresses might not be applicable, depending on the availability of soil data. Local field measurements could provide the soil compositions of the floodplains, but that would take much more time and expenses than using already collected data. This method is suitable for rivers in the USA and Europe, where soil databases are freely available (European Union, 2024).

4.4. Flood Impulse on the Floodplain

The concept of flood impulse was used to interpret the combined effect of the residual shear stresses and the overbank flood durations of the floods. On the datasets shown in Figure 3.9a, comparing the flood impulses between chute and neck cutoffs, a Student's t-test was applied. This returned a Student's t-value of 0.59 and a Student's p-value of 0.56 based on 50 floods for chute cutoffs and 15 floods for neck cutoffs. This indicates that these differences in flood impulses are, statistically seen, not significant. Since these flood impulse results are based on the combination of earlier results, some of which show great differences between chute and neck cutoffs and are considered statistically significant, conclusions will primarily be based on those earlier results. The values from the Student's t-tests performed on the other datasets of chute and neck cutoffs are shown below in Table 4.1. This table also includes the statistical values for the data of residual shear stresses and flood durations before excluding the negative values.

In addition to the Student's t-test, the Kolmorgov-Smirnov (K-S) test was applied to compare the distributions of the chute cutoffs dataset and the neck cutoffs dataset. For the flood impulses, this resulted in a K-S statistic (D-value) of 0.23 and a K-S p-value of $9.05 \cdot 10^{-3}$. While the Student's t-test results insinuated that the mean of the flood impulses of chutes is not so different from the mean of flood impulses of necks, the K-S test indicates that the datasets have distinctly different shapes of their distributions. The K-S test checks the similarities between the datasets on median, variability, and the shape of the distribution. At first glance, it is visible in Figure 3.9a that the tail of the chutes distribution is longer and the range of flood impulse values for chute cutoffs is greater than for neck cutoffs. This suggests that some chute cutoffs have been created by larger flood impulses than the majority of the neck cutoffs.

Table 4.1: Student's t-test and Kolmogorov-Smirnov test values from the chutes versus necks datasets presented in the results, in order of appearance. The number of data points per chutes or necks dataset are shown in the two columns on the right.

Chutes vs Necks	Student's t-value	Student's p-value	K-S D-value	K-S p-value	Chutes n	Necks n
Length ratio (L_{ox}/L_{cc})	-4.10	$1.44 \cdot 10^{-3}$	0.80	$1.06 \cdot 10^{-12}$	18	12
Width ratio (W_{ox}/W_{cc})	-0.58	$5.67 \cdot 10^{-1}$	0.19	$4.90 \cdot 10^{-1}$	18	12
Overbank flood height (h_{flood})	-1.55	$1.29 \cdot 10^{-1}$	0.30	$1.32 \cdot 10^{-5}$	62	29
Overbank flood shear stress (τ_{flood})	3.40	$1.08 \cdot 10^{-3}$	0.28	$9.47 \cdot 10^{-5}$	62	29
Local slope (S_{local})	3.04	$4.98 \cdot 10^{-3}$	0.58	$4.26 \cdot 10^{-20}$	62	29
Clay percentage	-1.73	$1.12 \cdot 10^{-1}$	0.64	$1.12 \cdot 10^{-7}$	18	12
Critical soil shear stress ($\tau_{c,soil}$)	-1.49	$1.63 \cdot 10^{-1}$	0.67	$1.76 \cdot 10^{-8}$	18	12
Residual shear stress (τ_{res}) (all values)	3.82	$3.01 \cdot 10^{-4}$	0.37	$2.73 \cdot 10^{-8}$	62	29
Flood duration (all values)	-2.61	$1.35 \cdot 10^{-2}$	0.45	$4.45 \cdot 10^{-12}$	62	29
Residual shear stress (τ_{res}) (only positive values)	2.05	$5.04 \cdot 10^{-2}$	0.25	$3.45 \cdot 10^{-3}$	50	15
Flood duration (only positive values)	-2.28	$3.79 \cdot 10^{-2}$	0.53	$9.10 \cdot 10^{-14}$	50	15
Flood impulses (I)	0.56	$5.60 \cdot 10^{-1}$	0.23	$9.05 \cdot 10^{-3}$	50	15

4.5. Evaluation of the Research Process

Overall, the use of multiple data types and sources seems to have paid off in the collection of data and comparisons. Although the time frame of 1985-2022 might seem small, the USA contains many rivers with cutoffs that have occurred during that time. During the data collection process, choices had to be made and only a few rivers were selected, limiting the total compilation of data and results. With research time and data gaps as the two major limiting factors during this research, many steps have still been made. These methods show to be useful to find and formulate general relationships between overbank flooding, soil properties, and chute versus neck cutoffs on a larger scale. Google Earth Pro, or another database containing detailed satellite imagery, can be used to find and measure cutoffs in other rivers in the USA or most other countries. Local limitations will arise and some cutoff bends might be more difficult to interpret than others, making assigning cutoff types challenging. During this process, the definitions for and differences between chute and neck cutoffs need to be precisely defined. When another single-thread meandering river of choice has river gauge data available, the conversions applied during this research can be applied to that river as well. Choices for definitions and conversion equations should be similar for each river to compare the datasets, which is also needed for the processing of soil data. These methods and the combination of data will contribute to the understanding of cutoffs in meandering rivers and the improvement of predicting and modelling river migration.

5

Conclusion and Recommendations

This final chapter contains the conclusion of this research, followed by recommendations for future researches. The main research question will be answered after the two sub-questions. For the recommendations, advises for a similar study will be listed, after which suggestions for further research are given.

5.1. Conclusion

This research is performed with data collected for four rivers in four different states in the USA. These rivers are Cheyenne River in South Dakota with a chute cutoff regime, Powder River in Wyoming and Montana with a mixed cutoff regime, Pearl River in Mississippi and Trinity River in Texas, both with a neck cutoff regime. The results presented with the gathered and processed data for these rivers led to the following conclusions.

First, the research sub-question, ”What is the relationship between the overbank flood shear stress and the frequency of chute versus neck cutoffs?” was used to find out if the overbank flood shear stresses in a river can be related to the cutoff regime of that river. For these four rivers, it was found that, on average, overbank floods associated with chute cutoffs exerted larger overbank flood shear stresses than the overbank floods linked to neck cutoffs. The overbank flood heights showed similar average values for the floods for chute cutoffs and the floods for neck cutoffs, which indicated that the effect of the local slopes was relatively great in the calculation of the overbank flood shear stresses. A river that is subject to large overbank flood shear stresses is more prone to have chute cutoffs than a river that is subject to smaller overbank flood shear stresses. Additionally, a river with a steeper slope is more likely to have a chute cutoff regime than a river with a gentler slope.

The overbank flood shear stress is applied onto the floodplain within a river bend, which led to the research sub-question, ”What is the relationship between the soil type and the frequency of chute versus neck cutoffs?”. The collected soil data showed that chute cutoffs occurred in soil textures with high sand percentages and low clay percentages, implying a need for soil with low cohesion for erosion of a chute cutoff channel. The soils in which neck cutoffs were formed were more diverse and not limited to a high sand percentage, indicating that neck cutoffs can occur on floodplains with higher soil resistance. When solely looking at the soil texture of the floodplains, a river with floodplains containing soil with a relatively low sand percentage seems to be more prone to a neck cutoff regime than a chute cutoff regime. Those rivers that have floodplains with very high sand percentages are more likely to have a mixed or chute cutoff regime.

Finally, the main research question, ”What is the relationship between the duration of overbank flooding and the formation of chute versus neck cutoffs?” required an evaluation of the floods with a positive

residual shear stress. By combining these with the durations of those floods, the flood impulses were calculated. Floods for chute cutoffs exerted overall larger residual shear stresses for shorter durations, compared to the floods for neck cutoffs. The flood impulses associated with chute cutoffs were greater overall than those related to neck cutoffs, but there is no significant difference for the mean values of these impulse data sets. The data sets have significantly different distributions, with a larger tail for the flood impulses for chute cutoffs. This suggests the possibility that when the flood impulses in a river with a neck cutoff regime increase, the cutoff regime could converge to a mixed, or even a chute cutoff regime.

The findings presented in this report canassist in formulating general relationships between river properties plus overbank flooding and the frequency of chute versus neck cutoffs. The general conclusion of this research is that the chute cutoffs are associated with higher overbank flood shear stresses and occur in soils limited by high sand percentages, in comparison with the neck cutoffs. The overbank floods creating chute cutoffs exerted larger residual shear stresses for shorter durations, as opposed to smaller residual shear stresses for longer durations of floods associated with neck cutoffs.

5.2. Recommendations

This research used a combination of different data sources and methods of collecting measurements. It would be interesting to see if different methods of measuring cutoff properties and defining cutoff time frames would result in significantly different outcomes. During data processing, certain choices were made regarding the methods and conversions. Especially the definitions and conversions for bankfull river discharge and bankfull river depth contained major uncertainties and could be sensitive to the use of different values and methods. With more detailed data and more time available, these parameters could be improved, which is recommended for a more certain outcome.

This research focused on the general relationship between overbank flooding and river bend cutoffs, but there are a lot of things unknown on different levels of detail. More research is needed to improve the understanding of the creation of neck and chute cutoffs, which would assist in the understanding of the broader relationships within rivers concerning the event of a cutoff. In addition, other factors such as the influences of riverbend locations and channel belt elevation on the frequency of chute versus neck cutoffs call for more analysis.

The shape of the overbank flood is simplified in this research, meaning that the average overbank flood height is taken as the effective overbank flood height on the floodplain. If the shape of the overbank flood could be directly related to the frequency of chute versus neck cutoffs, it would increase the detail with which meandering rivers could be modelled. The impacts of high peaks with short durations could then be analysed and included in a model.

In addition to the magnitude and duration of overbank flooding, the frequency of the floods is also an interesting aspect with relation to the cutoff regime of a river. This should especially be looked at in those cases where erosion of the floodplain happened gradually over time caused by multiple floods. Having more detailed hydrographs as input would result in a model that could show the effects of small changes as well as larger ones.

For further research, the impact of vegetation on the resistance of the floodplain should be included, since it can largely increase the resistance of the floodplain. A location-dependent factor could be added to the calculation of the residual shear stress. Depending on the scope and level of detail, any other objects that contribute to the resistance of the floodplain could be quantified with a factor as well. This would represent a more local reflection of reality, but the level of detail in the input and the desired use of the output needs to remain balanced.

Something that should definitely be looked at for future research are the possibilities for increasing the efficiency of data collection and data processing. In this research, cutoff properties were collected and measured through manually drawing paths on Google Earth Pro. Automation of data collection would significantly improve the efficiency. The increasing capabilities of Artificial Intelligence and Machine

Learning could be put to use for data collection, when the necessary tools are available (Chang et al., 2023; Ho & Goethals, 2022). That would expand the amount of data that can be collected and processed, building a stronger case. This can also enlarge the soil data set, which would then support the formulation of a relationship between the soil texture of the floodplain and the type of cutoff, when taking into account a larger number of rivers and regions.

Another method to increase the size of the data set is the inclusion of historic cutoffs, within the time frame of river gauge measurements. This can improve the certainty for relationships on a local scale, but also on a more global scale over a longer time span. One of the methods that is currently used by some researchers to detect oxbow lakes and assign the cutoff type is the use of LiDAR imagery (Q. W. Lewis et al., 2020; Mason & Mohrig, 2018). A combination of light pulses and other satellite data generates detailed three dimensional maps with information about the earth's surface (NOAA, 2023). LiDAR can also be used to estimate or calculate the bankfull depth, according to Lindroth et al. (2020). Combining the use of LiDAR and teaching a Machine Learning model to find and measure cutoffs would be a massive contribution to the research on river bend cutoffs. This would then help any researchers in the future with data collection and assist in predicting the migration of meandering rivers.

References

Abad, J. D., Mendoza, A., Arceo, K., Torres, Z., Valverde, H., Medina, G., Frias, C., & Berezowsky, M. (2022). Planform dynamics and cut-off processes in the Lower Ucayali River, Peruvian Amazon. *Water 2022, Vol. 14, Page 3059*, *14*(19), 3059. https://doi.org/10.3390/W14193059

AIRBUS. (2024). Satellite Imagery | Earth Observation | Airbus Space. https://www.airbus.com/en/space/earth-observation/satellite-imagery

Ashmore, P., & Sauks, E. (2006). Prediction of discharge from water surface width in a braided river with implications for at-a-station hydraulic geometry. *Water Resources Research*, *42*(3). https://doi.org/10.1029/2005WR003993

Basnayaka, V., Samarasinghe, J. T., Gunathilake, M. B., Muttil, N., Hettiarachchi, D. C., Abeynayaka, A., & Rathnayake, U. (2022). Analysis of meandering river morphodynamics using satellite remote sensing data — An application in the Lower Deduru Oya (River), Sri Lanka. *Land 2022, Vol. 11, Page 1091*, *11*(7), 1091. https://doi.org/10.3390/LAND11071091

Bjerklie, D. M. (2007). Estimating the bankfull velocity and discharge for rivers using remotely sensed river morphology information. *Journal of Hydrology*, *341*(3-4), 144–155. https://doi.org/10.1016/J.JHYDROL.2007.04.011

Chang, F.-J. ; Chang, L.-C. ; Chen, J., Chang, F.-J., Chang, L.-C., & Chen, J.-F. (2023). Artificial intelligence techniques in hydrology and water resources management. *Water 2023, Vol. 15, Page 1846*, *15*(10), 1846. https://doi.org/10.3390/W15101846

Constantine, J. A., & Dunne, T. (2008). Meander cutoff and the controls on the production of oxbow lakes. *Geology*, *36*(1), 23–26. https://doi.org/10.1130/G24130A.1

Constantine, J. A., McLean, S. R., & Dunne, T. (2010). A mechanism of chute cutoff along large meandering rivers with uniform floodplain topography. *Bulletin of the Geological Society of America*, *122*(5-6), 855–869. https://doi.org/10.1130/B26560.1

Copernicus Service information. (n.d.). Complementary data | Copernicus Data Space Ecosystem. https://dataspace.copernicus.eu/complementary-data

David, S. R., Edmonds, D. A., & Letsinger, S. L. (2017). Controls on the occurrence and prevalence of floodplain channels in meandering rivers. *Earth Surface Processes and Landforms*, *42*(3), 460–472. https://doi.org/10.1002/ESP.4002

Dunne, K. B., Arratia, P. E., & Jerolmack, D. J. (2022). A new method for in situ measurement of the erosion threshold of river channels. *Water Resources Research*, *58*(8), e2022WR032407. https://doi.org/10.1029/2022WR032407

Durkin, P. R., Hubbard, S. M., Holbrook, J., & Boyd, R. (2018). Evolution of fluvial meander-belt deposits and implications for the completeness of the stratigraphic record. *Bulletin of the Geological Society of America*, *130*(5), 721–739. https://doi.org/10.1130/B31699.1

Eekhout, J. P., & Hoitink, A. J. (2015). Chute cutoff as a morphological response to stream reconstruction: The possible role of backwater. *Water Resources Research*, *51*(5), 3339–3352. https://doi.org/10.1002/2014WR016539

European Union. (2024, June). European Soil Database & soil properties. https://esdac.jrc.ec.europa.eu/resource-type/european-soil-database-soil-properties

Evers, J., & MacPhee, M. (2023, October). Floodplain. https://education.nationalgeographic.org/resource/flood-plain/

Fisk, H. N. (1947, July). *Fine-grained alluvial deposits and their effects on Mississippi River activity* (tech. rep.). Louisiana State University. Baton Rouge, Lousiana. https://books.google.nl/books?hl=nl&lr=&id=prYKAQAAIAAJ&oi=fnd&pg=PA2&dq=fisk+1947&ots=JN5RBCrmP7&sig=4gfkbMnDHvMBiNex-qcUvN-ARpY&redir_esc=y#v=onepage&q&f=false

Forti, L., Mariani, G. S., Brandolini, F., Pezzotta, A., & Zerboni, A. (2022). Declassified intelligence satellite imagery as a tool to reconstruct past landforms and surface processes: The submerged

riverscape of the Tigris River below the Mosul Dam Lake, Iraq. *Earth Surface Processes and Landforms*, *47*(10), 2483–2499. https://doi.org/10.1002/ESP.5389

Frascati, A., & Lanzoni, S. (2013). A mathematical model for meandering rivers with varying width. *Journal of Geophysical Research: Earth Surface*, *118*(3), 1641–1657. https://doi.org/10.1002/JGRF.20084

Frost, R. L., & Kristof, J. (2004). Raman and infrared spectroscopic studies of kaolinite surfaces modified by intercalation. *Interface Science and Technology*, *1*(100), 184–215. https://doi.org/10.1016/S1573-4285(04)80041-3

Fuller, I. C., Large, A. R., & Milan, D. J. (2003). Quantifying channel development and sediment transfer following chute cutoff in a wandering gravel-bed river. *Geomorphology*, *54*(3-4), 307–323. https://doi.org/10.1016/S0169-555X(02)00374-4

Gay, G., Gay, H., Gay, W., Martinson, H., Meade, R., & Moody, J. (1998). Evolution of cutoffs across meander necks in Powder River, Montana, USA. *Earth Surface Processes and Landforms*, *23*(7), 651–662.

Ghinassi, M. (2011). Chute channels in the Holocene high-sinuosity river deposits of the Firenze plain, Tuscany, Italy. *Sedimentology*, *58*(3), 618–642. https://doi.org/10.1111/J.1365-3091.2010.01176.X

Ghosh, S., Mandal, P., & Bera, B. (2023). Dynamics of meander geometry and formation of neck cutoff of River Raidak-I within Himalayan Foreland Basin, India. *Journal of the Geological Society of India*, *99*(2), 247–258. https://doi.org/10.1007/S12594-023-2292-2/METRICS

Google. (2024). How images are collected - Google Earth Help. https://support.google.com/earth/answer/6327779?hl=en

Grenfell, M., Aalto, R., & Nicholas, A. (2012). Chute channel dynamics in large, sand-bed meandering rivers. *Earth Surface Processes and Landforms*, *37*(3), 315–331. https://doi.org/10.1002/ESP.2257

Güneralp, I., & Marston, R. A. (2012). Process-form linkages in meander morphodynamics: Bridging theoretical modeling and real world complexity. *Progress in Physical Geography*, *36*(6), 718–746. https://doi.org/10.1177/0309133312451989

Ho, L., & Goethals, P. (2022). Machine learning applications in river research: Trends, opportunities and challenges. *Methods in Ecology and Evolution*, *13*(11), 2603–2621. https://doi.org/10.1111/2041-210X.13992

Hydroacoustics. (n.d.-a). Mid-section Measurements | U.S. Geological Survey. https://www.usgs.gov/hydroacoustics/mid-section-measurements

Hydroacoustics. (n.d.-b). Moving-boat Measurements | U.S. Geological Survey. https://www.usgs.gov/hydroacoustics/moving-boat-measurements

Ielpi, A., Lapôtre, M. G., Finotello, A., & Ghinassi, M. (2021). Planform-asymmetry and backwater effects on river-cutoff kinematics and clustering. *Earth Surface Processes and Landforms*, *46*(2), 357–370. https://doi.org/10.1002/ESP.5029

Ijafiya, D. J., & Yonnana, E. (2018). Development of chute cutoff in the lower course of River Mayo-Inne, Yola South, Nigeria. *Asian Journal of Geographical Research*, *1*(1), 1–9. https://doi.org/10.9734/AJGR/2018/v1i124666

Jacobson, J., & Kitchen, J. (n.d.). Discharge Measurements.

Keller, E. A., & Swanson, J., Frederick. (1979). Effects of large organic material on channel form and fluvial processes. *Earth Surface Processes*, *4*, 361–380. https://andrewsforest.oregonstate.edu/publications/565

Knighton, A. D., & Nanson, G. C. (2002). Inbank and overbank velocity conditions in an arid zone anastomosing river. *Hydrological Processes*, *16*(9), 1771–1791. https://doi.org/10.1002/HYP.1076

Konsoer, K. M., Richards, D., & Edwards, B. (2016). Planform evolution of neck cutoffs on elongate meander loops, White River, Arkansas, USA.

Land, L. F., Moring, J. B., Van Metre, P. C., Reutter, D. C., Mahler, B. J., Shipp, A. A., & Ulery, R. L. (1998). Water quality in the Trinity River Basin, Texas, 1992-95. *U.S. Geological Survey Circular 1171*, 4–5. https://pubs.usgs.gov/circ/circ1171/circ1171.pdf

Lauer, J. W., & Parker, G. (2008). Net local removal of floodplain sediment by river meander migration. *Geomorphology*, *96*(1-2), 123–149. https://doi.org/10.1016/J.GEOMORPH.2007.08.003

Lazarus, E. D., & Constantine, J. A. (2013). Generic theory for channel sinuosity. *Proceedings of the National Academy of Sciences of the United States of America*, *110*(21), 8447–8452. https://doi.org/10.1073/PNAS.1214074110/-/DCSUPPLEMENTAL

Leopold, L. B., Wolman, M. G., & Miller, J. P. (1964). *Fluvial processes in geomorphology*. Dover Publications, Inc. https://books.google.com/books?hl=en&lr=&id=KXnCAgAAQBAJ&pgis=1

Lewis, G. W., & Lewin, J. (2009). Alluvial cutoffs in Wales and the Borderlands. *Modern and Ancient Fluvial Systems*, 145–154. https://doi.org/10.1002/9781444303773.CH11

Lewis, Q. W., Edmonds, D. A., & Yanites, B. J. (2020). Integrated UAS and LiDAR reveals the importance of land cover and flood magnitude on the formation of incipient chute holes and chute cutoff development. *Earth Surface Processes and Landforms*, *45*(6), 1441–1455. https://doi.org/10.1002/ESP.4816

Li, J., Grenfell, M. C., Wei, H., Tooth, S., & Ngiem, S. (2020). Chute cutoff-driven abandonment and sedimentation of meander bends along a fine-grained, non-vegetated, ephemeral river on the Bolivian Altiplano. *Geomorphology*, *350*, 106917. https://doi.org/10.1016/J.GEOMORPH.2019.106917

Li, Z., Gao, P., & Wu, X. (2022). Processes of neck cutoff and channel adjustment affected by seeding herbaceous vegetation and variable discharges. *CATENA*, *208*, 105731. https://doi.org/10.1016/J.CATENA.2021.105731

Li, Z., Wu, X., & Gao, P. (2019). Experimental study on the process of neck cutoff and channel adjustment in a highly sinuous meander under constant discharges. *Geomorphology*, *327*, 215–229. https://doi.org/10.1016/J.GEOMORPH.2018.11.002

Lindroth, E. M., Rhoads, B. L., Castillo, C. R., Czuba, J. A., Güneralp, İ., & Edmonds, D. (2020). Spatial variability in bankfull stage and bank elevations of lowland meandering rivers: relation to rating curves and channel planform characteristics. *Water Resources Research*, *56*(8), e2020WR027477. https://doi.org/10.1029/2020WR027477

Malik, S., Pal, S. C., Das, B., & Das, B. (2017). Chute cut-off processes along a small alluvial channel: a case study of Sangra Khal, sub-tributary of Gour Nadi, West Bengal, India. *Modeling Earth Systems and Environment*, *3*(1), 1–11. https://doi.org/10.1007/S40808-017-0307-Y/FIGURES/12

Martha, T. R., Sharma, A., & Kumar, K. V. (2015). Development of meander cutoffs—a multi-temporal satellite-based observation in parts of Sindh River, Madhya Pradesh, India. *Arabian Journal of Geosciences*, *8*(8), 5663–5668. https://doi.org/10.1007/S12517-014-1582-9/FIGURES/5

Mason, J., & Mohrig, D. (2018). Using time-lapse lidar to quantify river bend evolution on the meandering coastal Trinity River, Texas, USA. *Journal of Geophysical Research: Earth Surface*, *123*(5), 1133–1144. https://doi.org/10.1029/2017JF004492

Musselman, Z. A. (2006). Tributary response to the Lake Livingston impoundment - Lower Trinity River, Texas. *University of Kentucky Doctoral Dissertations*. https://uknowledge.uky.edu/gradschool_diss/361

NOAA. (2023, January). What is LIDAR.

Pannone, M., & De Vincenzo, A. (2022). On the prediction of the characteristic times of river meander cutoff sequence: Theoretical model and comparison with laboratory and field observations. *Water Resources Research*, *58*(7). https://doi.org/10.1029/2021WR031661

Qiao, Q., Yang, C., Hao, X., & Huang, L. (2024). Numerical modeling of two-dimensional hydrodynamics in an artificial chute cutoff under different hydrologic conditions. https://doi.org/10.21203/RS.3.RS-4041670/V1

Schwenk, J., & Foufoula-Georgiou, E. (2016). Meander cutoffs nonlocally accelerate upstream and downstream migration and channel widening. *Geophysical Research Letters*, *43*(24), 437–12. https://doi.org/10.1002/2016GL071670

Slowik, M. (2016). The influence of meander bend evolution on the formation of multiple cutoffs: findings inferred from floodplain architecture and bend geometry. *Earth Surface Processes and Landforms*, *41*(5), 626–641. https://doi.org/10.1002/ESP.3851

Smith, L. C., & Pavelsky, T. M. (2008). Estimation of river discharge, propagation speed, and hydraulic geometry from space: Lena River, Siberia. *Water Resources Research*, *44*(3), 3427. https://doi.org/10.1029/2007WR006133

Sylvester, Z., Durkin, P., & Covault, J. A. (2019). High curvatures drive river meandering. *Geology*, *47*(3), 263–266. https://doi.org/10.1130/G45608.1

Szewczyk, L., Grimaud, J. L., Cojan, I., & Piegay, H. (2022). Bedload infilling and depositional patterns in chute cutoffs channels of a gravel-bed river: The Ain River, France. *Earth Surface Processes and Landforms*, *47*(2), 459–476. https://doi.org/10.1002/ESP.5260

Thornton, C. I., Abt, S. R., Morris, C. E., & Fischenich, J. C. (2000). Calculating shear stress at channel-overbank interfaces in straight channels with vegetated floodplains. *Journal of Hydraulic Engineering*, *126*(12), 929–936. https://doi.org/10.1061/(ASCE)0733-9429(2000)126:12(929)

Trinity River Authority of Texas. (n.d.). Lake Livingston. https://www.trinityra.org/lake_information/water_storage/lake_livingston/index.php

Turnipseed, C. (2017). Characterizing the hydrodynamics of a meandering river neck cutoff. https://repository.lsu.edu/gradschool_theses/4431

UC Davis. (n.d.). SoilWeb: An online soil survey browser | California Soil Resource Lab. https://casoilresource.lawr.ucdavis.edu/gmap/

University of North Carolina at Chapel Hill. (2022). SWOT River Database (SWORD). https://www.swordexplorer.com/

U.S. Department of Agriculture, N. R. C. S. (2022, October). National soil survey handbook, title 430-VI. https://www.nrcs.usda.gov/resources/guides-and-instructions/national-soil-survey-handbook%20https://directives.sc.egov.usda.gov

Van Dijk, W. M., Van De Lageweg, W. I., & Kleinhans, M. G. (2012). Experimental meandering river with chute cutoffs. *Journal of Geophysical Research: Earth Surface*, *117*(F3), 3023. https://doi.org/10.1029/2011JF002314

Van Dijk, W. M., Schuurman, F., Van de Lageweg, W. I., & Kleinhans, M. G. (2014). Bifurcation instability and chute cutoff development in meandering gravel-bed rivers. *Geomorphology*, *213*, 277–291. https://doi.org/10.1016/J.GEOMORPH.2014.01.018

Van Dijk, W. M., Van de Lageweg, W. I., & Kleinhans, M. G. (2013). Formation of a cohesive floodplain in a dynamic experimental meandering river. *Earth Surface Processes and Landforms*, *38*(13), 1550–1565. https://doi.org/10.1002/ESP.3400

Viero, D. P., Dubon, S. L., & Lanzoni, S. (2018). Chute cutoffs in meandering rivers: formative mechanisms and hydrodynamic forcing. *Fluvial Meanders and Their Sedimentary Products in the Rock Record*, 201–229. https://doi.org/10.1002/9781119424437.CH8

Water Science School. (2018). How streamflow is measured | U.S. Geological Survey. https://www.usgs.gov/special-topics/water-science-school/science/how-streamflow-measured

Wolman, M. G., & Miller, J. P. (1960). Magnitude and frequency of forces in geomorphic processes. *The journal of geology*, *68*(1), 54–74. https://doi.org/10.1086/626637

Yin, K., Fauchille, A.-L., Filippo, E. D., Kotronis, P., & Sciarra, G. (2021). A review of sand–clay mixture and soil–structure interface direct shear test. *Geotechnics 2021, Vol. 1, Pages 260-306*, *1*(2), 260–306. https://doi.org/10.3390/GEOTECHNICS1020014

Zinger, J. A., Rhoads, B. L., & Best, J. L. (2011). Extreme sediment pulses generated by bend cutoffs along a large meandering river. *Nature Geoscience 2011 4:10*, *4*(10), 675–678. https://doi.org/10.1038/ngeo1260

A

Sources for Data Collection

During the initial search for rivers with cutoff bends, publicly accessible online sources were used. This appendix shows these sources, their data, and their website.

Table A.1: Overview of the collected data and the corresponding sources and links.

Data	Source	Link
River gauge data in the USA	USGS National Water Information System	https://maps.waterdata.usgs.gov/mapper/
Satellite imagery current	Google Maps	https://maps.google.com/
Satellite imagery historic	Google Earth Pro	https://earth.google.com/web/ or Desktop version
Soil information USA	Soil Web	https://casoilresource.lawr.ucdavis.edu/gmap/

Imagery for these particular rivers is collected by many different companies and sattelites, such as '2024 Airbus', '2024 Maxar Technologies', 'USDA/FPAC/GEO', 'NASA', 'CNES/Airubs', 'U.S. Geological Survey', and 'Image Landsat / Copernicus' on a greater elevation. These satellites provide detailed images of the surface of the earth which can be used for different causes. They are linked to organisations and companies such as Airbus, with the largest Earth observation constellation (AIRBUS, 2024). Others are owned by Maxar technologies, the US department of agriculture, NASA, CNES (French space station), and many more.

Further zoomed out, the Copernicus Landsat, part of the Landsat programme, which is "a joint USGS and NASA-led enterprise for Earth observation that represents the world's longest running system of satellites for moderate-resolution optical remote sensing for land, coastal areas and shallow waters", according to Copernicus Service information (n.d.). This satellite provides images which are dated to the 31st of December every year. The acquisition dates are provided by the image provider or, when the provider has not given date information, a reasonable range is shown (Google, 2024). For all images in this research, a singular date was shown, which indicates that those were provided by the image provider and Google ensures that a date is never newer than the actual image collection date. Google Earth Pro uses the computer's timezone, which for this research was GMT+2, so the image dates can be a few hours off.

B

Rivers and USGS stations

For each river, the elevation range and reach length were measured on Google Earth Pro based on the area of interest within the upstream and downstream coordinates. These values are shown in the tables below per river. The USGS measurement stations along those rivers are listed in the next table, together with their coordinates and availability of data.

B.1. Cheyenne River

Cutoff Regime	Elevation Range (m)	Reach Length (m)	Slope (m/m)	Upstream coordinates	Downstream coordinates
Chute	707 - 494	207297	1.03E-03	44.014737, -102.275279	44.413595, -101.133367

Gauge Station	ID	Gauge Station Coordinates	Daily discharge Availability	Field measurements Availability	River Width (m)
CHEYENNE RIVER NEAR WASTA, SD	06423500	44.080754, -102.400837	1914-2024	1975-2024	44
CHEYENNE RIVER NEAR PLAINVIEW, SD	06438500	44.531101, -101.929670	1950-2024	1994-2024	58

B.2. Powder River

Cutoff Regime	Elevation Range (m)	Reach Length (m)	Slope (m/m)	Upstream coordinates	Downstream coordinates
Mixed	1207 - 1080	125472	1.01E-03	44.111074, -106.083371	44.491835, -106.045154

Gauge Station	ID	Gauge Station Coordinates	Daily discharge Availability	Field measurements Availability	River Width (m)
POWDER RIVER AT ARVADA, WY	06317000	44.3900, -106.0737	1930-2024	1980-2024	45
Powder River at Moorhead MT	06324500	45.057268, -105.878426	1929-2024	1974-2024	58
Powder River near Locate MT	06326500	46.429155, -105.309737	1938-2024	1983-2023	72

B.3. Pearl River

Cutoff Regime	Elevation Range (m)	Reach Length (m)	Slope (m/m)	Upstream coordinates	Downstream coordinates
Neck	70 - 47	174503	1.32E-04	32.115180, -90.114305	31.242815, -90.002628

Gauge Station	ID	Gauge Station Coordinates	Daily discharge Availability	Field measurements Availability	River Width (m)
Pearl River nr Monticello, MS	02488500	31.3312, -90.0517	1938-2024	1982-2024	94
Pearl River nr Columbia, MS	02489000	31.237655, -89.847381	1999-2023	1979-1992 and 1999-2024	120
Pearl River nr Bogalusa, LA	02489500	30.4735, -89.4915	1938-2024	1938-2024	113

B.4. Trinity River

Cutoff Regime	Elevation Range (m)	Reach Length (m)	Slope (m/m)	Upstream coordinates	Downstream coordinates
Neck	7 - 4	84968	3.53E-05	30.153993, -94.472579	30.023036, -94.493143

Gauge Station	ID	Gauge Station Coordinates	Daily discharge Availability	Field measurements Availability	River Width (m)
Trinity Rv at Romayor, TX	08066500	30.2530, -94.5102	1924-2024	1924-2024	140

C

Google Earth Pro Imagery and Measurements

Based on measurements, of which an example is shown below in Figure C.1, the properties of the cutoff bends are measured and shown for each river in this appendix. The Google Earth Pro files with measurements and labels saved, can be requested.

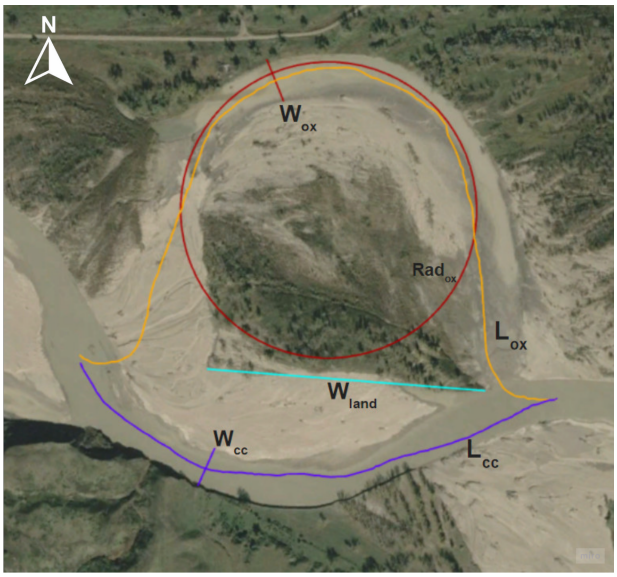

(a) Example for measurements drawn on a chute cutoff on Google Earth Pro. This is cutoff number 10 of Cheyenne River, South Dakota. The flow direction is West to East. Image taken from Google Earth Pro, image date: 5-10-2019.

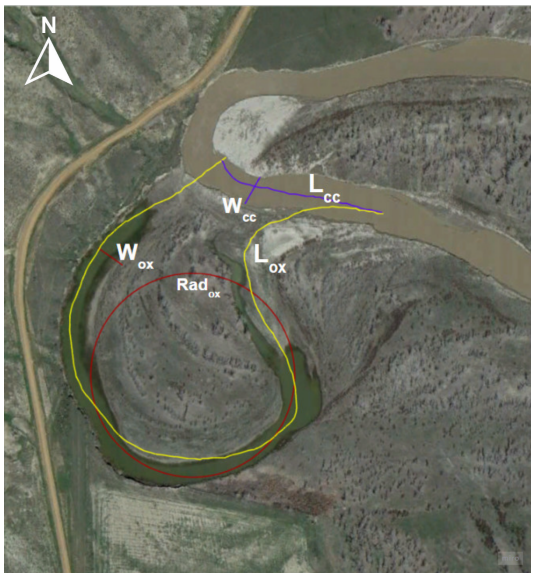

(b) Example for measurements drawn on a neck cutoff on Google Earth Pro. This is cutoff number 7 of Powder River, Wyoming. The flow direction is from South to North. Image taken from Google Earth Pro, image date: 1-5-2014.

Figure C.1: Measurements done on Google Earth Pro on images. W_{ox}: oxbow lake/channel width, L_{ox}: oxbow lake/channel length, W_{cc}: cutoff channel width, L_{cc}: cutoff channel length, Rad_{ox}: radius of the oxbow bend, and W_{land}: land width between two bends (only measured for chute cutoffs).

C.1. Cheyenne River

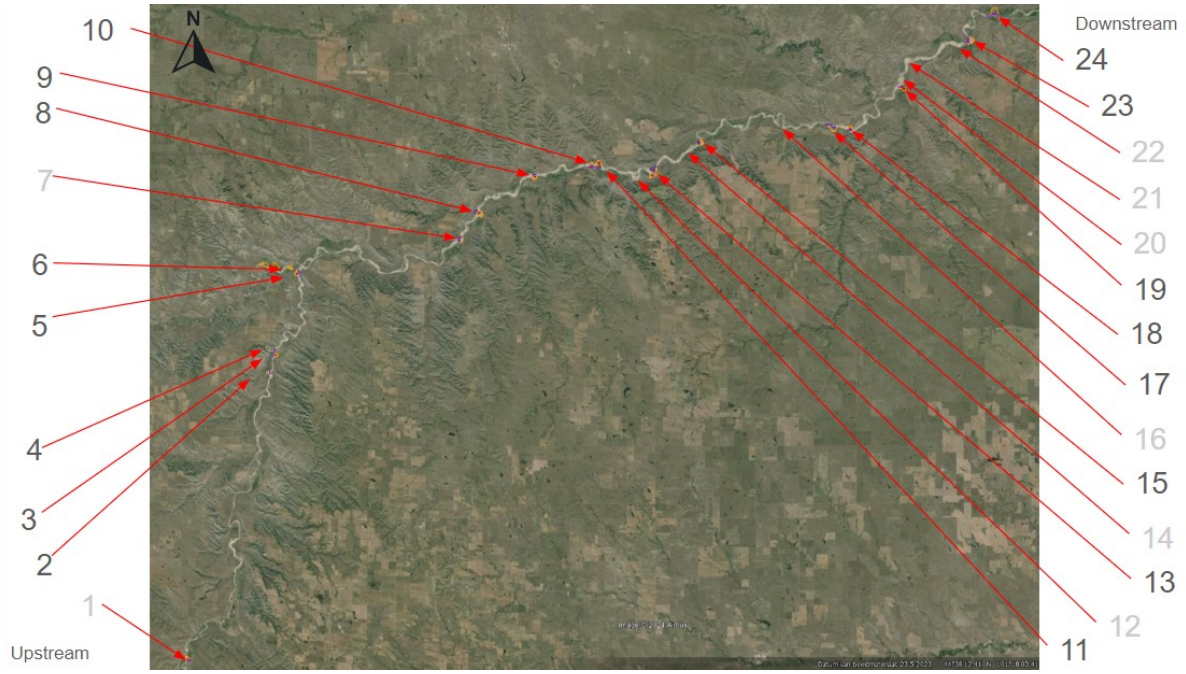

Figure C.2: Overview of the locations of the found cutoffs in the Cheyenne River, South Dakota, numbers starting upstream. Numbers shown in light grey were eventually excluded from the data analysis. Photo taken from Google Earth Pro.

The cutoffs shown above were measured and cutoff dates were assigned, which can be seen in Table C.1 on the next page.

Table C.1: Cutoff dates, locations, and measurements for cutoffs in Cheyenne River.

Cutoff	Year	Coordinates	Rad_{ox}	W_{ox}	W_{cc}	L_{ox}	L_{cc}	W_{land}	$W_{straight}$	Type	Extra
1	2016-2020	44.021838, -102.272470	170	50	50	1550	730	383	44	Chute	Exclude. Too far upstream.
2	2000	44.193622, -102.204800	136	39	33	905	477	271	44	Chute	
3	1998-1999	44.204174, -102.202751	180	49	47	1569	700	355	38	Chute	
4	2004-2005	44.205689, -102.202270	110	23	35	730	560	252	38	Chute	
5	1999-2000	44.253208, -102.182477	157	45	29	1346	780	321	57	Chute	
6	2015-2016	44.254159, -102.182366	160	37	44	808	488	323	57	Chute	
7	2004-2016	44.274135, -102.045338	258	58	54	1332	908	528	79	Chute	Exclude. Incomplete cutoff or parallel channel.
8	2019	44.291666, -102.033384	297	74	68	2055	730	504	73	Chute	Images have no clear collection date.
9	2008-2009	44.313116, -101.583843	214	54	74	1474	524	582	97	Chute	Old channel cutoff.
10	2019	44.315985, -101.534875	207	63	59	1262	754	393	68	Chute	Old/Parallel channel cutoff.
11	2019	44.315677, -101.531210	201, 251	74	71	1907	694	450	68	Chute	Cutoff happened in the same event as 10.
12	2011-2012	44.313997, -101.500423								Chute	Exclude. Many parallel channels.
13	2010-2011	44.314933, -101.483597	172, 296	67	49	3110	1147	576	68	Chute	Possibly contribution of earlier erosion.
14	2016-2019	44.330246, -101.453317								Chute	Exclude. Unsure if it is a cutoff.
15	2019	44.333021, -101.444537	308	40	70	1434	687	406	76	Chute	Images have no clear collection date.
16	2014-2019	44.344818, -101.380787								Chute	Exclude. Double cutoff not within scope.
17	1997	44.342603, -101.332982	278	59	55	2174	1392	845	79	Chute	
18	2008-2009	44.341553, -101.320823	212	42	78	1472	668	428	79	Chute	
19	1995	44.364949, -101.274071	178, 235	64	40	2054	704	336	98	Chute	
20	2014	44.371396, -101.274454								Chute	Exclude. Lack of images.
21	2010-2012	44.382231, -101.270965								Chute	Exclude. Lack of images.
22	2014	44.391917, -101.224238								Chute	Exclude. Lack of images.
23	2009-2010	44.393535, -101.215529	351	56	55	2192	1124	525	103	Chute	
24	1997	44.410909, -101.194312	368	75	59	2796	1637	617	103	Chute	

C.2. Powder River

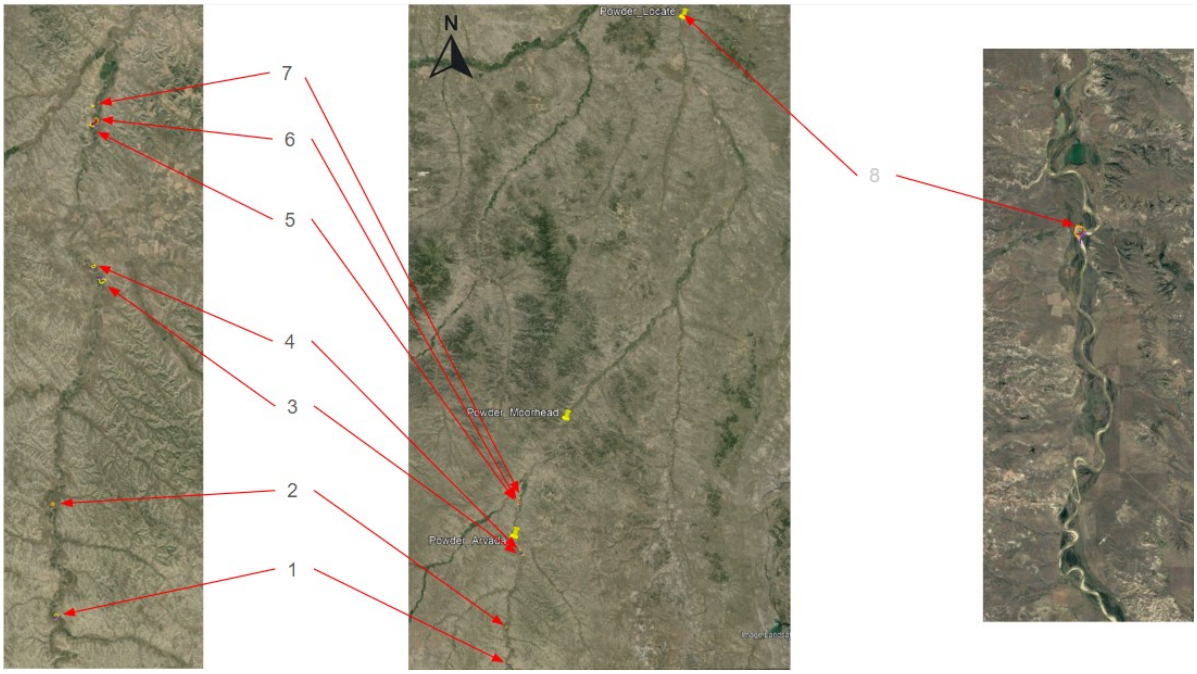

Figure C.3: Overview of the locations of the found cutoffs in the Powder River, Wyoming, numbers starting upstream. The left and right photos are close ups of the overview in the middle. Numbers shown in light grey were eventually excluded from the data analysis. Photos taken from Google Earth Pro.

Table C.2: Cutoff dates, locations, and measurements for cutoffs in Powder River.

Cut off	Year	Coordinates	Rad_{ox}	W_{ox}	W_{cc}	L_{ox}	L_{cc}	W_{land}	$W_{straight}$	Type	Extra
1	2000	44.141739, -106.083811	156	47	37	2100	1049	-	47	Neck	
2	1994-2006	44.214976, -106.090200	116, 88	23	28	790	369	294	46	Chute	
3	1984-1987	44.364971, -106.044423	289	60	57	2397	885	-	54	Neck	Questionable, lack of images.
4	1995	44.373436, -106.053429	180	57	93	1655	355	-	41	Neck	
5	2008	44.470293, -106.051990	201, 173	44	40	2203	302	-	50	Neck	
6	2011	44.471160, -106.053258	255, 183	47	41	2301	871	-	59	Chute	Questionable, difficult situation.
7	2009	44.482791, -106.052932	119, 113	36	37	1043	206	-	59	Neck	
8	2011	46.281181, -105.185771	152	57	67	1073	477	240	77	Chute	Exclude. Too far downstream.

C.3. Pearl River

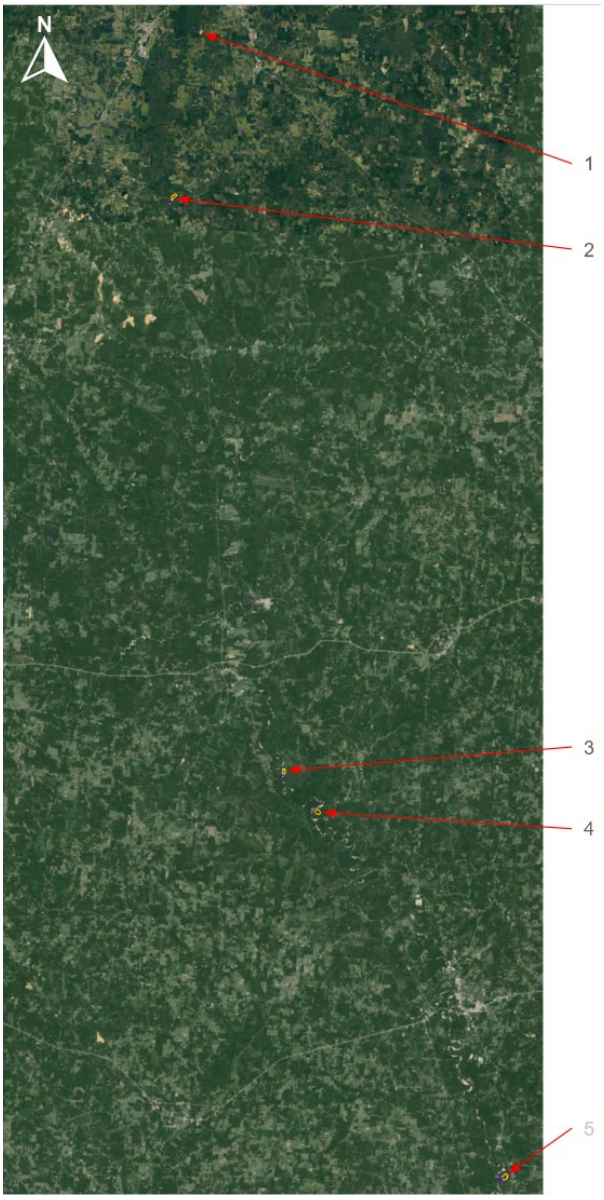

Figure C.4: Overview of the locations of the found river bend cutoffs in the Pearl River, Mississippi, numbers starting upstream. Numbers shown in light grey were eventually excluded from the data analysis. Photo taken from Google Earth Pro.

Table C.3: Cutoff dates, locations, and measurements for cutoffs in Pearl River. W_land column is not present here since neck cutoffs have a land width equal to or smaller than the river width before the cutoff event.

Cutoff	Year	Coordinates	Rad_{ox}	W_{ox}	W_{cc}	L_{ox}	L_{cc}	$W_{straight}$	Type	Extra
1	2010	32.111833, -90.115263	138, 87	74	69	1454	422	75	Neck	
2	1999	32.010739, -90.130811	142, 135	61	74	2433	611	80	Neck	
3	2015	31.273833, -31.273833	141	117	83	2179	896	109	Neck	
4	1990-1991	31.254077, -90.004300	245	149	120	2462	691	94	Neck	
5	2010	31.042468, -89.462347	260	145	95	2786	1254	125	?	Exclude. Difficult to define.

C.4. Trinity River

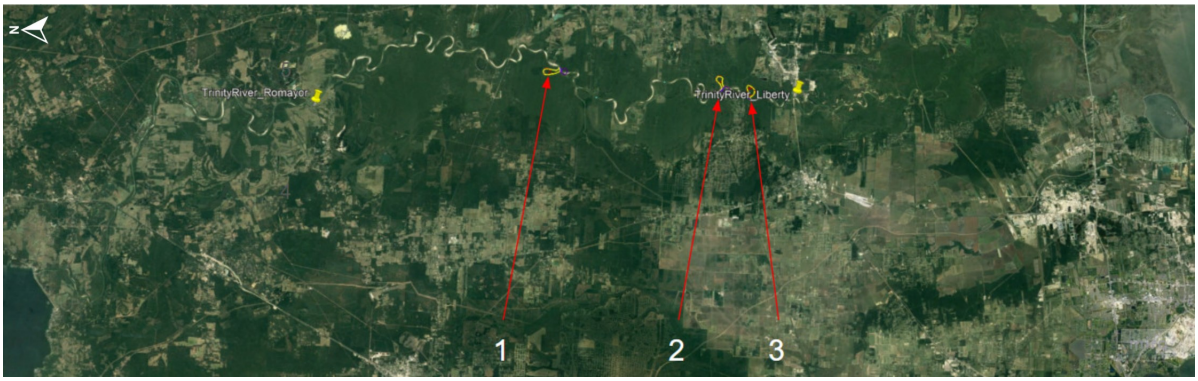

Figure C.5: Overview of the locations of the found river bend cutoffs in the Trinity River, Texas, numbers starting upstream. Photo taken from Google Earth Pro.

Table C.4: Cutoff dates, locations, and measurements for cutoffs in Trinity River. W_land column and Extra column are not present here since neck cutoffs have a land width equal to or smaller than the river width before the cutoff event, and no extra information was given for these cutoffs.

Cutoff	Year	Coordinates	Rad_{ox}	W_{ox}	W_{cc}	L_{ox}	L_{cc}	$W_{straight}$	Type
1	1990	30.142250, -94.482113	276	135	147	3419	442	105	Neck
2	1990	30.064788, -94.484956	277	109	72	2877	534	130	Neck
3	1997	30.053518, -94.491511	330, 164	127	113	3243	857	130	Neck

D

Discharges and River Depths

This appendix contains graphs for all nine stations that were evaluated in the four rivers. First the daily discharges, after which a representing station was selected for each river. The power law scaling is visualised, followed by the river depths.

D.1. Daily Discharge and Bankfull Discharge

For all 9 USGS stations that were initially found and analysed, the discharge and calculated bankfull discharge are shown below. In blue: the daily discharge measured by USGS measurement stations and converted to the metric system. Red horizontal line: the bankfull discharge limit, per Bjerklie (2007). The orange range: the 95% confidence interval. Values are shown in the legend of each graph.

Figure D.1: Discharge plots for all USGS measurement stations

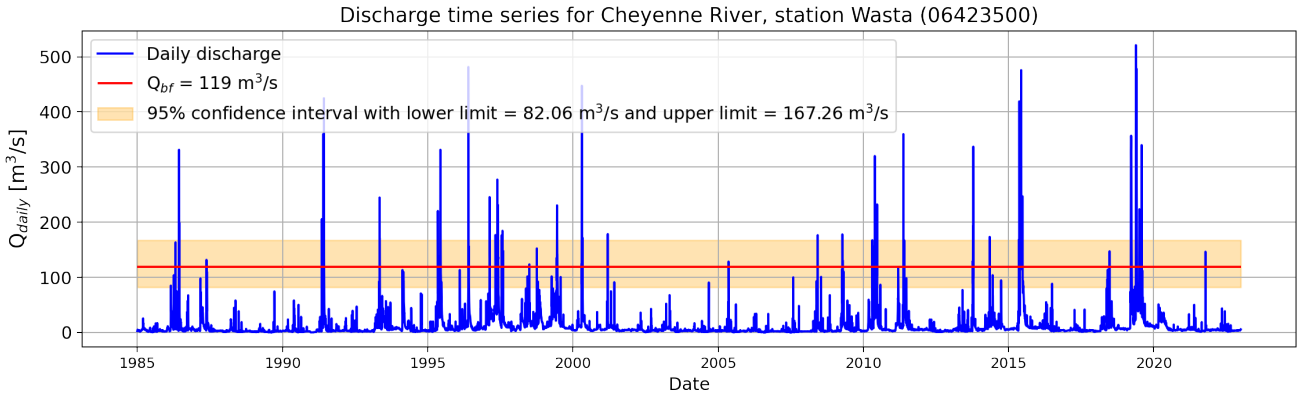

(a) Cheyenne River, Wasta station

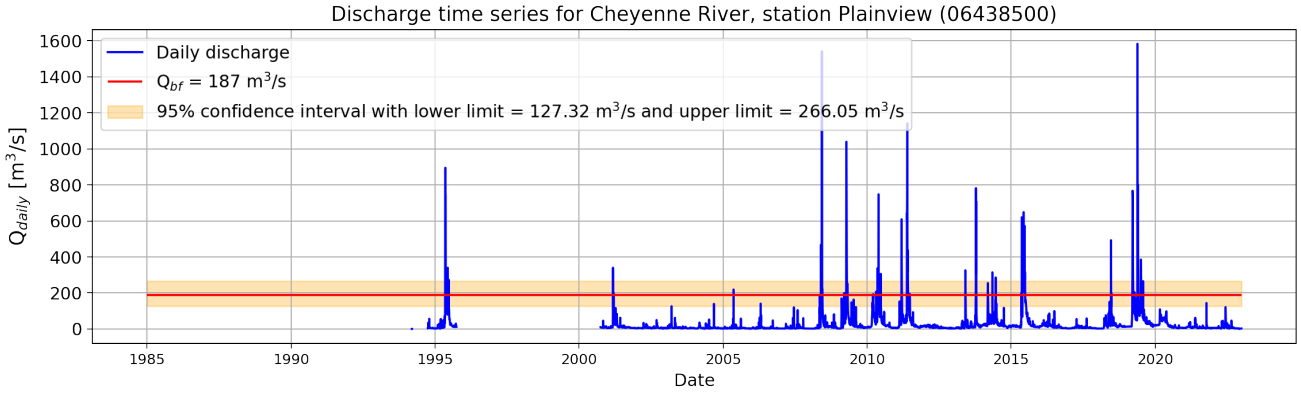

(b) Cheyenne River, Plainview station

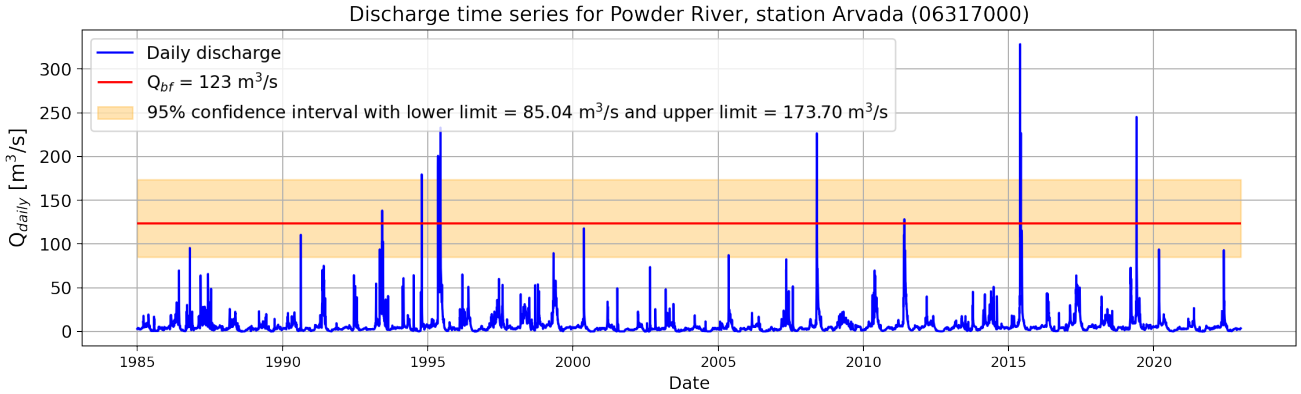

(c) Powder River, Arvada station

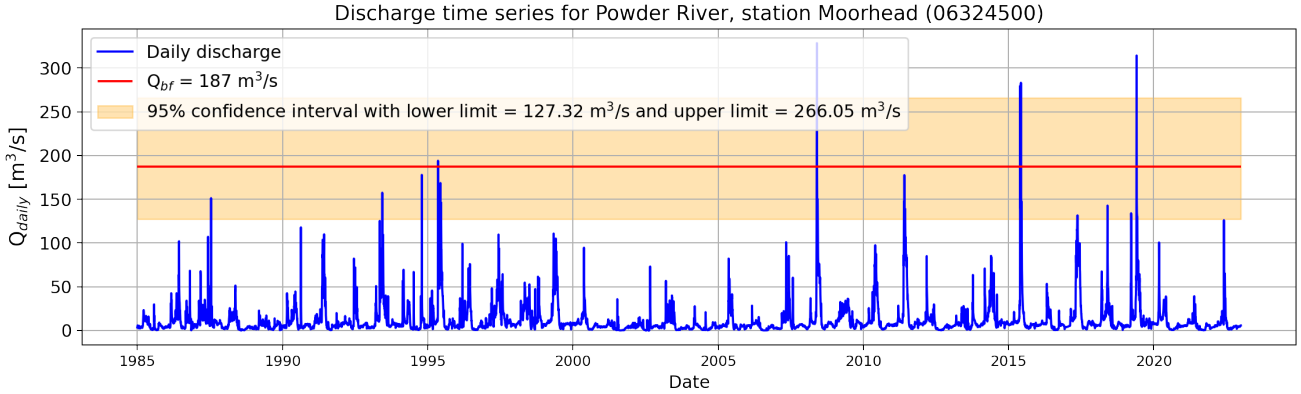

(d) Powder River, Moorhead station

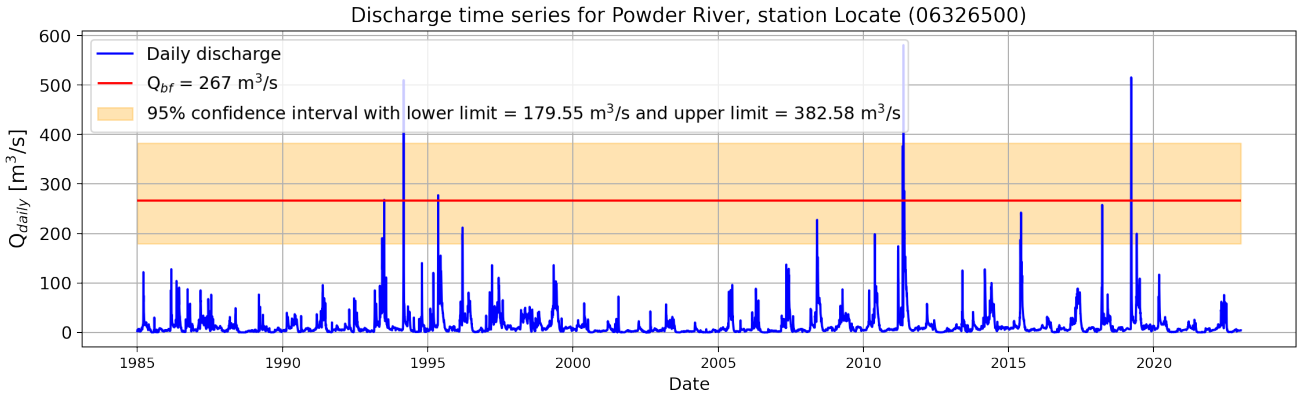

(e) Powder River, Locate station

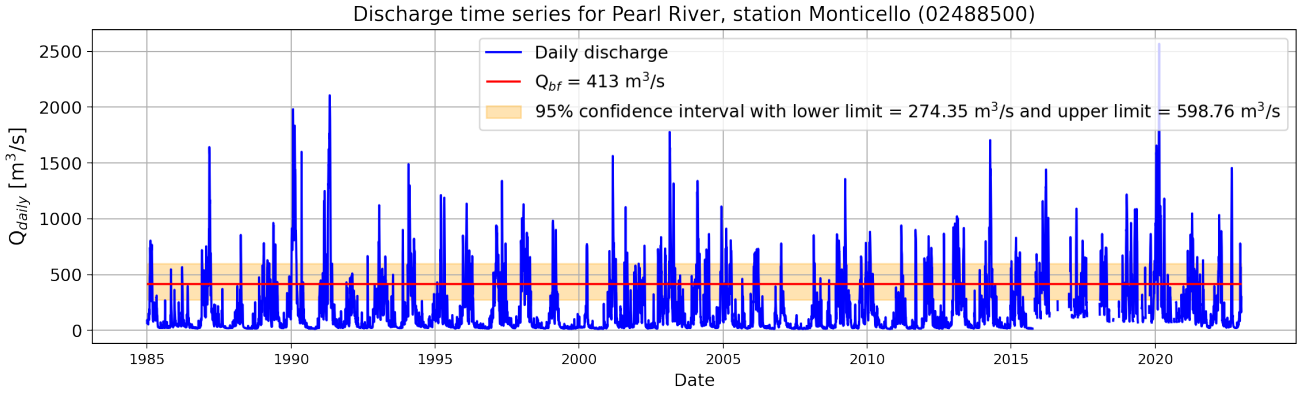

(f) Pearl River, Monticello station

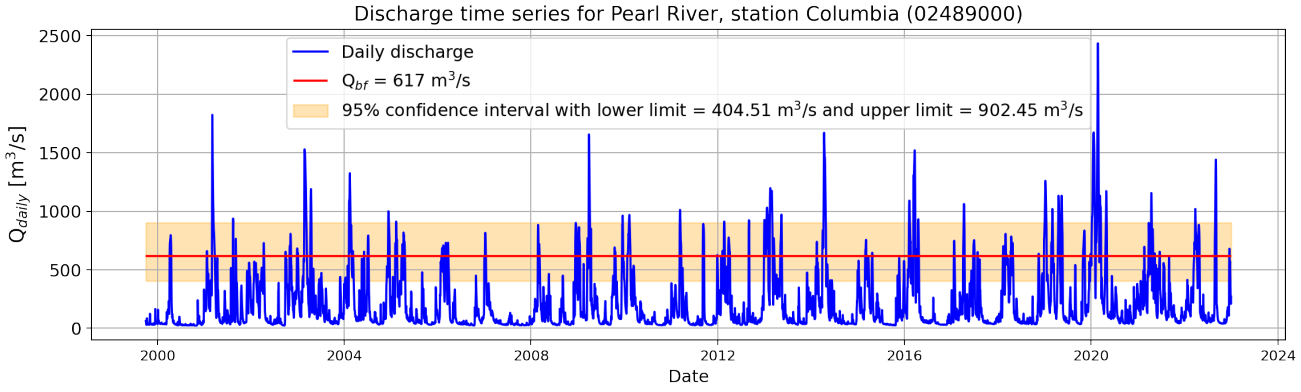

(g) Pearl River, Columbia station

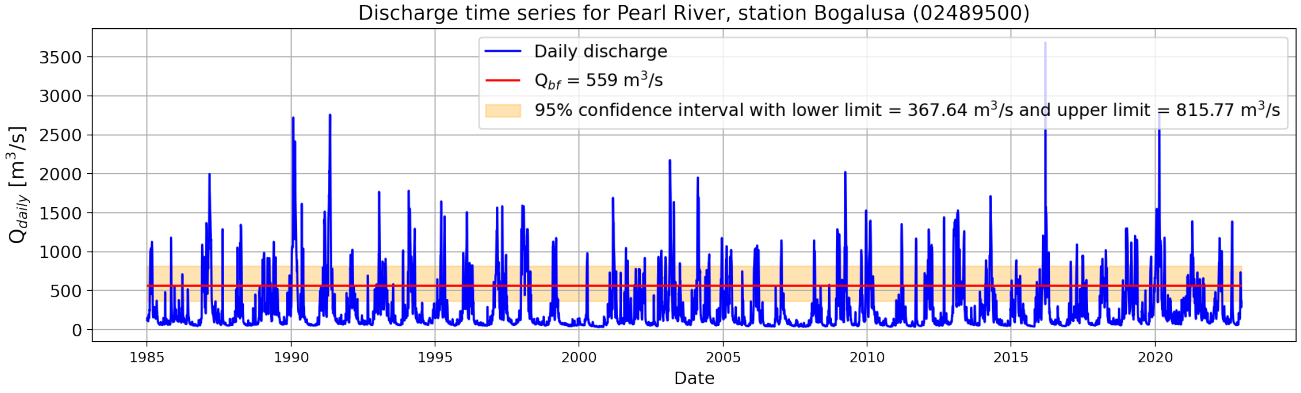

(h) Pearl River, Bogalusa station

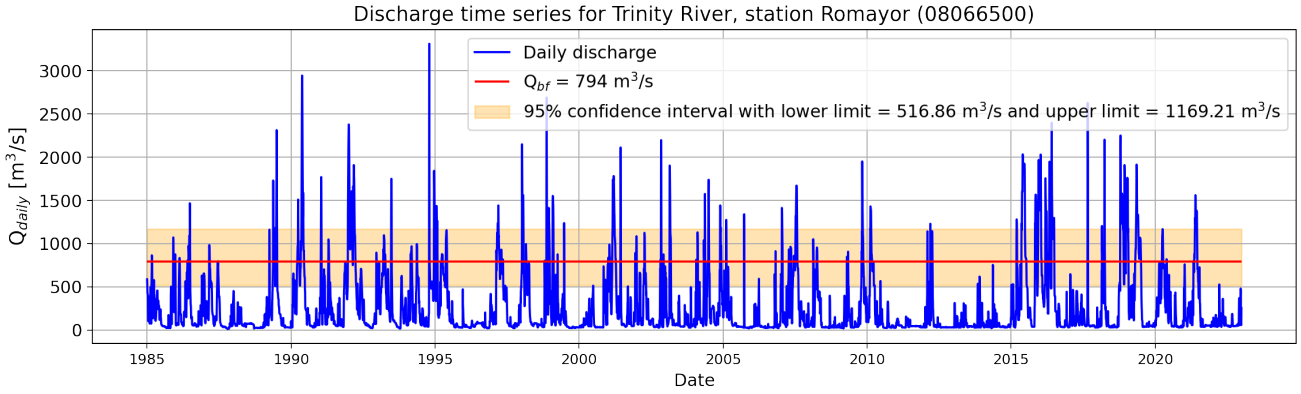

(i) Trinity River, Romayor station

D.2. Power Law Scaling

For the four selected USGS stations, a power law fit was applied to convert the measured discharges to river depths. The next figures show the Q_{fm} in m^3/s on the x-axis and the calculated river depth in m on the y-axis. The vertical line is the Q_{bf} calculated with Equation (2.1). The horizontal dashed line is the estimated corresponding bankfull river depth. Within these limits, a power law fit is applied on the data points, resulting in the orange line. The values of the scaling factor and exponent are shown in the legend.

Figure D.2: The four selected stations

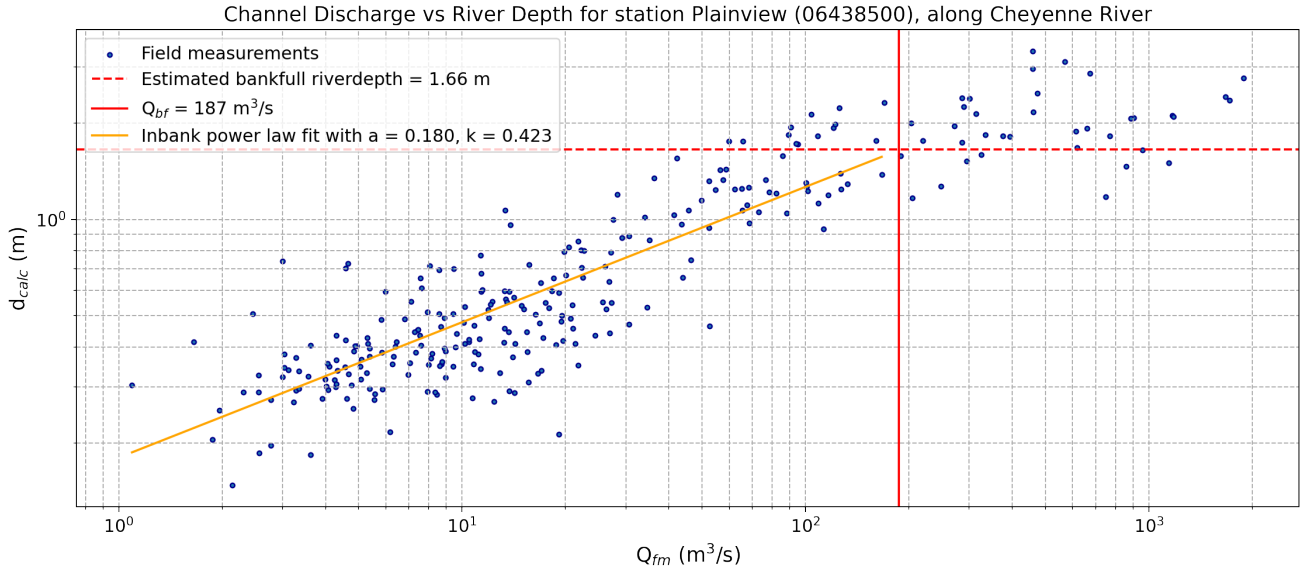

(a) Cheyenne River, Plainview station, r^2 = 0.720

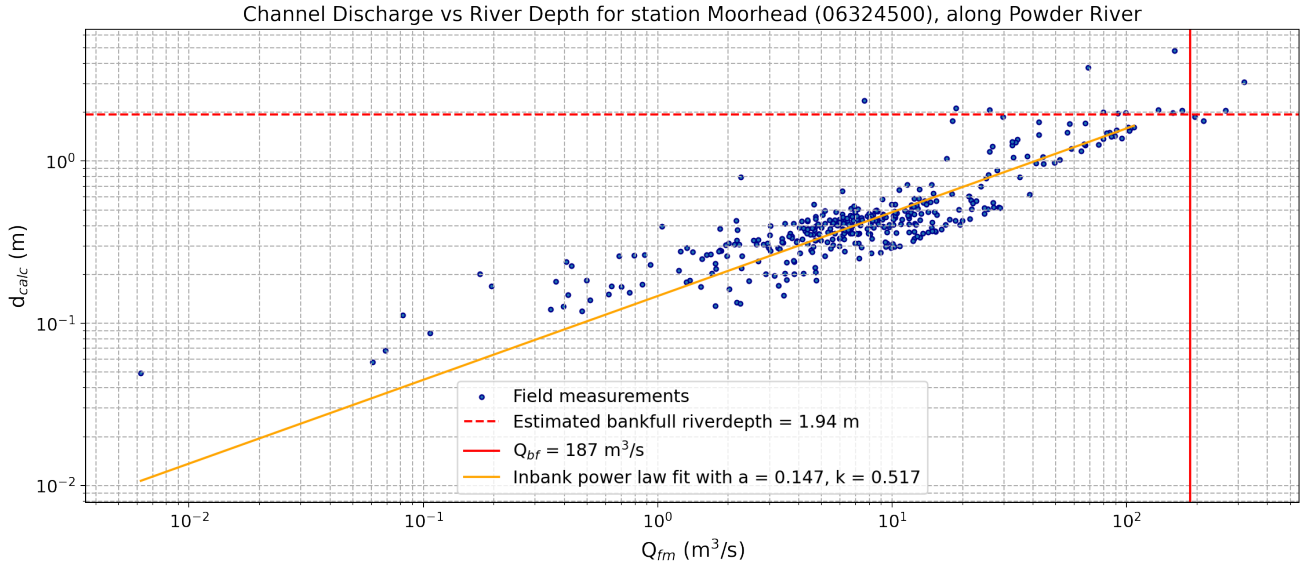

(b) Powder River, Moorhead station, r^2 = 0.774

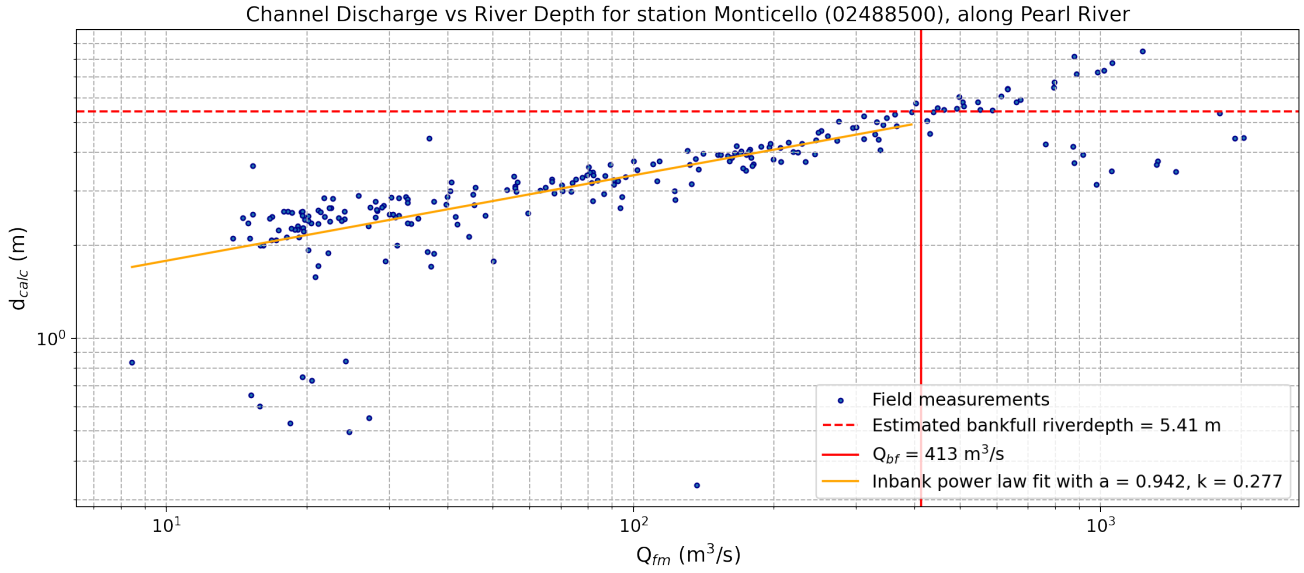

(c) Pearl River, Monticello River, r^2 = 0.710

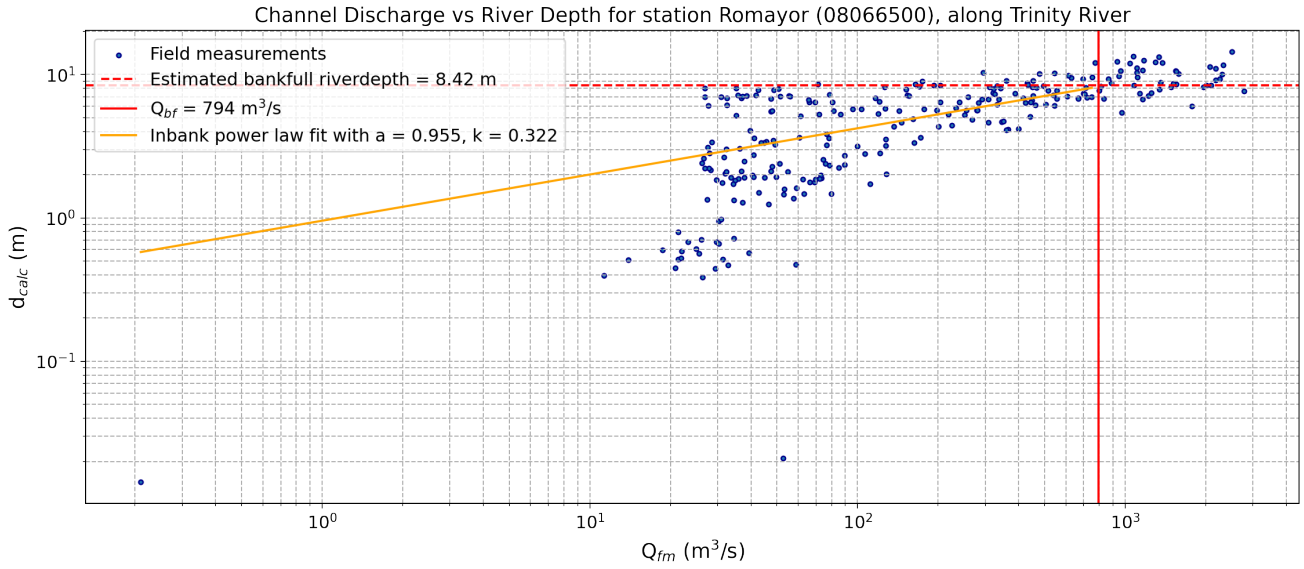

(d) Trinity River, Romayor station, r^2 = 0.401

Figure D.3: The other stations in the rivers

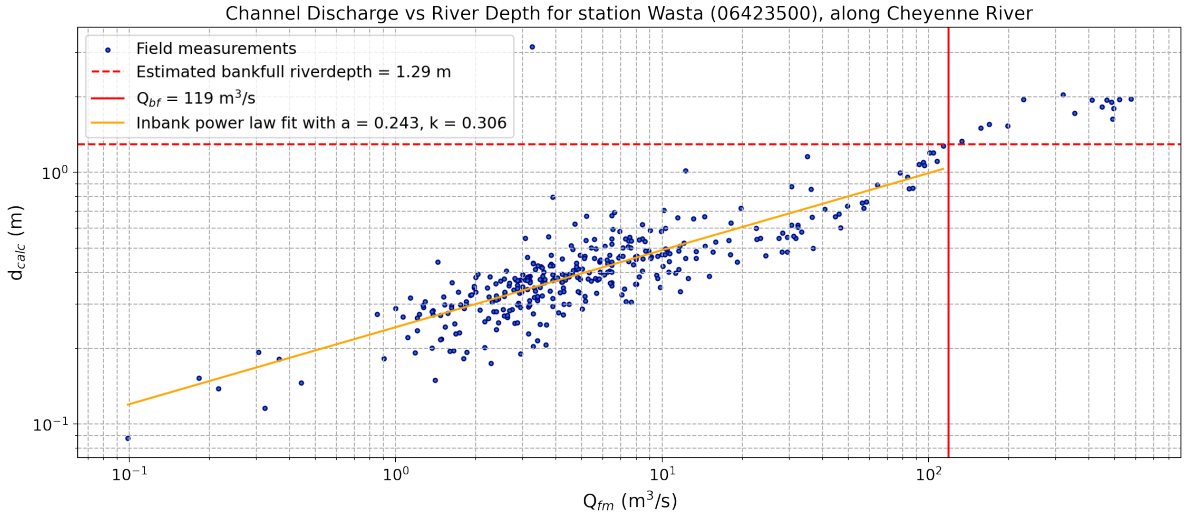

(a) Cheyenne River, Wasta station, r^2 = 0.749

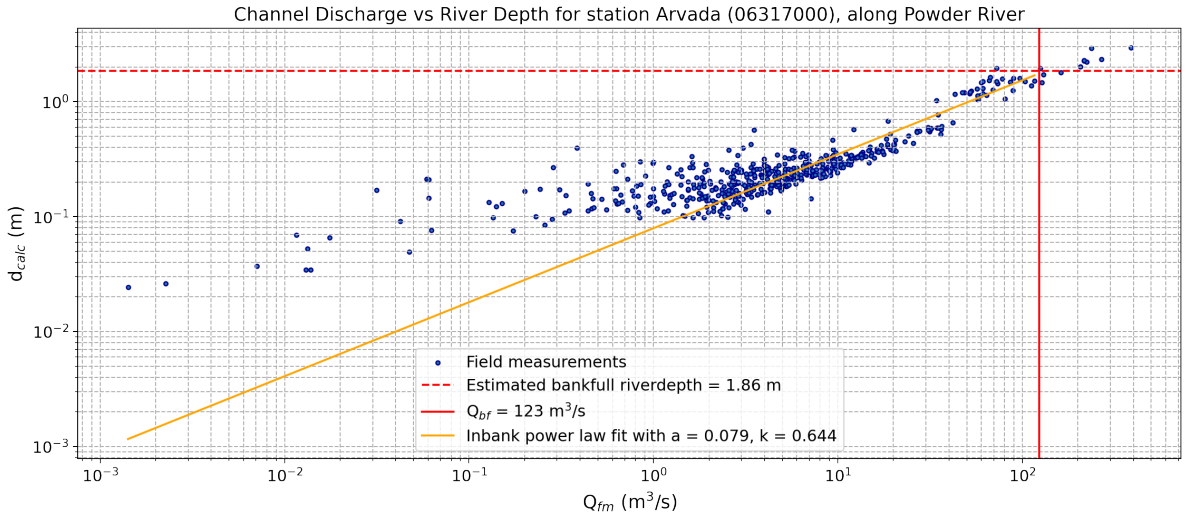

(b) Powder River, Arvada station, r^2 = 0.873

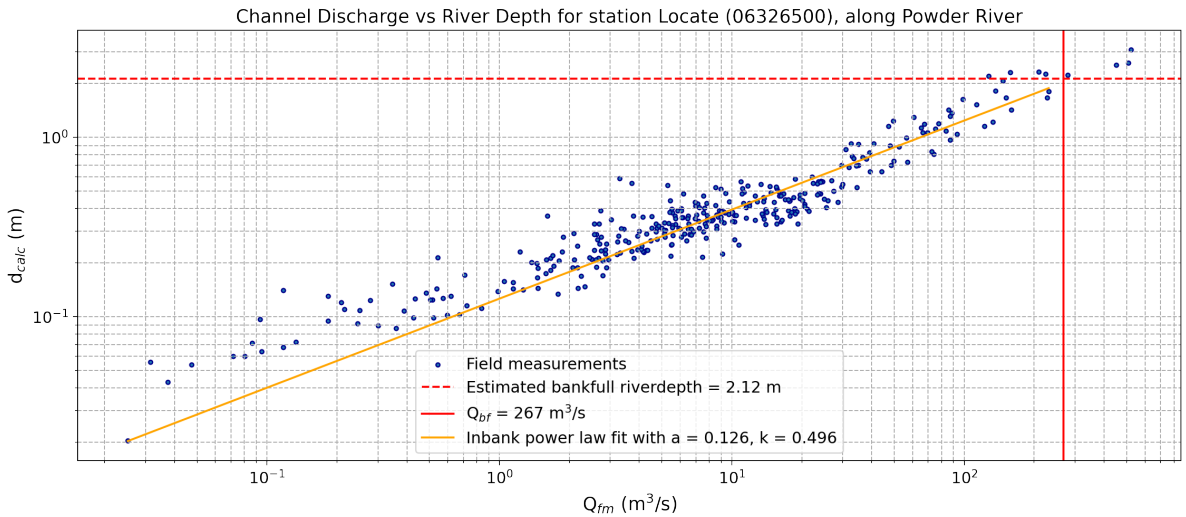

(c) Powder river, Locate station, r^2 = 0.873

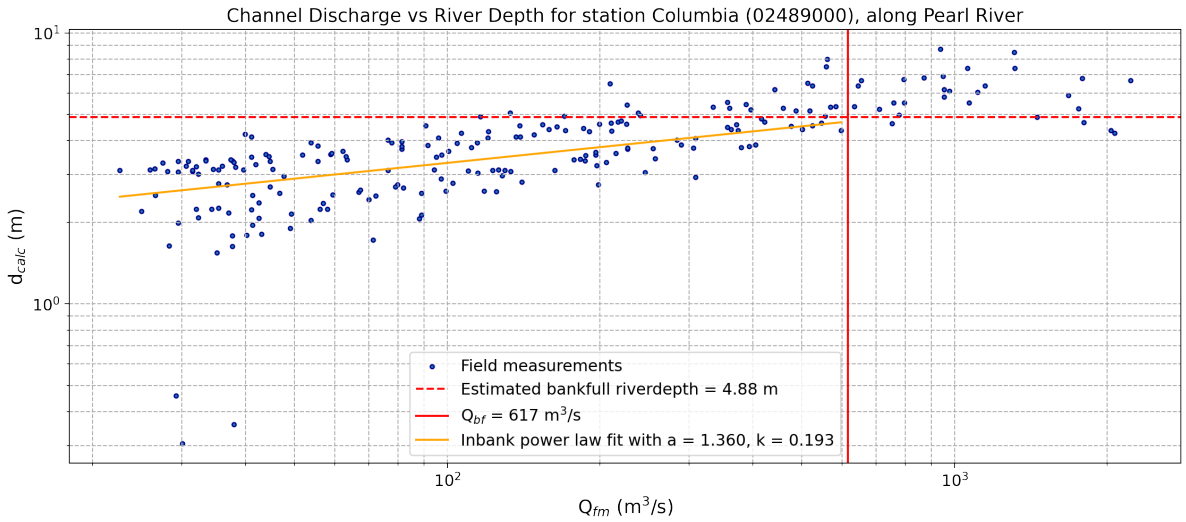

(d) Pearl River, Columbia station, r^2 = 0.382

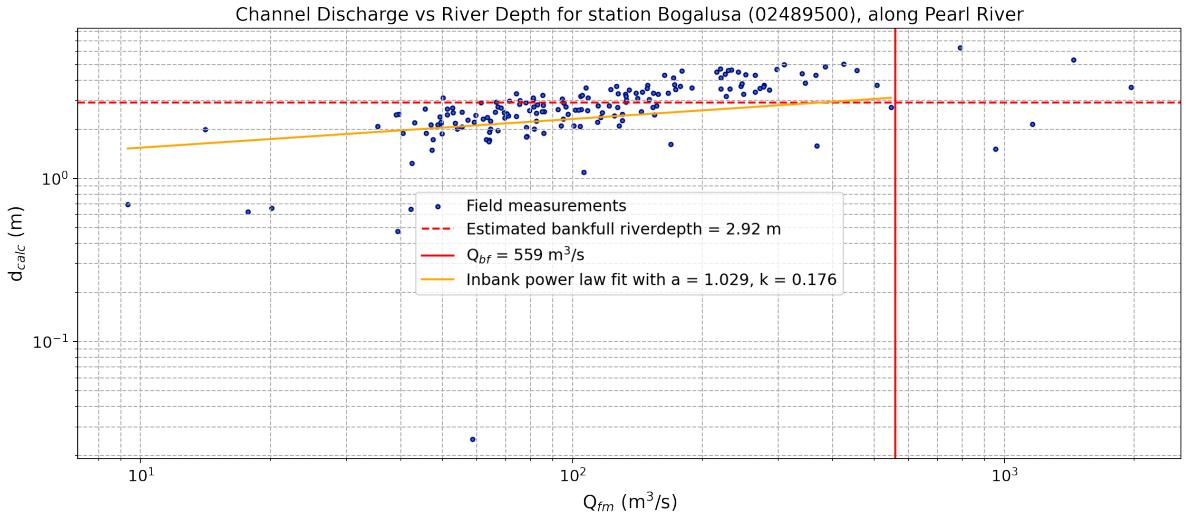

(e) Pearl River, Bogalusa station, r^2 = 0.171

D.3. Scaled River Depth

The resulting values of the power law fitting were used to convert daily discharge data to daily river depth data and a corresponding bankfull river depth Rd_{bf}. These are shown in the next figures, with the daily river depths in blue and Rd_{bf} as a green horizontal line, with the value shown in the legend.

Figure D.4: For the four selected stations

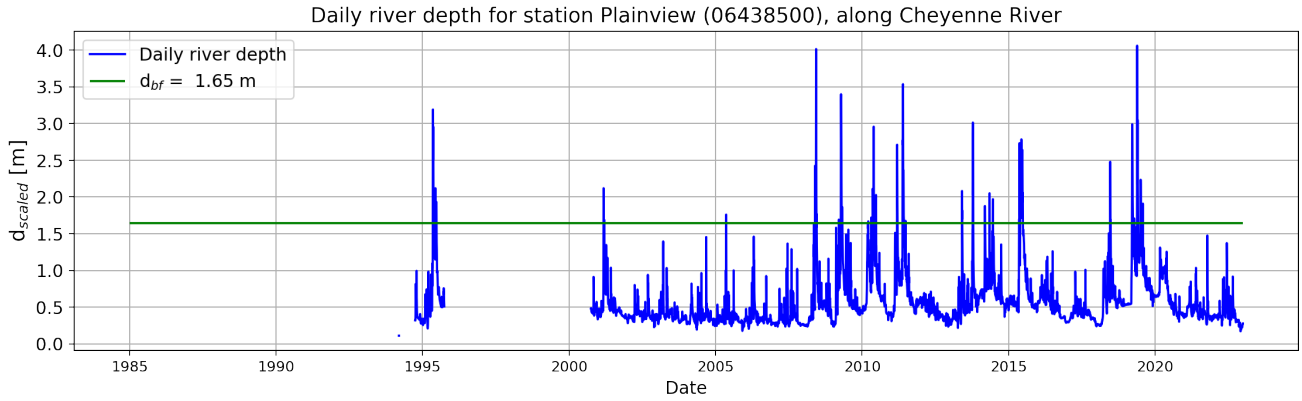

(a) Cheyenne River, Plainview station

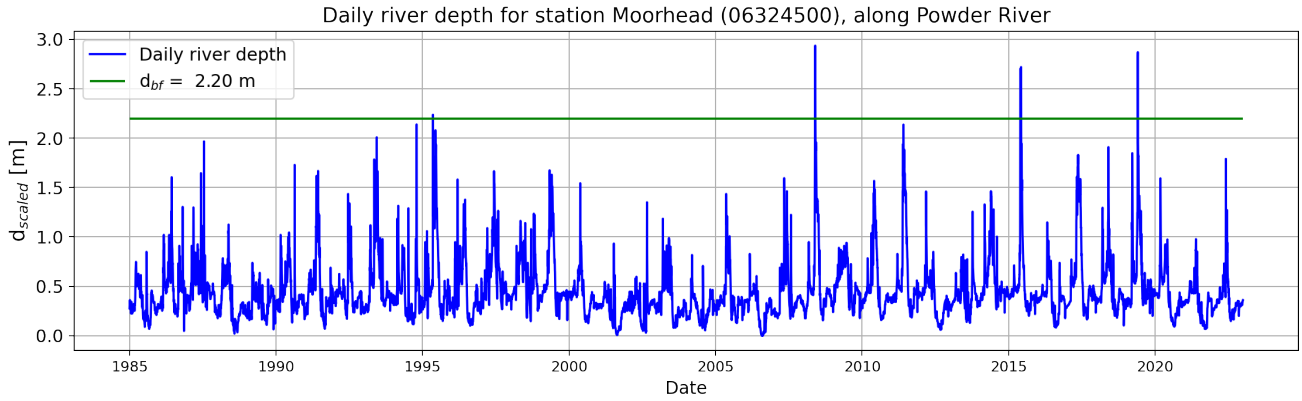

(b) Powder River, Moorhead station

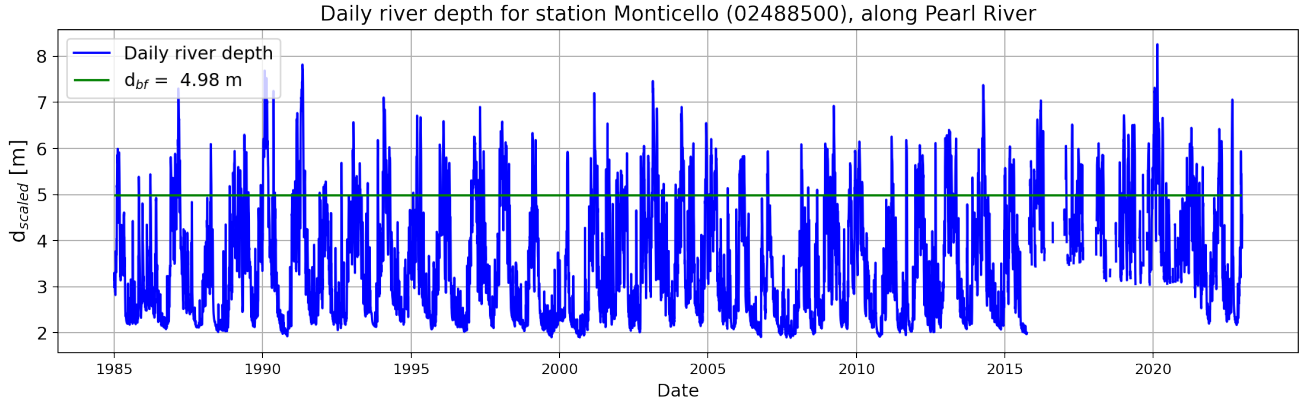

(c) Pearl River, Monticello station

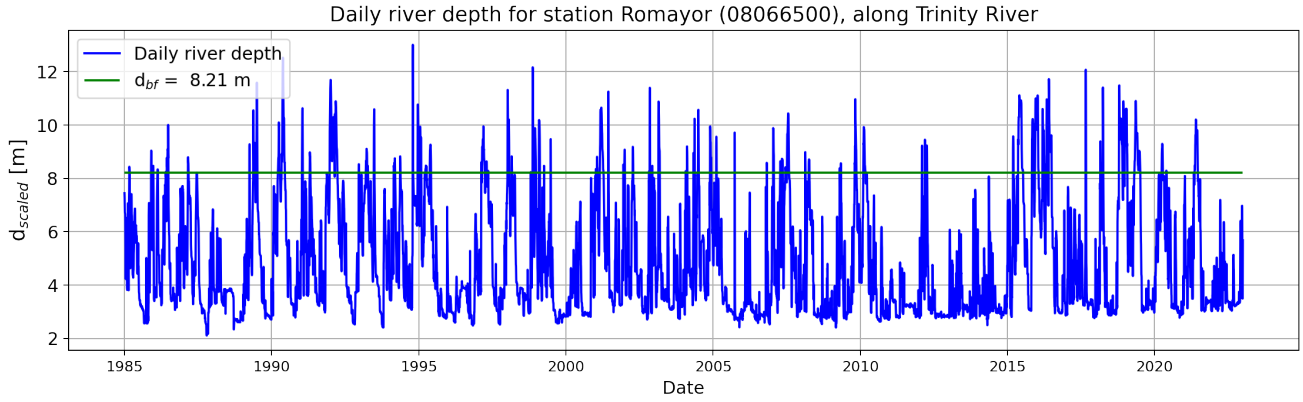

(d) Trinity River, Romayor station

Figure D.5: Scaled river depths for the other stations in the rivers

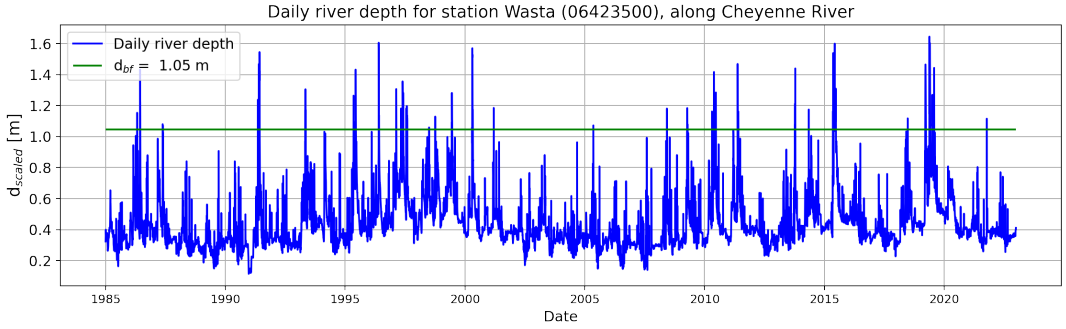

(a) Cheyenne River, Wasta station

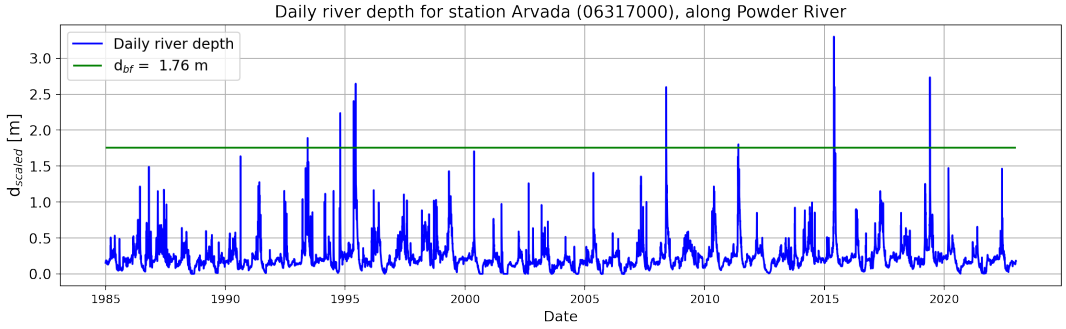

(b) Powder River, Arvada station

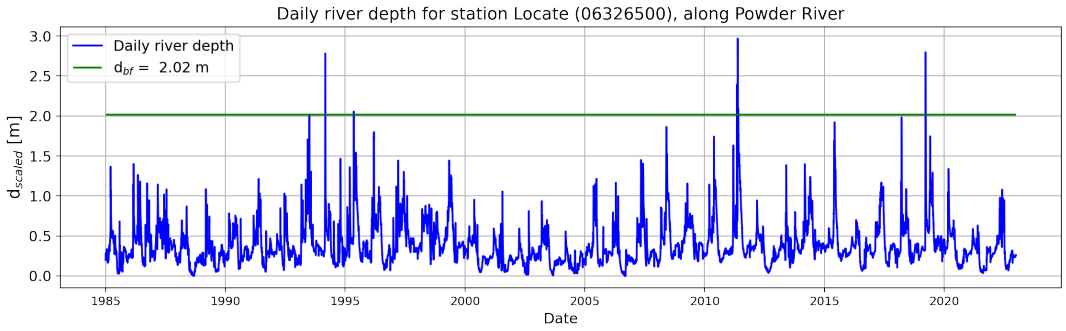

(c) Powder River, Locate station

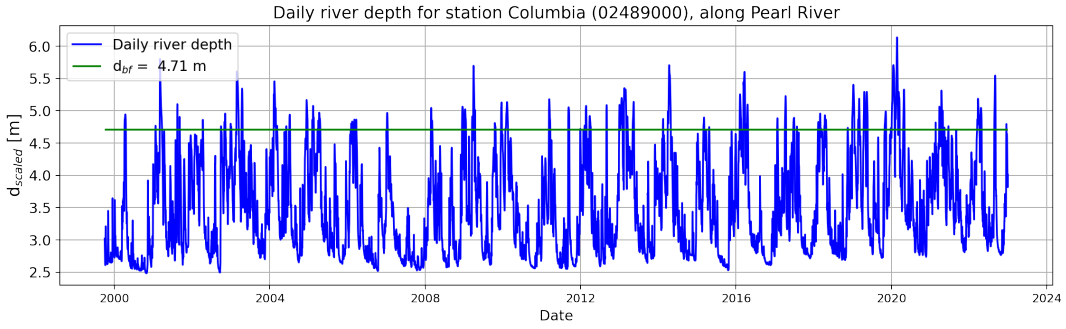

(d) Pearl River, Columbia station

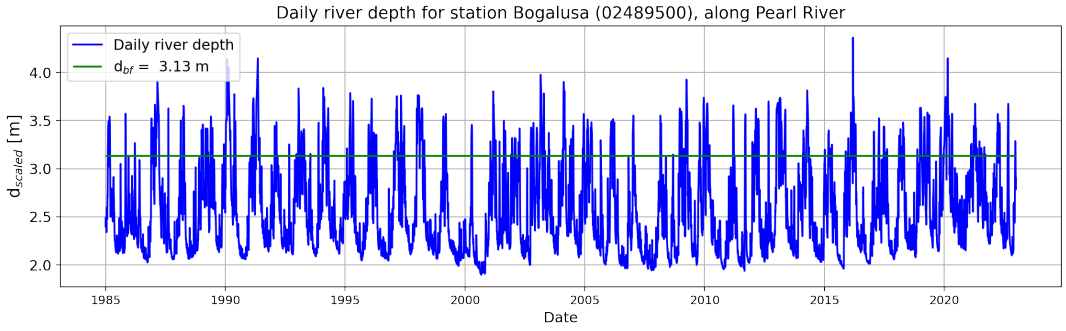

(e) Pearl River, Bogalusa station

E

Soil Data

Per cutoff location, soil data of the floodplain was found through SoilWeb and is displayed in this appendix. The names for the soil types were assigned by the creaters of SoilWeb. The percentages for Clay and Sand were calculated based on the values given on SoilWeb. The Silt percentage was calculated with the assumption that Clay, Sand, and Silt make up 100% of the soil.

According to UC Davis (n.d.), ”Sand percentage” is the weight percentage the particles with 0.05 mm < diameter < 2 mm. This contains the total sand fraction. For ”Total clay percentage” the particles have a diameter smaller than 0.002 mm (U.S. Department of Agriculture, 2022).

E.1. Cheyenne River Floodplain Soil

Table E.1: Cutoffs of Cheyenne River with dates and soil percentages gathered from SoilWeb.

Cutoff	Year	Silt	Clay	Sand	Soil Type	Type	Extra
1	2016-2020	4.37%	12.78%	82.85%	Gb: Glenberg fine sandy loam	Chute	Exclude.
2	2000	17.14%	9.80%	73.07%	Ba: Bankard soils	Chute	
3	1998-1999	17.14%	9.80%	73.07%	Ba: Bankard soils	Chute	
4	2004-2005	1.95%	10.45%	87.60%	Rw: Riverwash	Chute	
5	1999-2000	17.14%	9.80%	73.07%	Ba: Bankard soils	Chute	
6	2015-2016	4.49%	13.05%	82.46%	Gb: Glenberg fine sandy loam	Chute	
7	2004-2016	1.95%	10.45%	87.60%	Rw: Riverwash	Chute	Exclude.
8	2019	6.59%	13.23%	80.18%	Gb: Glenberg fine sandy loam	Chute	
9	2008-2009	1.95%	10.45%	87.60%	Rw: Riverwash	Chute	
10	2019	1.95%	10.45%	87.60%	Rw: Riverwash	Chute	
11	2019	1.95%	10.45%	87.60%	Rw: Riverwash	Chute	
12	2011-2012	6.70%	10.00%	83.30%	Bk: Bankard loamy fine sand	Chute	Exclude.
13	2010-2011	6.70%	10.00%	83.30%	Bk: Bankard loamy fine sand	Chute	
14	2016-2019	1.95%	10.45%	87.60%	Rw: Riverwash	Chute	Exclude.
15	2019	1.95%	10.45%	87.60%	Rw: Riverwash	Chute	
16	2014-2019					Chute	Exclude.
17	1997	6.70%	10.00%	83.30%	Bk: Bankard loamy fine sand	Chute	
18	2008-2009	8.89%	6.80%	84.31%	Bc: Bankard loamy sand, hummocky	Chute	
19	1995	7.15%	6.30%	86.55%	Bn: Bankard loamy fine sand, gravelly substratum	Chute	
20	2014					Chute	Exclude.
21	2010-2012					Chute	Exclude.
22	2014					Chute	Exclude.
23	2009-2010	1.95%	10.45%	87.60%	Rw: Riverwash	Chute	
24	1997	7.42%	7.48%	85.10%	Bd: Bankard very fine sandly loam	Chute	

E.2. Powder River Floodplain Soil

Table E.2: Cutoffs of Powder River with dates, coordinates and soil percentages gathered from SoilWeb.

Cutoff	Year	Silt	Clay	Sand	Soil Type	Type	Extra
1	2000	5.75%	5.35%	88.90%	611: Draknab sandy loam	Neck	
2	1994-2006	5.75%	5.35%	88.90%	611: Draknab sandy loam	Chute	
3	1984-1987	22.44%	13.16%	61.40%	158: Haverdad-Draknab complex	Neck	
4	1995	25.44%	13.16%	61.40%	158: Haverdad-Draknab complex	Neck	
5	2008	25.44%	13.16%	61.40%	158: Haverdad-Draknab complex	Neck	
6	2011	25.44%	13.16%	61.40%	158: Haverdad-Draknab complex	Chute	
7	2009	25.44%	13.16%	61.40%	158: Haverdad-Draknab complex	Neck	
8	2011	11.89%	9.36%	74.75%	4621A: Hanly-Glendive complex	Chute	Exclude.

E.3. Pearl River Floodplain Soil

Table E.3: Cutoffs of Pearl River with dates, coordinates and soil percentages gathered from SoilWeb.

Cutoff	Year	Silt	Clay	Sand	Soil Type	Type	Extra
1	2010	59.75%	23.84%	16.42%	CY: Cascilla-Chenneby ass.	Neck	
2	1999	23.91%	5.10%	70.99%	Br: Bruno sandy loam	Neck	
3	2015	12.43%	6.59%	80.98%	Je: Jena fine sandy loam	Neck	
4	1990-1991	28.02%	6.30%	65.69%	Nu: Nugent soils	Neck	
5	2010	16.70%	8.33%	74.98%	JN: Jena-Nugent association	?	Exclude.

E.4. Trinity River Floodplain Soil

Table E.4: Cutoffs of Trinity River with dates, coordinates and soil percentages gathered from SoilWeb.

Cutoff	Year	Silt	Clay	Sand	Soil Type	Type
1	1990	30.07%	17.08%	52.86%	HatA: Hatliff-Pluck-Klan complex	Neck
2	1990	30.27%	64.13%	5.60%	KamA: Kaman clay	Neck
3	1997	30.27%	64.13%	5.60%	KamA: Kaman clay	Neck